THE TRANSCELLULAR PATHWAY IS A SIGNIFICANT CONTRIBUTOR TO WATER FLOW THROUGH VASCULAR ENDOTHELIA

by

YAN XUE

A dissertation submitted to the Graduate Faculty in Biology in fulfillment of the requirements for the degree of Doctor of Philosophy, The City University of New York

2011

This manuscript has been read and accepted for the
Graduate Faculty in Biology in satisfaction of the
dissertation requirement for the degree of Doctor of Philosophy.

Date	Professor Karen Hubbard, Ph.D. Chair of Examining Committee

Date	Professor Laurel A. Eckhardt, Ph.D. Executive Officer

Professor, David S. Rumschitzki Ph.D.

Professor Mark Pezzano, Ph.D.

Professor Kamilah S. Ali, Ph. D.

Professor John M. Tarbell, Ph.D.

Kung-Ming Jan, M.D. Ph. D.

Supervision Committee

THE CITY UNIVERSITY OF NEW YORK

Abstract

THE TRANSCELLULAR PATHWAY IS A SIGNIFICANT CONTRIBUTOR TO WATER FLOW THROUGH VASCULAR ENDOTHELIA

by

Yan Xue

Advisor: Professor Karen Hubbard

Aquaporin-1 (AQP1) is a ubiquitous water channel protein that facilitates transmembrane water flow. The aim of our study is to determine the contribution of the AQP1 transcellular pathway to water filtration through aortic endothelial cells (AECs). In this thesis, we use both *in vitro* and *ex vivo* models of rat AECs to characterize the transport properties of such cells to water and/or small solutes.

In vitro water flux (*Jv*) studies show that 67.9% knockdown of AQP1 in rat AECs by small interfering RNA (siRNA) significantly reduces *Jv* by 56.4±8.2% (n=7). A study of the permeability to tetramethylrhodamine (TAMRA) and albumin has provided an interesting insight into what portion of this *Jv* reduction is due directly to AQP1 suppression, since these solutes traverse only inter-endothelial junctions. As a result, AQP1 suppression leads to a 21.8±7.04% drop in TAMRA convective permeability and a 29.79.1±1.72% /25.69±8.19% drop in albumin permeability under convection/diffusion conditions between control and treated monolayers.

We have constructed an *ex vivo* culture system that allows for the perfusion of the vessel lumen and application of a hydrostatic pressure that yields a physiological shear stress and transmural pressure. We note that maintenance of both pressure and shear flow preserves isolated AEC integrity, as assessed by hydraulic conductivity (*Lp*) and morphology studies. This culture model enables us to employ molecular manipulation of AECs in intact rat aortas. We showed that downregulation of AQP1 via siRNA results in a pressure-dependent decrease in total *Lp* (*Lp* of endothelium + subendothelial intima (SI)), Lp_t (Lp_{e+i}), by 37.35±12.97% (n=5) (59.8±11.6 % (n=3)) and 8.71±3.76% (n=5) (15.5±9.1% (n=3)) at 60 and 100 mmHg respectively. Our study indicates that AQP1 contributes significantly to transendothelial *Lp*. Transendothelial water flow is critical in determining whether low-density-lipoprotein (LDL) molecules can spend enough time at high enough local concentration in the SI to bind to SI extracellular matrix, a critical step in early atherosclerotic lesion formation. Our data suggest that regulation of AQP1, an important contributor to water filtration, may affect lipid transport in a beneficial way with regards to early disease progression.

Acknowledgements:

游子吟　　孟郊

慈母手中线，游子身上衣。

临行密密缝，意恐迟迟归。

谁言寸草心，报得三春辉。

谢谢我的爸爸妈妈。。。

Table of Contents

List of Figures:

List of Tables:

Chapter 1 Introduction

1. Atherosclerosis

Atherosclerosis, a disease that affects the aorta and other major high-pressure arteries, is the leading causes of death in America and all Western countries. It is manifested by a gradual narrowing of the vessel lumen due to atherosclerotic plaques, leading to reduced blood supply to major organs. When the plaques rupture, the resulting thrombosis can lead to myocardial (heart attack) and cerebral infarction (stroke). Risk factors associated with atherosclerosis include: hypertension, smoking and diabetes mellitus (Insull, 2009).

Lipid metabolism plays an important role in atherogenesis. Low-density-lipoprotein (LDL) is the most abundant artherogenic lipoprotein in plasma and accumulation of LDL, referred in the popular press to as the "bad" cholesterol, in the arterial subendothelial intima is considered the fundamental event that triggers early lesion formation (Nielsen, 1996). Lipoproteins are cholesterol carriers. The LDL particle is 22nm in diameter and is one of the five cholesterol carriers in the body. Its outer phospholipid layer contains a single chain of apolipoprotein B. Its hydrophobic core comprises cholesterol esters and triglycerides. High-density- lipoprotein (HDL) cholesterol is referred to as the "good cholesterol". It is believed to be protective of cardiovascular disease because HDL can remove cholesterol from the blood stream and transport it back to the liver (Rader e Daugherty, 2008).

The structure of the aorta is divided into multiple layers. The inner-most layer (facing the lumen) is a monolayer of endothelial cells, followed by a very thin layer of subendothelial intima (SI) (0.1-0.5μm in rat), which consists of a loose fiber matrix of proteoglycan and collagen fibers bordered by a fenestrated internal elastic lamina (IEL). The dense media (~100μm in rats) mainly consists of smooth muscle cells, extracellular matrix and elastic tissue. It is covered on the outside by a layer of loose adventitial tissue (Lusis, 2000).

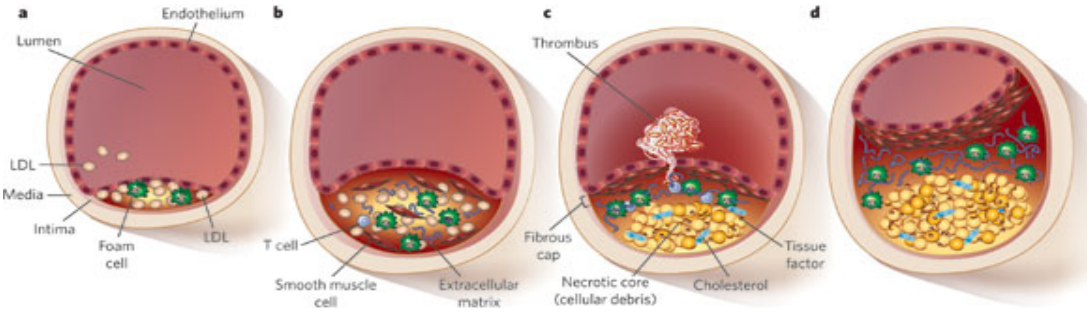

Figure 1.1: Sequential steps of the genesis of atherosclerosis a: Early lesions (fatty streaks); b: Intermediate lesion; c: Fibrous lesion that can easily rupture inducing thrombus formation; d: More advanced lesion that can lead to occlusion (see text). (Rader e Daugherty, 2008)

Atherogenesis is a multi-step process. (See Figure 1.1) The earliest recognizable lesion of atherosclerosis is called “fatty streaks”, which is an accumulation of lipid-rich macrophages and lymphocytes in the arterial wall. Low-density-lipoproteins (LDL) transmigrate from the lumen to susceptible sites on the vascular endothelium and accumulate in the subendothelial intima (SI) space. These accumulated LDLs are then oxidized through interaction with reactive oxygen species (ROS). It is believed that this modification process contributes to monocyte recruitment by stimulating overlying endothelial cells to producing pro-inflammatory factors (Ross, 1993). Another line of thinking suggests that they stimulate neighboring endothelial cells to shed part of their

surface glycocalyx, thereby exposing receptors for blood-borne monocytes, that attach and cross the endothelium (Grundmann, Schirmer *et al.*, 2009). In the SI, monocytes mature to become macrophages that subsequently phagocytose bound lipids, when overwhelmed, they can become foam cells. The aggregation of foam cells leads to the formation of fatty streaks. The intermediate lesion, the "fibro-fatty lesion", is composed of a growing mixture of foam cells as well as smooth muscle cells. Oxidized LDL also recruits media smooth muscle cells into the SI. The smooth muscle cells can proliferate there, producing extracellular matrix (i.e., collagen), which is deposited to facilitate further lipids retention. In addition to monocytes, lymphocytes are also recruited to help maintain a state of chronic inflammation. The lumen begins narrowing down by the growth of the lesion. Eventually, the more complex advanced lesion called "fibrous plaques" form. A cap of fibrous connective tissue forms over the mass of lipids and the necrotic core, which is comprised of cellular debris and crystalline cholesterol released by dead foam cells. The lesion can now project into the lumen of the artery and impede blood flow. This thin fibrous cap is vulnerable to rupture, which can lead to thrombosis. If the plaque does not rupture, it continues to grow, gradually occluding lumenal blood flow, which can result in life-threatening disease state such as myocardial infarction and stroke (Ross, 1993).

2. Endothelial barrier function, transendothelial water and macromolecule transport

The endothelial monolayer that composes the lining of the vessel lumen is a major contributor to the blood-tissue barrier. The endothelial cells (ECs) form continuous tight

junctions that formulate a semi-permeable exchange surface through which selective transport of fluid and small molecules can take place. Tight junctions (TJs) are responsible for the sealing between neighboring cells, see Figure 1.2. They appear in electron micrographs as a series of belts around cell-cell focal points, usually on the apical surface of the cells. TJs are composed of transmembrane proteins (occludin, claudins) linked to the actin cytoskeleton via cytoplasmic zonular occludens (ZO) proteins (Anderson, 2001). Endothelial barrier dysfunction is associated with the disruption and/or injury of endothelial cells by mechanical force, i.e., shear stress. It results in the disruption of barrier function and hyperpermeability to macromolecule transport leading to a vascular diseased state. Vascular endothelia are regarded as active sensor to various mechanical forces, for instance, shear stress exerted by blood flow. Under culture conditions, endothelia grow in a symmetric, cobblestone pattern. In contrast, with an application of steady shear stress, the endothelial cells can undergo drastic morphological changes from polygonal to elongate while aligning themselves in the direction of shear flow over a period of 24-48 hours. In regions of the vessel where the flow is uniform, the endothelial cells align parallel to the direction of the flow. Near the inner curvature, branching or bifurcation areas, however, the blood flow is disturbed and often unsteady, and shear stress is reduced resulting in alterations in the shape of the endothelial cells and in a loss of their particular axial alignment. It turns out that this is where endothelial permeability to macromolecules is highest, and where vessels are most susceptible to plaque formation (Dewey, Bussolari *et al.*, 1981; Langille e Adamson, 1981) (Friedman e Fry, 1993; Gimbrone, 1999) The unsteady and even oscillating shear flow in these regions influences the rate of cell proliferation (mitosis) and death

(apoptosis). Decreasing shear flow can induce apoptosis (Dimmeler, Haendeler *et al.*, 1996; Cho, Mitchell *et al.*, 1997). As we shall explain, increased cell turnover in this region is at least partly responsible for increasing macromolecular endothelial permeability.

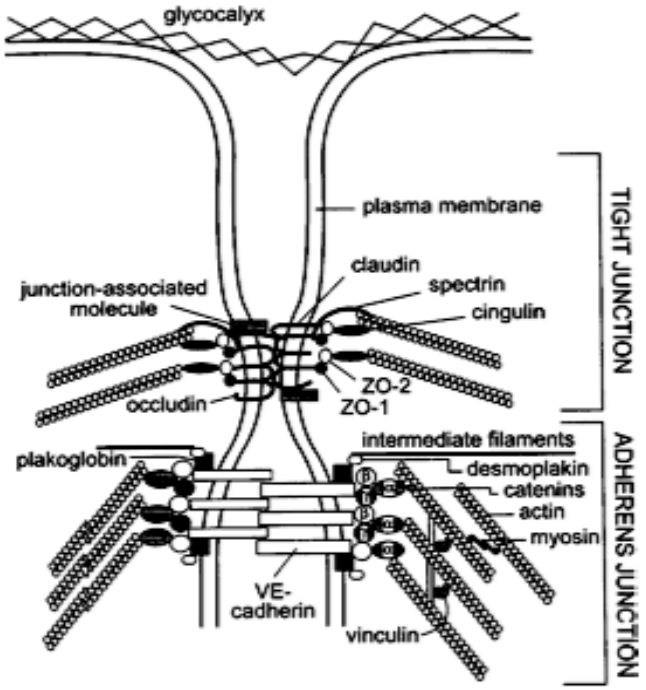

Figure 1.2: Tight junction protein complexes, starting from the apical surface, tight junction followed by adherens junctions. (Tarbell, 2003)

A hallmark of atherosclerosis is the accumulation of LDL in the arterial SI. How a large molecule like LDL crosses the endothelial barrier has been an important puzzle. There are believed to be two major transendothelial transport pathways: paracellular and transcellular pathways, by which macromolecules can traverse through the arterial endothelium:

(1) Paracellular transport pathway and tracer spot studies

The paracellular pathway allows for the transport of water and hydrophilic solutes smaller than the size of albumin (5-6nm in diameter) through the functional clefts between endothelial cells (ECs). This transport can be mediated either by convection, where solutes are carried by the flow of bulk fluid (usually water), driven by a transmural pressure gradient; or by diffusion, the random Brownian motion movement of solutes driven by a chemical potential, which at concentration, reduces to a concentration gradient. Weinbaum proposed a 'leaky junction' theory, where there exists rare, transient widened junctions (1 out of 1,000-10,000 cells), referred to as 'large pores', that occur during the processes of cell turnover either by mitosis or cell death (Weinbaum, 1985). These transient "leaky junctions" induce local endothelial hyperpermeability to macromolecules. Stemerman used horseradish peroxidase (HRP, 4-5nm) and ^{125}I-LDL as large molecular tracers. When one examines perfusion-fixed aortic endothelium *en face* after 10-minute HRP circulation time, the HRP appears on the luminal surface as small punctuate brown foci (less than 1mm in diameter). Aortas with ^{125}I-LDL must be put on photographic plates in the dark and one eventually develops the films to measure counts per unit area. This focal hyperpermeability to LDL turns out to be 47 times greater in leaky bifurcation regions than in nonleaky, straight ones and, as noted, these leaky regions tend to concentration around aortic branches (Stemerman, Morrel *et al.*, 1986). Leaky sites are also associated with the branching sites of the intercostals. Lin's Evan blue albumin (EBA) tracer study shows that albumin (6nm in diameter) can pass through transiently opened junctions but experiences near impermeability through normal junctions. They found that 99% of mitotic cells are associated with spots leaky for EBA, but these account for only 26% of the total number of leaky sites; 63% of dying cells

correlate with EBA leakage, and these account for 37% of the total number of leaky sites (Lin, Jan *et al.*, 1988). Thus mitotic plus dying cells together account for nearly 60% of all leaky sites to EBA, thereby leaving the reason for leakage in ~40% of EBA leaks unexplained (Lin, Jan *et al.*, 1990). Lin used Lucifer yellow-LDL (LY-LDL), which is 22nm in diameter, for analogous tracer studies; these larger particles can only passes through a maximally widened junction. It turned out that 80% of dividing cells are associated with spots leaky for LY-LDL, and these accounts for 45% of total LY-LDL leaky sites. These LY-LDL numbers seem spuriously high, since a higher proportion of dividing cells seem to leak the larger LY-LDL than the smaller EBA. These numbers are likely due to a too small sample size (Lin, Jan *et al.*, 1989). Consistent with this suspicion are the generally lower numbers from Truskey, who used ^{125}I-labeled LDL to study LDL permeability and concentration in the arterial wall. Their *en face* nuclear emulsion radiograph shows that only 60% of the mitotic cells correlate with regions of LDL hyperpermeability, but these account for only 25% of all leaky sites (Truskey, Roberts *et al.*, 1992). Similarly, Herman found that although 71-90% of mitotic cells leaked, they accounted for only 1/6 of all macromolecular leaks and for only 8% of LDL leaks (Hermann, 1994). Finally, Chen found that, even though at any given time only a small proportion of ECs undergo mitosis (0.01%) or death (0.1%), HRP traverses ECs in turnover far more rapidly than normal endothelium. In fact, 90-100% of mitotic ECs correlate with leaky sties, accounting for 48% of all cellular leaky sites between 1-5 minutes of HRP circulation. 90% dying cells are associated with leaky sites, accounting for 10% of all leaky sites (Chen, Jan *et al.*, 1997) .

Chuang measured *en face* EBA and horseradish peroxidase (HRP, 4-5nm in diameter) spot sizes in thoracic aortas after various tracer circulation times. The spot sizes increase rapidly with increasing circulation times up to ~four minutes. Beyond that, leakage through normal EC junctions leads to diffuse EBA or HRP staining areas, which make it difficult to distinguish localized spots from background. They found that leaky spots are more frequently associated with mitotic than dying cells in the arteries, but they coincide predominantly with dead cells in the veins (Chuang, Cheng *et al.*, 1990). Chen also found that, as circulation times increases, HRP spot sizes increases. Silver nitrate staining of the inter-endothelial junction revealed widened junction associated with mitotic cells, which might be responsible for hyperpermeability to dye around those regions. Since HRP is smaller in size than EBA, it can passed through normal as well as more easily through transiently leaky junctions, explaining why there are, in general, more HRP spots than EBA or LDL spot a given tissue (Chen, Jan *et al.*, 1997).

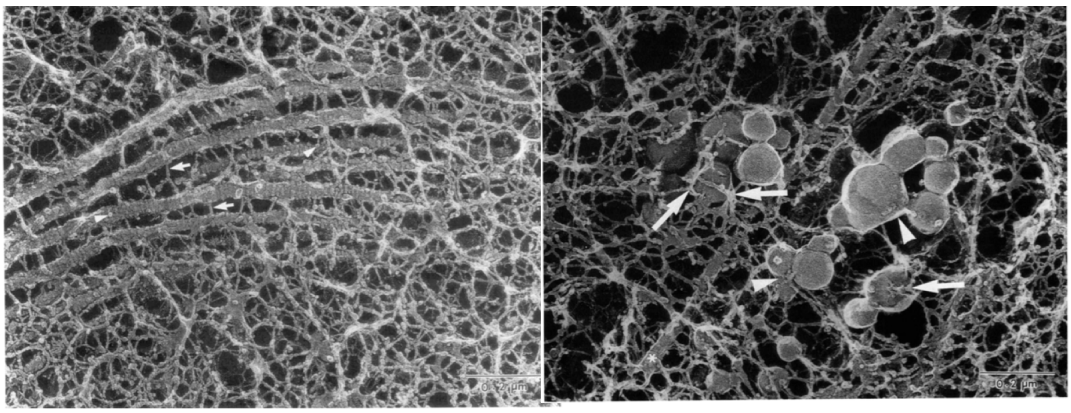

Figure 1.3: Electron micrograph of the arterial subendothelial intima (SI) showing how the loose matrix in the subendothelial space is intertwined with cross-banding branching collagen fibrils (the thick fibers) with no lipid deposit (left). Extracellular lipids vesicles (spheres) that are attached to collagen fiber are seen on the right in the aortic SIs of cholesterol-fed rabbits (Frank e Fogelman, 1989).

We turn now to longer studies that reflect lipid accumulation. Electron micrographs show that free cholesterol and apolipoprotein B are found to accumulate in the extracellular matrix in the subendothelial intimas of hypercholesteremic rabbits even before there are any detectable lesions in their vessel walls (Mora, Lupu *et al.*, 1987). Frank and Fogelman used ultra-rapid freezing and rotary shadow etching to produce electron micrographs of exceptional clarity. These micrographs reveal the ultrastructure of the SI, which is composed of an extensive network of collage fibrils that are connected by thin filament and proteoglycans. Aggregated of lipid vesicles are found between the collagen fibrils in the SI and linked to matrix filaments, see Figure 1.3 (Frank e Fogelman, 1989).

(2) Theoretical studies

Yuan developed a two-dimensional filtration and advection-diffusion model for water and macromolecular transport through a localized EC leak and its neighborhood. This theory predicts that the transmural pressure difference across a vessel lumen drives water flow through both normal and leaky clefts. The early growth of leaky sites is too rapid to be explained by diffusion alone (for HRP, 150-200 μm in diameter after 1 minute), but Yuan *et al.*'s inclusion of fluid advection only improved the diffusive prediction marginally, and its predictions for localized tracer spot growth with tracer circulation time were still an order of magnitude too slow. Their theory assumed that the permeability and diffusivity for the SI, the IEL fenestrae and the media are all the same (Yuan, Chien et al., 1991). Huang *et al.* considered the possibility that the permeability and diffusivity of SI and media matrices may indeed be different. They used Frank and Fogelman's micrographs to extract SI ultastructure, e.g., fiber sizes and spacing, and used them as a basis for an *ab initio* fiber matrix theory to predict these transport parameters for the all-important, ultra-thin SI. They found that the far more porous subendothelial intima matrix's permeability is two orders of magnitude greater (130-250 times) than that of media. They then extended Yuan *et al*.'s advection-diffusion-filtration model and successfully explained the rapid growth of HRP leaky sites in the arterial SI without the need to invoke immeasurable adjustable parameters. Their theory explains spot growth by showing how the transmural pressure drives a water flow that advects solute across the localized leak into the SI and then, when inside the SI, parallel to the endothelium and radially away from the leaky junction. This SI spread slows as water and macromolecules find the fenestrated pores of internal elastic lamina (IEL) and cross into the far thicker and denser media (Huang, Rumschitzki *et al.*, 1994). The SI lateral water flow is central

to macromolecular spread in the vessel wall around a focal endothelial leak. Zeng reworked Huang *et al.*'s theory using subsequently measured parameters that Huang had incorrectly guessed and corrected certain errors in Huang *et al.*. Fortunately, these changes actually slightly improved the theory's agreement with experiment and extended to a theory for the water and macromolecular transport in the pulmonary artery, which also agrees well with experimental measurements (Zeng *et al*, 2011, in review).

Transmural water flux is also responsible for the drainage of unbound macromolecules i.e., LDL, from the SI by advection into and through the arterial media and adventitia. Lever et al showed that the steady state LDL concentration in the media of the carotid artery was 50 times higher with collars around the vessel than without collars. They explained their results as being the result of collars restricting transmural water flux; therefore, LDL cannot be flushed out of the vessel wall, and this results in LDL rapid accumulation in the media (Lever, Jay *et al.*, 1996).

(3) Transcellular pathway

Normally large-molecular-weight molecules (such as LDL) cannot pass through the clefts of tight junctions. They can, however, attach to endothelial cell (EC) surface receptors that accumulate in clathrin-rich coated pit regions on the cell surface that enter the cell via endocytosis. LDL molecules internalized in this manner are digested and their cholesterol content can be used for membrane synthesis or storage in the form of cholesterol esters (Goldstein e Brown, 2009). It has long been believed that LDL can also

enter and even traverse ECs via moving plasmalemmal vesicles either involving or independent of the LDL receptor to deliver cholesterol to neighboring cells. Using *in situ* perfusion of either native or reductively methylated LDL (which is unable to bind to the LDL receptor), such uptake was visualized using colloidal gold immunolabeling on rat arterial endothelial cells. Snelting-Havinga showed that the vesicular pathway is the major pathway for LDL transport and that this intracellular transport is most likely LDL receptor independent (Snelting-Havinga, Mommaas *et al.*, 1989). Vasile studied the transport of LDL through rat aortic endothelia via vesicles using electron microscopy. They found that any receptor-mediated endocytosis transport could at most account for a small fraction of the transport through the receptor-independent pathway. Thus the majority of the transcellular transendothelial transport of circulating LDL molecules must occur via plasmalemmal transcytosis vesicles. These membrane-bound vesicles are homogenous in size (60-80nm), which seem to act as passageway for LDL from luminal to abluminal surface, with a discharge of LDL to abluminal side or to other cells (Vasile, Simionescu *et al.*, 1983). Note that ultrathin serial sections appear to show that what appear in one plane to be free vesicles are, in fact, attached to one membrane or the other in another plane; this result appears to refute the plasmalemmal transcytosis transport hypothesis (Frokjaer-Jensen, 1984).

3. Aquaporin water channel transport proteins

Water transport is essential for all biological processes. The lipid bilayer of the cell's plasma membrane is slightly permeable to water either by diffusion or by water-selective channels. Diffusion is slow but for decades was considered the predominant

water pathway for most of the cells. During this time, scientists were puzzled why erythrocytes and certain proximal tubules epithelia demonstrate an exceptionally high osmotic water permeability with an usually low Arrhenius activation energy (*Ea*) (King e Agre, 1996). In addition, this fast water osmotic water permeability proved to be reversibly inhibited by mercuric compounds in red blood cells (Macey e Farmer, 1970) and proximal tubules epithelia (Whittembury, Carpi-Medina *et al.*, 1984).

The discovery of the aquaporin-1 (AQP1) membrane water channel protein offered a clear explanation to this puzzle. AQP1 (also called Channel-forming Integral Protein (CHIP28)) was discovered while isolating Rh polypeptides from human erythrocytes. It was originally thought to be a proteolytic degradation product of Rh antigen on erythrocytes, but was later identified as a distinct integral membrane protein of 28kDa size (Denker, Smith *et al.*, 1988). The cDNA encoding AQP1was cloned by Preston and coworkers and has demonstrated high homology with the Major Intrinsic Protein (MIP) family, an ancient family of membrane channels that are involved with water and small solute transport (Preston e Agre, 1991). Since then, 13 mammalian AQP isoforms are identified (Verkman, 2009).

AQP1 is abundant in erythrocytes and kidney proximal tubules. The homology with the MIP family suggested that it might be a channel protein, in addition, radiation inactivation studies showed that an approximately 30kDa size functional unit protein, similar to the size of AQP1, existed in the renal proximal tubules apical membrane (Van Hoek, Hom *et al.*, 1991) and erythrocytes (Van Hoek, Luthjens *et al.*, 1992) as a

moderator to rapid water transport. However, the physiological function of CHIP28 was still unresolved. The first evidence of the water permeation function of AQP1 (CHIP28) was presented by complementary RNA (cRNA) expression in swelling studies in Xenopus laevis oocytes. Oocytes naturally have very low permeability to water. When injected with AQP1 cRNA in a hypotonic solution; however, they swell and rupture within 5 minutes. The increased osmotic water permeability (*Pf*) was 8 times greater than that of the non-injected oocytes at 22°C and 30 times greater at 10°C, while the activation energy (Ea<3 kcal/mol) of this permeability is at least 3 times lower in comparison with the non-injected groups. Incubation with mercuric chlorides reduced this osmotic water permeability while β-mercaptoethanol can reverse this reduction (Preston, Carroll *et al.*, 1992). In order to rule out the possibility that AQP1, instead of being the water channel itself, might be a water channel regulator, Zeidel inserted functionally reconstituted purified RBC AQP1 into proteoliposomes. The water permeability of these liposomes was 50 times (*Pf*=0.054cm/s) greater than that of the control group (*Pf*=0.0097cm/s) at 37°C. And this permeability is also very sensitive to inhibition by a mercuric sulfhydril reagent and can be reversed by reducing agents. It also exhibited low Arrhenius activation energy. Based on the calculated osmotic water permeability of a single AQP1 (11.7E-14cm^3/s) from proteoliposomes containing pure AQP1, the calculated water permeability of human RBC (approximately 2×10^5 AQP1 molecules over a surface area of 1.4×10^{-6} cm^2) is 0.017cm/s, which agrees with the observed *Pf* value of human RBCs (0.02cm/s). The unit water permeability of reconstructed proteoliposomes is 3×10^9 molecules/single AQP1subunit/second (Zeidel, Ambudkar *et al.*, 1992). Van Hoek and coworker also confirmed Zeidel's observation that AQP1 exhibited water channel

properties. Water permeability of erythrocytes membrane depleted of non-AQP1 proteins is high (0.03cm/s) at 37°C while *Ea* is very low (2.2 kcal/mol) (Van Hoek e Verkman, 1992). Therefore, AQP1 is considered as the water channel protein that assists fast water transport. Preston and coworkers has indicated that cysteine189 is the mercurial susceptible site in AQP1. Four site-directed mutagenesis of four cysteine residues (87, 102, 152, or 189) with cysteine substituted by serine were constructed and injected into oocytes. Water permeability of oocyte injected with C189S RNA was not inhibited by 1mM $HgCl_2$ and this is not affected by changing concentration of $HgCl_2$ up to 3mM. Additionally, injection of a mix of cRNAs encoding mercurial-sensitive and resistant AQP1 resulted in a sum of *Pf* as measured by individual constructs. When inhibited, *Pf* decreased to that of C189S RNA. These results indicated that each subunit is functional as a water pore. Finally, note that the AQP1 membrane channel is very selective for water transport; it does not conduct urea or protons (Preston, Jung *et al.*, 1993).

AQP1 is an integral membrane protein that is very abundant in erythrocytes and in the epithelia of the proximal tubules and the descending limbs of Henle as well as other water-permeable secretory and resorptive epithelia (Preston e Agre, 1991; Nielsen, Smith, Christensen, Knepper *et al.*, 1993). It is believed to be involved in numerous physiological functions from glomerular filtrate fluid reabsorption, to cerebrospinal fluid secretion and maintenance of interstitial fluid (Nielsen, Smith, Christensen e Agre, 1993).

As noted, there are about 2×10^5AQP1 monomer copies per human RBC, which is the major site of AQP1 immunolabeling. It is postulated that mammalian RBC exhibits

high water permeability to allow for rapid cell volume changes so as to withstand the hypertonic environment (high salt and urea concentration) in the renal medulla. In addition, urea can permeate through RBC membrane independently of water transport, which is also helps to ensure the osmotic stability of the erythrocytes (Macey, 1984). Because of its abundance distribution on RBC membranes, AQP1 depletion or absence might lead to lethality. However, AQP1-null humans do not demonstrate any apparent clinical symptoms such as anemia, associated with RBC damage. Their RBCs appear normal in shape while exhibiting reduced osmotic water permeability (by as much as 80%) compared with the wild-type. This prompted a re-consideration of the physiological function of AQP1 on RBCs (Preston, Smith *et al.*, 1994).

In the kidney, AQP1 plays an essential role in renal osmotic driven transcellular water transport. AQP1 expression is identified in the apical and the basolateral sides of the proximal tubules, the descending thin limbs of Henle and the endothelial cells of the vasa recta, where closely to 90% of the nearly 200 liters of glomerular filtrate are reabsorbed so as to form concentrated urine (Nielsen, Smith, Christensen, Knepper *et al.*, 1993). When given water, transgenic AQP1-knockout mice exhibit polyuria. When deprived of water, these mice exhibited a severely deficient ability to concentrate urine resulting in inability to conserve fluid and dehydration. AQP1 deficiency caused a 78% decrease in transepithelial water permeability (*Pf*) and reduced net fluid reabsorption by 50% in isolated segments of the proximal tubules relative to the wild-type mice (Schnermann, Chou *et al.*, 1998). In the thin descending limb of Henle, loss-of-function of AQP1 resulted in an 88% decrease in an originally very high osmotic water

permeability (from *Pf* = 0.26 cm/s to 0.031cm/s) (Chou, Knepper *et al.*, 1999). In the Outer Medullary Descending Vasa Recta (OMDVR) of AQP-1 knockout mice, there is a nearly 60% decrease in NaCl-driven water transport compared with wild-type mice, providing evidence that such transcelluar water transport is AQP1 dependent (Pallone, Edwards *et al.*, 2000).

In lung microvessels, AQP1 is strongly expressed in the vasculature surrounding the alveoli, bronchioles and visceral pleura which are involved with fluid water transport between the airspace and the capillary compartment; such transport helps to maintain adequate hydration in the airway for gas exchange and for the absorption of alveolar fluid which resolves pulmonary edema. Three separate patterns of AQP1 expression are revealed during the development of fetal rats. AQP1 protein first begins to express in the perinatal phase, increases drastically in the neonatal phase and remains at a high level of expression throughout adult life (King, Nielsen *et al.*, 1996). In the eyes, AQP1 is expressed in lens epithelia and in cornea endothelia. AQP1-mediated water transport is believed to help maintain the transparency of the cornea. In brain tissues, the apical membrane of the choroid plexus epithelium was heavily stained, implying a role for AQP1 in the secretion of cerebrospinal fluid (Jung, Bhat *et al.*, 1994). AQP1was also found to strongly stained in the apical and basolateral membrane in the continuous capillaries of various tissues, including cardiac, skeletal and smooth muscles and in the mammary glands. It has been suggested that the water-permeable endothelia in continuous capillaries are responsible for the water balance between the plasma and interstitial fluid compartments (Nielsen, Smith, Christensen e Agre, 1993).

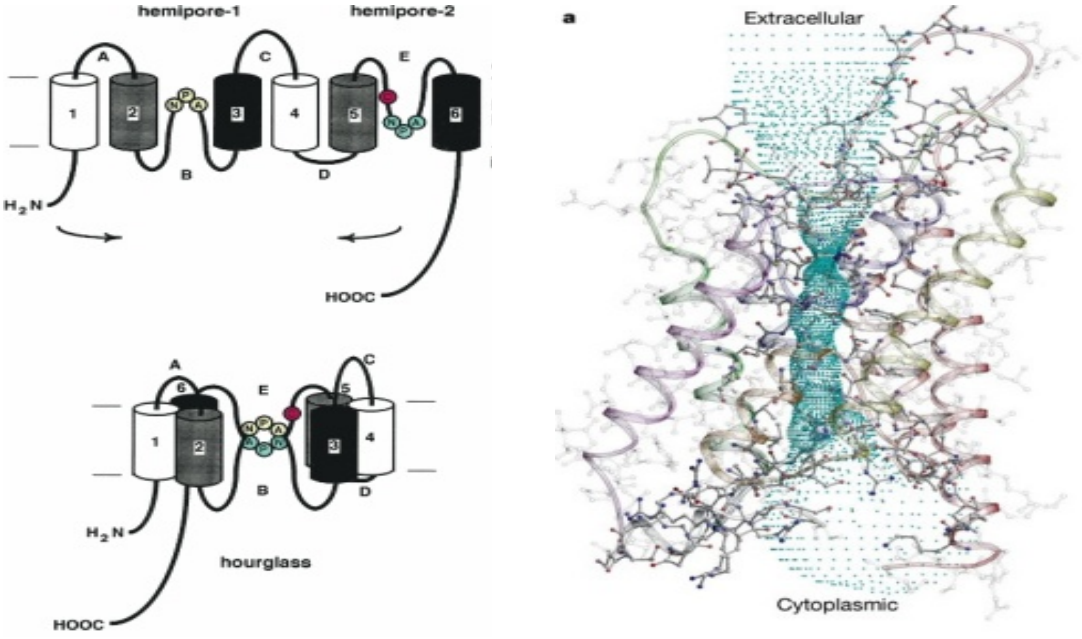

Figure 1.4: Left, the hourglass model of AQP1 (Jung, Preston *et al.*, 1994). The six lipid-membrane spanning α-helices are connected by five loops with amino and carboxyl termini located on the cytoplasmic side of the membrane, Loops B and E are oriented 180° to each other on the opposite sides of the membrane. They form a narrow aqueous channel. The figure on the right highlights the constriction region of AQP1. It has hydrogen-binding residues that line the inside wall of the channel. The selective filter is mainly hydrophobic with a few hydrophilic nodes (Sui, Han *et al.*, 2001).

As noted above, AQP1 allows the rapid transport of water in response to an osmotic gradient with no known ATP cost, but is, at the same time, rejects the transport of many other solutes, such as urea or even of protons (or $H3O^{+}$). It has been shown more recently that certain dissolved gases, such as carbon dioxide (Nakhoul, Davis *et al.*, 1998) ammonia in oocytes (Nakhoul, Hering-Smith *et al.*, 2001) do in fact traverse the AQP1 pore. NO is a physiological gas that serves as cell signaling molecule to endothelium-dependent vasodilation. It is produced by vascular endothelial cell and believed to freely and passively diffused through its lipid bilayer to act on neighboring smooth muscle cells. Recently it is shown that NO transport is AQP1 dependent, as NO permeability correlates with water permeability and can be blocked by $HgCl_2$ and DMSO in Chinese hamster

ovary cells (CHO-K1). In addition, a 316% increase in NO influx was observed in liposomes containing purified AQP1. The aortic ring of AQP1-/- mice displays reduced vasorelaxation. It is suggested that AQP1 can facilitate NO transport, which enables a cell to actively control its intracellular NO concentration resulting in active (not just passive) diffusion to smooth muscle cells to regulate blood pressure and flow. (Herrera, Hong *et al.*, 2006; Herrera e Garvin, 2007)

In order to understand AQP1's very easy water transport properties while maintaining unusually high selectivity, one generally turns to the molecule's molecular structure. AQP1 has been proposed to exist *in vivo* as a non-covalently bonded tetramer. This tetramer is composed of non-glycosylated and N-linked glycosylated monomers in a 3:1 ratio. The glycosylated subunit is subject to cleavage by a family of glycosidases (Smith e Agre, 1991). This tetramer structure theory is supported by freeze-fracture transmission electron microscopy studies using AQP1 reconstituted into proteoliposomes (Zeidel, Nielsen *et al.*, 1994). Based on the deduced amino acid sequence from a cDNA isolated from human bone marrow, it has been inferred that AQP1 contains six lipid-spanning hydrophobic α-helices connected by five loops with amino and carboxyl termini located on the cytoplasmic side of the membrane (Preston e Agre, 1991). The cytoplasmic Loop B and the extracellular Loop E contain highly conserved asparagine-proline-alanine (NPA) motifs. These motifs are critical to water permeability, since site-directed mutations that disturb of this triad lead to loss-of-function in osmotic water permeability (*Pf*). There are also two internal tandem repeats close to the amino and carboxyl halves of the polypeptides. It is proposed that the cytoplasmic Loop B and the

extracellular Loop E align structurally adjacent to each other by virtue of a folding path that has them move towards opposite sides of the cytoplasmic membrane (with cytoplasmic Loop B towards the extracellular side, and extracellular Loop E towards the intracellular side) as well as the juxtaposition of the COOH- termini. This is thought to be how the NPA motifs are able to form a narrow hourglass-like aqueous channel within the lipid bilayer (Figure 1.4A) (Jung, Preston *et al.*, 1994). Murata *et al*. proposed an atomic model of human RBC using electron crystallography studies at 3.8Å resolution. In it, the two non-lipid membrane spanning helices form a long hydrophobic channel that provides the structural basis for the exclusive selectivity of AQP1 for water molecule but not to protons (Murata, Mitsuoka *et al.*, 2000). A similar strategy is at work in *E. coli* glycerol facilitator Glp F (Fu, Libson *et al.*, 2000). In 2001, Sui and Jap determined a more accurate, a 2.2Å resolution X-ray crystallographic structure of AQP1 derived from bovine RBC. AQP1 consists of three regions: an extracellular and a cytoplasmic vestibule, connected by a constricted water pore of about 20Å in length. The mouth of extracellular vestibule is calculated to be 15Å in diameter. This opening cone narrows down to the molecule's narrowest point, about 2.8Å in diameter, roughly the diameter of a water molecule, which forms the restriction region. This steric resistance permits aquaporin to transport molecules with selectivity, water but not other solutes. The hydrogen-binding residues of certain amino acid side-chains in the constriction region allow for the favorable hydrophilic interaction with water molecules. These interactions help them to readily pass through, though the constriction region is predominantly hydrophobic. Similarly, the selectivity filter (4Å) is also amphipathic, with a few hydrophilic punctuated sites that allow for water molecule binding down the length of the

pathway. Thus the amphipathic nature and steric hindrance selectively facilitate rapid transport of water in AQP1. (Figure 1.4) (Sui, Han *et al.*, 2001).

4. Our group's work and current objectives

As discussed above, the artery's transmural pressure difference drives a flow of plasma, mostly water and solutes, from the blood across the arterial endothelium, and this flow both advects macromolecules into the subendothelial space and flushes unbound macromolecules from it. As such, the water transport characteristics of the vessel wall are of great interest for the study of early atherogenesis. After numerous studies on slabs of artery wall, A. Tedgui and J. Lever were the first to study of water filtration property through aortic walls on whole vessels *ex vivo* two and a half decades ago. They discovered that when the transmural pressure (ΔP) changed from 70 to 180mmHg, the hydraulic conductivity (*Lp*) of intact rabbit aorta decreased by nearly 40%. Not surprisingly, *Lp* increased when one denuded the endothelium, since denudation removed of one layer of resistance to flow (Tedgui e Lever, 1984). Baldwin and Wilson improved the techniques by measuring *Lp* at more intermediate ΔPs and by using the same rabbit aorta for *Lp* measurement at all of the multiple hydrostatic pressures. Their study showed a similar *Lp* trend. However, their data obtained at the lower pressures (50 and 75mmHg) showed far higher standard deviations than at the higher pressures and their *Lp* values were nearly double that of Tedgui and Lever. Whereas Tedgui and Lever's data showed that the *Lp* of the rabbit aorta's wall is dependent on ΔP as well as on the integrity of the endothelial monolayer, and whereas Baldwin and Wilson's mean *Lp*(ΔP) values were

consistent with these inferences, the latter group's very high standard deviations at 50 mmHg meant that the higher *Lp* value at that pressure could not be asserted from their data with any statistical significance (Baldwin, Wilson *et al.*, 1992).

Y. Huang developed a theoretical framework and a mathematical model to explain Tedgui and Lever's result for the dependence of the hydraulic conductivity on transmural pressures. They posited that high transmural pressure loading compresses the arterial subendothelial intima (SI), and this causes wall permeability to decrease drastically. The reason for this is that the compressed SI has a denser and therefore more resistant fiber matrix in it and, in addition, the compressed SI leads to endothelial cells partially blocking the fenestrated pores of the IEL. This latter effect increases resistance to transendothelial water flow significantly. The stiffer collagen prevents the SI from further compression after the maximal compaction (roughly to 1/6-1/7 of its unloaded thickness) is reached. Deendothelialization removes the endothelial resistance as well as the blocking of fenestrate, resulting in an elevated *Lp* that is, as seen in experiment, ΔP-independent. This theory indeed explained Tedgui and Lever's, Baldwin and Wilson's and Shou *et al*.'s results and predicted a 5-6-fold SI maximal compression (Huang, Rumschitzki *et al.*, 1997). Huang *et al.* fixed rat aortas under various pressures and measured average SI thicknesses in hundreds of random electron microscopy sections to confirm this prediction. Moreover, light micrographs of thick transverse aortic sections fixed under 100 mmHg showed aortic ECs blocking IEL fenestrae (Huang, Jan *et al.*, 1998). Shou *et al.*'s rat pulmonary artery and inferior vena cava *Lp* data suggest that SI

compression under pressure loading may also play a role in *Lp*(ΔP) in these other vessels, particularly in the former (Shou, Jan *et al.*, 2006).

Y. Shou, T. Nguyen and Y. Sun of our lab have all measured hydraulic conductivity (*Lp*) for whole rat thoracic aorta as a function of transmural pressure (ΔP), both with intact and denuded endothelium on the same vessel. Shou's result showed that *Lp* dropped by 40% as ΔP was increased from 60mmHg to 100mmHg and remained pressure insensitive to 140mmHg, which agrees with Tedgui and Lever's *Lp* data of rabbit aorta. Moreover, her results had acceptable standard deviations. Shou has also shown that *Lp* measured from the lowest to the highest ΔP is only slightly, but not significantly larger, on an average, than that is measured from high to low ΔP. This is probably due to a slight pre-conditioning effect (Shou, Jan *et al.*, 2006). T. Nguyen's measurements showed similar trends, a drop of 27.5% from 60 to 100mmHg, but consistently 20% lower at each ΔP than that of Shou's data. *Lp* of the deendothelialized vessel is roughly double the intact high-pressure value and pressure insensitive. By using a difference of resistances argument for the intact and denuded *Lp* data, we found that the aortic endothelium and SI accounted for about 47% (by Shou) and 37% (by Nguyen) of the total aortic resistance (1/*Lp*) (Shou, 2005; Nguyen, 2008).

J. Toussaint in our lab used both qualitative and quantitative immunohistochemistry to verify the presence/expression of AQP1 in the endothelial cells of excised rat aorta of both male Sprague-Dawley and Wystar Kyoto rats. His results show that AQP1 is found both on the luminal and abluminal surfaces as well as in the

interior of endothelial cells in transverse sections of rat aorta. He also found that, in both genetically bred spontaneous hypertensive rat (SHR) and Goldblatts surgery-induced hypertensive rats (2K1C) (Goldblatt, 1934), AQP1 expression on rat aortic endothelial cells was 2-3 times higher than in the analogous cell of normotensive controls of the same rat strain (Toussaint, 2009). Nguyen's complementary functional study showed that the measured *Lp* of SHR and 2K1C hypertensive rat aorta was significantly higher than their normotensive littermates (Nguyen, 2008). These results strongly suggest that AQP1 plays an important role in the regulation of transcellular water flow in response to chronic hypertension by actively switching its AQP1 gene expression on and off (Toussaint, 2009).

$HgCl_2$ is a known AQP1 blocker and has been used extensively for its effect on water permeability of erythrocytes and renal tubules epithelial cells in response to a step change in extracellular osmolarity. Our group's goal was/is to see if endothelial AQP1 contribute to endothelial as well as overall aortic wall *Lp*. As a first test to see if AQP1 plays an active role in transendothelial water transport, our group began to investigate if low doses (so as to avoid toxicity) of this effective, if nonspecific, AQP1 blocker, reduce endothelial *Lp* significantly. Nguyen measured titrated sufficiently low doses of $HgCl_2$ (25μM concentration of $HgCl_2$, under a 10cm hydrostatic pressure) in monolayers of bovine aortic endothelial cells (BAECs) so as to avoid toxicity and used this concentration to show a 22.1±6% drop in water permeability (*Jv*), and thus in *Lp*, in treated vs. control BAEC monolayers (Nguyen, 2008). S. Russell using a bovine-specific siRNA custom-designed to knockdown AQP1 on BAECs, reported an average of

62.4±1.7% drop in monolayers *Jv*, while there is no significant difference in *Jv* for BAECs with either Lipofectamine (a lipid carrier) alone or Lipofectamine and scrambled siRNA (a fluorescent-tagged control RNA) to control. It seems that siRNA reagent was able to induce a much greater decrease in *Jv* while avoiding the cytotoxic side effect (Russell, 2008). To compliment these studies, Shou, in preliminary experiments, and later Nguyen, in comprehensive experiments, measured *Lp*(ΔP) under multiple transmural pressures in excised rat aorta, introduced $HgCl_2$ into its lumen, flushed, remeasured *Lp*(ΔP) at the same transmural pressures, and then either flushed with β-mercaptoethanol or denuded the vessel endothelium, and then again remeasured *Lp*(ΔP) at the same transmural pressures. Shou's pilot *Lp* experiments, using 10μm $HgCl_2$ and not using the β-mercaptoethanol, showed an *Lp* decrease throughout the entire range of ΔP, but mostly notably by 27.5% at 60 mmHg (Shou, 2005). Nguyen's studies, using a 5μm $HgCl_2$, showed that AQP1 blocking induced a significant decrease in *Lp* at 60mmHg by 32±4% (mean ±SEM), 11± 2% % at 100mmHg, and 5±3% at 140mmHg. This inhibitory effect was reversed by addition of β-mercaptoethanol (ME). *Lp* of denudated aorta showed no significant change due to $HgCl_2$ treatment, indicating that water transport happened mainly around the AQP1-rich medial SMCs, and not across them (Nguyen, 2008).

In order to explain the trends seen by Shou and Nguyen, we first noticed that the *Lp* values of the $HgCl_2$ aortas at 60 and 100 mmHg were nearly identical. Since, under normal $HgCl_2$-free conditions, the aortic SI is fully compressed at 100 mmHg and partially uncompressed at 60 mmHg, these data suggest that $HgCl_2$ treatment may in fact cause the SI to compress at the lower pressure. The rationale for this is that, by blocking

one of two parallel pathways for transendothelial water transport, $HgCl_2$ treatment lowers endothelial *Lp* and thereby shifts a lager portion of the total transmural pressure difference from the media to the endothelium. Thus the trans-endothelial pressure difference can reach the critical value needed for full SI compression at lower overall transmural pressure (ΔP). S. Joshi in our group has worked out a theoretical/ fluid mechanical theory demonstrating the plausibility of this idea to account for the observed effects. Abrams, Toussaint and Joshi are using the technique of Huang (Huang, Jan *et al.*, 1998) to try to directly observe this SI compression at lower pressure with $HgCl_2$ treatment. However, if $HgCl_2$ treatment causes SI compaction at pressures where the SI would otherwise not be fully compressed, this change in wall geometry should impact the spread of macromolecular tracers in the subendothelial space. Y. Sun used HRP, a tracer that has been widely used to study the transport property of large vessels such as aorta, to test this idea. Using Zeng's corrected version of Huang *et al.*'s theoretical model for water and macromolecular transport in the artery wall, Sun predicted a maximal difference in the growth of focal HRP spots between the aortas of rats treated with $HgCl_2$ and controls, with spots from the treated rat growing faster. Subsequent rat experiments confirmed this prediction (Sun, 2008).

Both our *in vitro* and *ex vivo* experiments have used $HgCl_2$ to demonstrate that the AQP1-mediated transcellular pathway contributes significantly to endothelial as well as whole aorta *Lp*. $HgCl_2$ impedes water conduction by covalently binding to cysteine 189 located near the entrance of the restricted region of the AQP1 water channel (Preston, Jung *et al.*, 1993). This action, however, is non-specific and, despite our extensive

controls showing reversibility and lack of toxicity, $HgCl_2$'s well-known cytotoxicity potential is likely to leave many unconvinced. Thus, what is solely missing to solidify this picture of AQP1's important role in transendothelial water transport is to show that AQP1 knockdown in the rat aortic endothelial cells of an excised vessel significantly reduces the *Lp* of that whole vessel relative to what it was on that vessel before knockdown. For an *in vitro* water permeability study, we proposed to use rat aortic endothelial cells (RAECs) so as to be consistent with our *ex vivo Lp* study. In a nutshell, that and the associated experiments on rat aortic endothelial cells *in vitro* constitute the basis of this thesis. In subsequent chapters we shall detail our successes in this effort.

Chapter 2 An *in vitro* water and solute permeability study of rat aortic endothelial cells (RAECs) with AQP1 siRNA knockdown

Abstract

Plasma, mostly water and solutes, advects low-density-lipoprotein (LDL) cholesterol across the arterial endothelium. Subendothelial LDL deposition triggers pre-atherogenic lesion formation. This water flux is believed to occur paracellularly. We investigate the potential significance to total transmural water flow of the transcellular pathway through the ubiquitous aquaporin-1 (AQP1) water channel protein. Rat aortic endothelial cell (RAECs) monolayers cultured on a porous polycarbonate substrate were used as an *in vitro* model to study water and solute transport properties. Water flux (*Jv*) was measured by a bubble tracking system under a hydrostatic pressure of 10-cm of water. Simultaneously solute permeability (*Pe* convection or *Po* diffusion) was observed by measurement of the amount of fluorescence-tagged solute flux (tetramethylrhodamine,TAMRA and tetramethyl-rhodamine-iso-thiocyanate (TRITC)-albumin) that crossed the monolayers either with or without the hydrostatic pressure differences. Our results demonstrate that AQP1 downregulation by small interference RNA (siRNA) induces a significant 56.4±8.2% decrease in RAEC monolayer *Jv* and permeability to water and small solutes *in vitro*. This large reduction is likely only partially due to the direct effects of the suppressing the transcellular AQP1 pathway. Suppression of this pathway also increases flow resistance, likely causing the transmural pressure to compress the cells against the rigid support and increase cell-cell junction

overlap. This would increase the flow resistance for the paracellular route and therefore accounts for a portion of the observed *Lp* reduction. A study of RAEC permeability to TAMRA and TRITC-albumin, solutes that traverse only the cell-cell junctions, provides evidence consistent with this interpretation. AQP1's suppression led to a 21.8±7.04% drop in TAMRA convective permeability and a 29.79.1±1.72% /25.69±8.19% drop in albumin permeability under convection/diffusion respectively, consistent with increased cell-cell overlap. Thus AQP1 contributes significantly, both directly and indirectly, to the hydraulic conductivity of endothelial cell monolayers. Regulated AQP1 expression might have the potential to affect lipid transport in a beneficial way with regard to disease progression.

Introduction

1. Endothelial monolayer's permeability to water and solutes

The vascular endothelia form a tight barrier to serve as a selective exchange surface where water and solute transport occur. The *in vitro* endothelial cell culture model has been extensively used to study many aspects of endothelial cell characteristics ranging from proliferation to biochemical responses to mechanical stresses. Tarbell *et al*. have developed an *in vitro* culture model of bovine aortic endothelial cells (BAECs) to examine water and solute flux across such monolayers grown on a porous transwell filters (Dull, Jo *et al.*, 1991). Both water flux and solute flux can be measured simultaneously under the condition of various hydrostatic pressures by lowering a pressure reservoir relative to the apparatus and by the application of various

concentrations of fluorescence-tagged macromolecules (i.e., albumin, LDL) to the solution on the luminal side of the monolayer (Cancel, Fitting *et al.*, 2007). Water flux is measured by tracking the displacement of a bubbled introduced into a precision-calibrated diameter tube in series with the abluminal chamber. A spectrophotometer tracks the motion of the bubble's leading meniscus and records it in a digital computer. The water flux *Jv* across the monolayer is calculated based on the following equation:

$$J_V = \frac{\Delta d}{\Delta t} \times \frac{F}{S_A}$$

$\frac{\Delta d}{\Delta t}$ (cm/s) is change in bubble position per unit of time, i.e., the bubble velocity, S_A (cm^2) is the surface area of cell culture insert and F (cm^2) is the surface area of the tubing underneath the spectrophotometer.

Solute flux is measured by detecting the fluorescent tracer's concentration in an abluminal chamber below the monolayers after the addition of such tracer on to the top (luminal) change above the monolayer. Solute flux permeability equals:

$$Pe = \left[\left(\Delta Ca / \Delta t \right) \times Va \right] / A \times Cp$$

$\Delta Ca / \Delta t$ (mol/L/sec) is the rate of change of the abluminal fllurophore concentration with time, *Va* (cm^3) is the volume of fluid at the abluminal chamber, *A* (cm^2) is the surface area of filter, *Cp* (mol/L) fluorphore concentration in the luminal chamber.

The major macromolecular and water transendothelial transport pathways are believed to be tight junction, breaks in tight junction strands and leaky junction. Tight junctions (TJs) zipper up neighboring endothelial cells and appear as a series of belts around cell-cell focal points, usually on the apical surface of the cells. TJs are composed of transmembrane proteins (occludin, claudins) linked to the actin cytoskeleton via cytoplasmic zonular occludens (ZO) proteins (Anderson, 2001). TJs provide a size-selective pathway for the passage of solute molecules smaller than 2nm. Breaks in the tight junction broaden the entrance of macromolecules to the size of 20nm for molecules such as albumin to pass through the underlying adherens junction. For much larger macromolecule such as LDL (22nm), only leaky junctions could accommodate its paracellular passage. As predicted by Weinbaum, these transient large pores are associated with rare cell turnover events (Weinbaum, 1985). For transport of macromolecules such as albumin and LDL, there is evidence in the literature that a vesicular pathway may also be involved in their transport across the monolayer through the invagination and internalization of of clathrin-coated pits (Tarbell, 2010).

Using the Tarbell group's apparatus, Cancel *et al.* measured the permeability of water, albumin and low-density-lipoprotein (LDL) to bovine aortic endothelial cell (BAEC) monolayers under convective and diffusive conditions. These experiments, together with certain assumptions and a three-pore model allowed them to calculate the contribution to the total water and macromolecule fluxes for each one of the above-mentioned pathways. The vesicular pathway (*Pore1, LDL and albumin transport*), breaks

in the tight junction (*Pore2, water and albumin transport*) and leaky junctions (*Pore3, for water, albumin and LDL transport*) are considered as the 3 pores, with the species they are assumed able to transport. *Pore2* and *Pore 3* allow both diffusive and convective transport. They calculated that breaks in the tight junction accounts for 77% of water transport, while leaky junctions carry most (90%) of the LDL 40% of the albumin and 23% of the water transport. They found that the vesicular endocytotic pathway is not a major contributor for LDL transport, since it accounts for less than 10% of LDL permeability (Cancel, Fitting *et al.*, 2007).

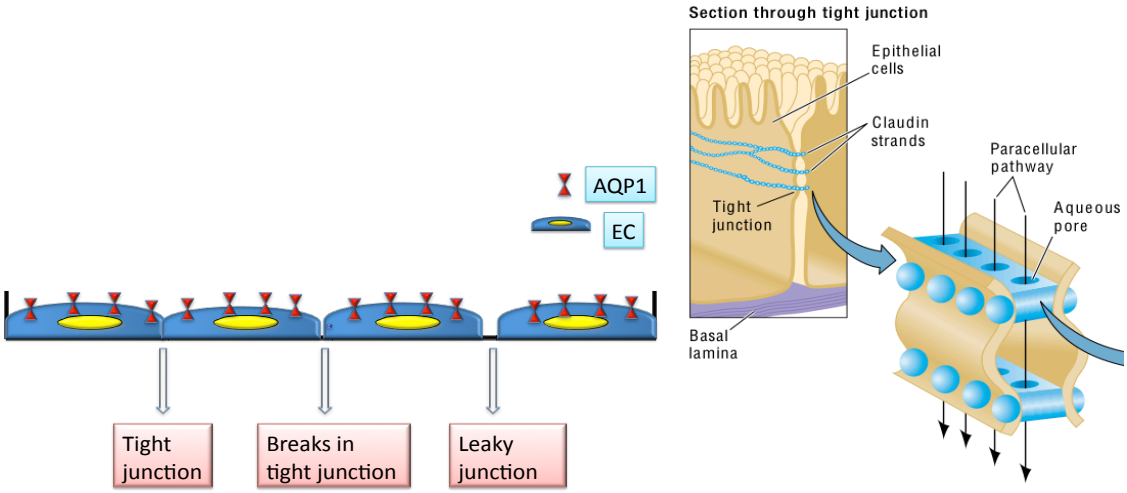

Figure 2.1: Left: a cartoon representation of what Cancel *et al*. take to be the major transport pathways across an endothelial cell (EC) monolayer: vesicles, breaks in tight junctions, leaky junctions. We shall invoke a fourth pathway, the AQP1 water channel protein for transcellular water transport. Right: a cartoon of tight junction complex showing claudin strands, which provide selective aqueous pores(Van Itallie e Anderson, 2004).

2. The sealing effect

An interesting phenomenon that endothelial cells monolayers exhibit is the so-called "sealing effect." After application of a transmural pressure gradient, an endothelial

monolayer that had been cultured with no transmural pressure responds by a sudden increase in its permeability to water and solutes. However, after a period of tens of minutes to an hour, the permeability gradually attenuates until eventually reaching a steady state. This is a natural biological response of cells to an increase in hydrostatic pressure under pathological situation such as edema (Turner, 1992). This temporarily increased permeability can be explained by the dynamic breakdown and reassembly of tight junctions via the recruitment of intracellular stores of ZO-occludin to the junctions (Demaio, Tarbell *et al.*, 2004).

S. Russell of our group has formulated a protein diffusion model of this sealing effect. In response to an application of hydrostatic pressure and subsequent increase in water flow through breaks in the tight junctions, junctional proteins, which are initially evenly distributed on the inside of the endothelial cells, diffuse towards the tight junctions located at the cell-cell borders. These additional junctional proteins help to close the breaks in the junctions. The model generates biologically meaningful parameters including (1) the protein diffusivity inside the cell, which governs the rate at which ZO and other proteins migrate to the remodeling junction. The diffusivity can be used to evaluate the validity of endothelial water transport data; (2) *Jv*, the steady state water flux; and (3) the sealing potential, a measure of the maximum magnitude that flow can attenuate (Russell, Cancel *et al.*, 2009). Figure 2.2 shows a typical water flux as a function of time across a monolayer of cultured rat aortic endothelial cells under a hydrostatic pressure of 10cm of water. The water flux is initially high at around 36×10^{-6} cm/s. It tapers down to nearly $6\text{-}7\times10^{-6}$cm/s after an hour.

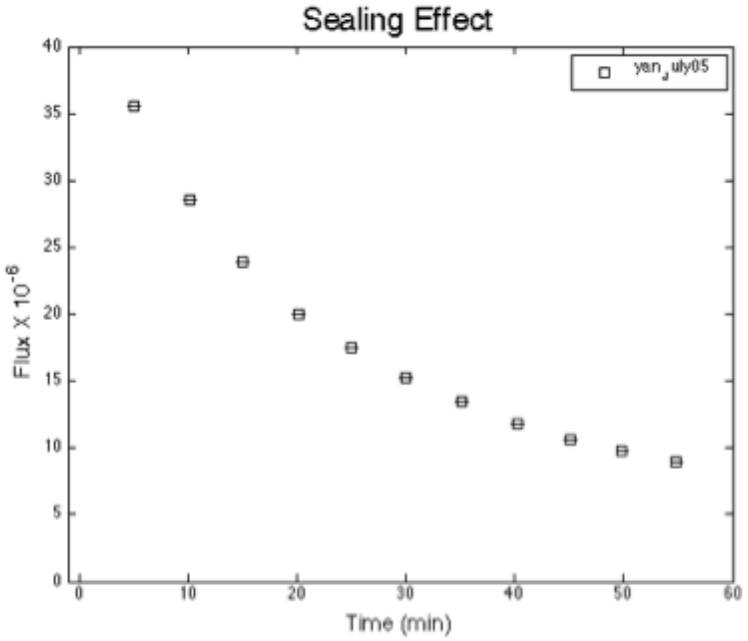

Figure 2.2: A sealing effect curve generated by a protein diffusion mathematical model of S. Russell (Russell, Cancel *et al.*, 2009).

This sealing effect has also been observed in a whole vessel whose pressure was raised precipitously. Upon introducing a sustained step change towards in pressure, there is dynamic change in *Lp* in intact microvessels from rat mesentery. *Lp* was initially increased by an amount proportional to the pressure step change, but later attenuated via the production of nitric oxides (Kim, Harris *et al.*, 2005).

3. The effect of the chemical blocker mercuric chlorides on in vitro water permeability

The AQP family of constitutively active transmembrane channel proteins that are water-selective pores and facilitate high water transport across cell membranes in response to osmotic gradients. Each monomer within the aquaporin tetramer provides an

independent and biologically active aqueous pore that allows for the single-file passage of water molecules through it. AQP1was also found to strongly stain the apical and basolateral membranes of the continuous capillaries of various tissues, including cardiac, skeletal and smooth muscles and the mammary glands. It has been suggested that the water-permeable endothelium in continuous capillaries are responsible for the water balance between the plasma and interstitial fluid compartments (Nielsen, Smith, Christensen e Agre, 1993).

Mercuric chloride is a known aquaporin blocker; it may inhibit water permeability by simple occlusion of the water molecule's passage through the aquaporin's pore via covalently binding to the free sulfhydryl residue of cysteine 189 (Cys189) near the entrance of the narrow pore region (Preston, Jung *et al.*, 1993). X-ray crystallography study of a bacterial homologue, aquaporinZ, mutant revealed no conformational change with $HgCl_2$ binding (Savage e Stroud, 2007). A decrease in water permeability upon mercuric compounds treatment was demonstrated in RBCs (Macey e Farmer, 1970), renal proximal tubule epithelium (Whittembury, Carpi-Medina *et al.*, 1984) and in a variety of cell types such as lung alveolar epithelia (Folkesson, Matthay *et al.*, 1994).

All of these studies were performed in the presence of an osmotic gradient, rather than a hydrostatic pressure difference. T. Nguyen of our group treated cultured BAEC monolayers with $HgCl_2$, Since $HgCl_2$ is well-known to be cytotoxic at high enough concentrations and exposure times, she first titrated a dosage/exposure that did not result in propidium iodide entering the cell cytoplasm, a marker of cell death. With this 25μM

concentration of $HgCl_2$ Nguyen reported an average of 22.1±6% (n=4) drop in water permeability (*Jv*) of treated BAECs as compared with control BAEC monolayers upon exposure to a 10cm hydrostatic pressure difference. The treated and control monolayers were otherwise identically treated as matched pairs (Nguyen, 2008).

Small interfering RNAs (siRNA) are a group of 15–25 base-pair long, double-stranded RNA molecules. They can be generated endogenously through fragmentation of precursor dsRNA or introduced as chemically synthesized oligonucleotides. When in cells, they are closely associated with an RNA-induced silencing complex (RISC) which facilitates the destruction of target complementary messenger RNA (mRNA) in a process called short interfering RNA (siRNA) (Fire, Xu et al., 1998). Using bovine-specific siRNA custom-designed to knockdown AQP1 on BAECs, S. Russell reported an average of 62.4±1.7% drop in monolayers *Jv* from (7.08±0.27 to 2.59±0.18×10^{-6} cm/s n=3), while there is no significant difference in *Jv* for BAECs with either Lipofectamine (a lipid carrier) alone (6.19±0.42×10^{-6} cm/s) or Lipofectamine and scrambled siRNA (a fluorescent-tagged control RNA) (5.64±0.34×10^{-6} cm/s) to control. This drop in *Jv* is much larger than that observed upon treatment with $HgCl_2$, likely the result of the low $HgCl_2$ concentration needed to avoid toxicity. According to a calibration in Verkman (Yang, Kim *et al.*, 2006), this concentration likely blocked only about 30% of aquaporins on BAECs. The siRNA reagent is much less cytotoxic and quantitative immunohistochemistry indicated that it achieved 50% knockdown, whereas our Western blot protein analysis indicated a 70.3% knockdown with these siRNAs (n=4, using NIH ImageJ) (Russell, 2008).

4. Aquaporins and cell volume regulation

Cells are filled with and surrounded by water and separated from their neighboring environment by a plasma membrane. In response to a small osmotic change, a cell can drastically change its volume by an immediate loss or gain of water in order to reach an osmotic equilibrium. This change in volume, however, is undesirable for a cell since a constant cell volume is critical to cell viability and functions; such as proliferation and apoptosis, cellular signal transduction, metabolism and gene regulation (Desjardins e Macmanus, 1995).

Swollen and shrinking cells, however, are able to restore their normal volume subsequent to an extracellular tonicity challenge by either regulatory volume decrease (RVD) or by regulatory volume increase (RVI), depending on the challenge. As cells sense their volume changes through mechanisms such as cytoskeleton disruption or intracellular ion concentration, they can activate membrane transport pathways to import or export small inorganic ions (such as sodium, potassium and chlorides) via membrane transporters such as Na^+-K^+-ATPase pumps or Na^+-H^+ exchangers, or to change their concentration of small organic solutes (called osmolytes, including polyols, animo acids and methylamines) by cellular uptake or by generation (Mcmanus, Churchwell *et al.*, 1995).

It takes a cell less than a minute, sometimes only seconds, to reach an osmotic equilibrium, but a much longer time (many minutes) to regulate its volume change. It is possible to speculate that water permeability through aquaporin channels plays a role in this volume regulation. AQP5-/- mice have shown decreased acinar membrane water permeability and a close to 60% decrease in RVD (volume recovery) in response to a hypotonic shock, suggesting that AQP5-mediated water flux is important in regulating cell volume (Krane, Melvin *et al.*, 2001). Similarly, following a hypotonic challenge, cultured corneal endothelial cell of AQP1-/- mice exhibit significantly impaired volume restoration (Kuang, Yiming *et al.*, 2004). The mechanism by which aquaporins are involved in volume regulation needs further investigation in such studies and their interaction with primary ion and solute transporters must be considered (Verkman, 2005).

Mercury treatment can lead to cell swelling and impaired normal regulation, which accounts for its cytotoxicity. It is possible that mercury might disrupt membrane transporter proteins that are responsible for ion and solutes exchange, resulting in an inability of the cell to effectively regulate its volume. An almost abolished RVD in skate hepatocytes after mercury treatment was observed in skate hepatocytes. Mercury-induced sodium influx and impaired function of ATP-dependent osmolyte channels, but not Na^+-K^+-ATPase, seem to be responsible for this failed volume recovery (Ballatori e Boyer, 1996). Sarkadi and coworkers have also demonstrated impaired normal volume regulation in lymphocytes after mercury treatment, they argued that this impairment may be due to an inhibited K^+-Cl^+ transport (Sarkadi, Cheung *et al.*, 1985).

5. The hypothesis of this chapter's work

We have previously presented data that bovine aortic endothelial cells (BAECs) and rat aortic endothelial cells in the whole aorta express aquaporin water channel proteins. Blocking aquaporins by chemical blocker $HgCl_2$ and biologically active small interference RNA can significantly reduce pressure-driven water flow in *in vitro* BAECs monolayer. To dissect more precisely the contribution of aquaporins transcellular pathway to the total transendothelial water flow and to make these studies species-consistent with our *ex vivo* whole vessel hydraulic conductivity measurements (see Chapter 3 and 4), we use siRNA reagent to knock down rat AQP1 in rat aortic endothelial cells (RAECs), and measure water and small solute flux of knocked down and of control monolayers. Since small solutes, such as TAMRA and albumin cannot traverse aquaporins but only the inter-endothelial junctions, their permeability can be used to gauge whether inhibiting trans-aquaporin-1 water flow could indirectly affect junctional transport. Thus, a portion of the observed siRNA-induced reduction in water flux might be due to the overlapping/increased complexity of the cell-cell junctions.

Materials and methods

1. Immunohistochemistry

Rat aortic endothelial cells (RAEC) (*VEC* Technologies (Rensselaer, NY)) were plated from passage 4 to passage 7 either on slides or in Transwell filters, 0.4μm pore size (Corning 3460) pretreated with fibronectin for one hour, or in a 24-well plate

(Corning 3548) at a seeding density from 1/8 to ½ confluence (16 to 64×10^3cells/cm^2). Cell doubling time was determined to be approximately 36 hours. The experimental preparation was cultured to confluence plus one day in minimum essential medial with 1% Pen/Strep, 1% L-glutamine and 10% fetal bovine serum, in a cell culture incubator, 5% carbon dioxide, 37°C, in the dark. RAECs plated on slides were fixed in 1% paraformaldehyde for 15 minutes, permeabilized with saponin solution for 20 min, followed by an incubation in blocking solution (15% goat serum, 0.3%Triton-X, 20mM sodium phosphate, 0.9mM sodium chloride) for 30 minutes. Rabbit anti-rat AQP1 antibody (AQP11-A, Alpha Diagnostic International, san Antonio, TX) diluted in PBS with 3% goat serum, 0.2% bovine serum albumin (Sigma) to a final concentration of 10μg/ml was applied at 4°C overnight. Alexa 488 conjugated goat anti-rabbit IgG antibody (Molecular Probes, Carlsbad, CA) at a dilution of 1:500 in PBS was applied for 90 minutes at room temperature. Anti-fade DAPI nuclear stain (Invitrogen) was applied before confocal imaging.

2. siRNA transfection

siRNA was designed and utilized to selectively target AQP1. (Dharmacon, Lafayette, CO) Target A: sense: CCAGCGAGUUCAAGAAGAAUU, antisense: UUCUUCUUGAACUCGCUGGUU; Tareget B: sense: GCGGUCAGGUGGAGGAGUAUU, antisense: UACUCCUCCACCUGACCGCUU. siRNA was designed to be specific for rat AQP1 (Invitrogen): Target 1 (AQP1-RSS351943) anti-sense: CACACUUUGGGCCAGAGUAGCGAUG; Target 2 (AQP1-RSS351944) anti-sense AUACAUGACAGCCCGGAGGAUGCUG; Target 3 (AQP1-

RSS351945) anti-sense: AAGAGCUUCUUCUUGAUUUCGCUGG. Non-targeting oligonucleotide (siGLO, Thermo Fisher Scientific) tagged with a fluorescent indicator allowed for visual detection and assessment of transfection efficiency. siRNA transfection was performed based on Michel's optimized BAEC transfection protocol (Gonzalez, Nagiel *et al.*, 2004). Briefly, upon 70% confluency, BAECs/RAECs were transfected with siRNA reagent by a lipid carrier: Lipofectamine 2000 in reduced serum media (OPTI-MEM). OPTI-MEM was removed 6-8 hour after transfection reagent incubation. Cells were analyzed after 48 hours after transfection either by Western blot or by PCR.

3. siRNA reagent concentration optimization

AQP1 siRNA reagent would be cytotoxic at high concentration since completely abolishing aquaproins are likely to induce injury or even death to cells. Since water permeability measurement is extremely sensitive to the integrity of the monolayer, we performed a series of optimization experiments by using various siRNA concentrations of 10, 20, 40, 80pmol per 1.5×10^5 cells BAECs/RAECs until maximal values of both of percentage protein knockdown as well as a minimal value of water flux were obtained. Monolayers incubated with siRNA reagent for over 20pmol showed compromised monolayer examining from light microscopy. This was consistent with the observed increase in J_v for these monolayers.

4. In vitro water and solute permeability apparatus

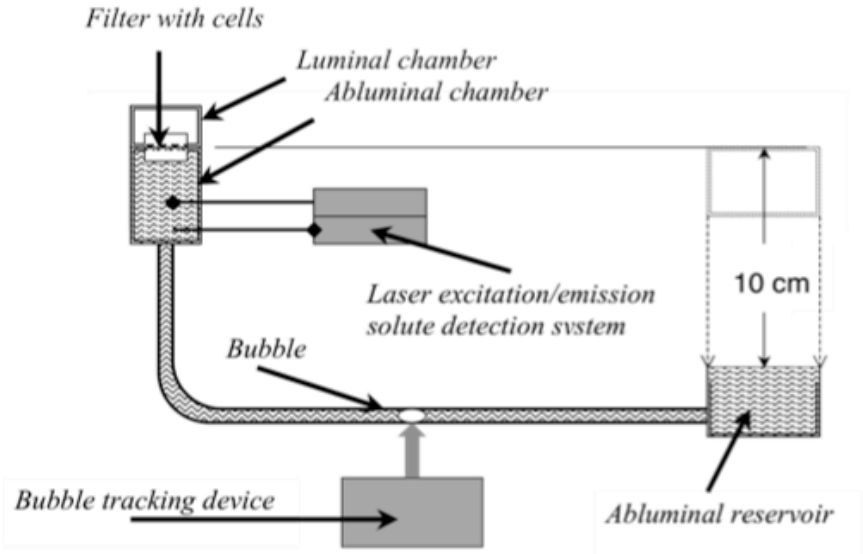

Figure 2.3: *Jv* measurement set-up, graph adapted from (Russell, 2008), see text.

The experimental set-up, the same as used by the Tarbell group, is housed in a Plexiglass box with a temperature control of 37°C. Rat aortic endothelial cells (RAEC) grown on Transwell filters (surface area=1.1cm^2, 12mm in diameter, 0.4μm pore size) 1-2 days post-confluence with or without siRNA treatment were situated in an aluminum support ring and an O-ring to create a tight seal. This complex is then inserted into the black ethylene tetraphthalate (PET) chamber, thus dividing it into a luminal (top) and an abluminal (bottom) compartment. The luminal chamber is continuously supplied with 5% CO_2. The bottom chamber is connected via Tygon tubings to a borosilicate glass tube followed, via more Tygon tubing by a fluid reservoir. This reservoir can be lowered to apply a 10cm hydraulic pressure across the monolayer. The water flux (*Jv*) was measured based on tracking the position of the front meniscus of a bubble in the precision diameter borosilicate tube over time. The steady state *Lp* was determined (from Jv_∞)

using a non-linear predictive curve-fitting algorithm as described previously (Russell, 2008; Russell, Cancel *et al.*, 2009)

The same chamber was also custom-fabricated to detect fluorescence intensity in the abluminal compartment so that solute and water flux can be measured simultaneously. Light is excited at 534.5nm by a uniphase helium-argon laser excitation machine (Manteca, CA) and transmitted through optic-fibers to each chamber. A photomuliplier detects the emission signals generated by the dissolved fluorophores via a separate optic-fiber oriented 90° to the excitation fiber. Data were collected by FluroMeasure program. At the beginning of the experiment, the fluorophores carboxytetramethylrhodamine (TAMRA) and tetramethyl-rhodamine-iso-thiocyanate (TRITC)-labeled-albumin (6nm) (Invitrogen) were added to the luminal chamber above the monolayer. After a 60-minute equilibration period under diffusive condition, the differential 10cm hydrostatic pressure was applied across the monolayer and fluorescence intensity was recorded for two hours. The pressure difference was then eliminated and fluorescence data was collected for one additional hour to indicate the passage of solutes by diffusion. Calibration curves were acquired on the same device so as to allow for the conversion of fluorescence intensity to fluorophore concentration.

Solute measurement follows the following equations: Solute permeability equals:

$$Pe = \left[\left(\Delta Ca / \Delta t \right) \times Va \right] / A \times Cp$$

$\Delta Ca/\Delta t$ is the time rate of change of the abluminal fluorophore concentration, *Va* is the volume of fluid at the abluminal chamber, *A* is the surface area of the filter, *Cp* is the fluorophore concentration at the luminal chamber, which is assumed time-independent. This formula assumes that *Cp* remains much larger than the fluorophore concentration in the abluminal compartment over the entire duration of the experiment.

5. Western Blot analysis

BAECs/RAECs were grown to confluence and lysed with ice-cold RIPA buffer (150mM NaCl, 25mM Tris pH 7.6, 1% NP-40, 1% deoxycholate, 0.1% SDS) containing protease inhibitor cocktails (Roche Diagnostics) for 20 minutes, followed by sonication for 10 seconds. Protein concentration was determined by Bradford's method (Caymen protein determination kit, Caymen Chemical Co., Ann Arbor, MI). An appropriate amount of protein sample was subjected to digestion with PNGase F (New England Biolabs, Ipswich, MA). 20μg protein/well was loaded after incubating with sample buffer for 10 minutes at 60°C and separated on a 12% SDS-polyacrylamide gel. The proteins were transferred to PVDF membranes and blocked with 5% non-fat dry milk in 1X Tris-buffered saline Tween-20 (TBS-T) for 1 hour. Immunoblot was performed using rabbit anti-rat AQP1 polyclonal antibody at a 1:1000 dilution (AQP11-A, Alpha Diagnostics, San Antonio, TX) at 4 °C overnight and horseradish-conjugated donkey anti-rabbit secondary antibody at a dilution of 1:4000 for 1 hour at room temperature (Amersham, Arlington Heights, IL). Immunoreactivity was visualized using an enhanced chemoluminescence kit (Amersham, Arlington Heights, IL). The membrane was reprobed with β-actin antibody as a loading control. Densitometry was determined using

Image J. AQP1 blocking peptides, (AQP11-P, Alpha Diagnostics, San Antonio, TX), designed to disrupt antigen-antibody binding in the immunoblotting, were used for AQP1 antibody blocking control.

6. Polymerase Chain Reaction (PCR)

RNA was extracted from RAECs using Trizol reagent and RNeasy Mini kit according to the manufacturer's protocol (Qiagen). RNase inhibitor was added (NewEngland Biolabs). cDNA was synthesized by reverse transcription using oligo(dT) primer and M-MLV reverse transcriptase (NewEngland Biolabs). PCR was performed and the PCR product was separated by 2.5% agarose gel with ethidium bromide and detected with ultraviolet light (UV). RT-qPCR amplification was carried out using ABI PRISM 7000 sequence detection system (Applied Biosystems). A reaction mixture of 25μl total volume was prepared by adding the following ingredients: 2X SYBR green fluorescein mix (Thermo Fisher Scientific), 70nm primers, 250ng cDNA templates. There was an initial denaturation step of 5 minutes at 95°C, which was followed by 50 cycles of 30 seconds at 94°C, 30 seconds at 55°C and 30 seconds at 78°C. A negative nontemplate control was used. Following each PCR, a dissociation curve analysis was used to assess the specificity of product amplification.

Table 2.1: Primer sequences selected for RT-PCR and RT-qPCR

Target gene	Primer sequence	Reference
AQP1-1 NM-012778	F: 125-144 CCCTCTTCGTCTTCATCAGC R: 543-562 CTGAGCCACCTAAGTCTCGG	(Dolman, Drndarski *et al.*, 2005)
von Willebrand factor (vWF) XM-342759	F: 4296-4316 GCAGTCAGTTGGCCTCTACCA R: 4366-4346 ACGGTCAATTTTGCCAAA GATC	Custom-designed
GAPDH NM_017008	F: 372-390 5'TCTTCACCACCATGGAGAA-3' R: 603-585 5'ACTGTGGTCATGAGCCCTT-3'	(Shi, Ji *et al.*, 2010)
Smoothelin NM_001013049.2	F: TCGGAGTGCTGGTGAATAC R: CCCTGTTTCTCTTCCTCTGG	(Rensen, Niessen *et al.*, 2006)

Results

1. AQP1 immunohistochemistry on RAEC monolayer

Figure 2.4 is a confocal section through RAEC monolayer. It shows the immunolocalization of AQP1 (green) on RAECs. Alexa488 fluorescence green staining indicates the presence of AQP1 antibody in the cytoplasm. There is very localized and intense staining especially around the nuclei (stained with nuclear stain DAPI). This constitutes evidence that AQP1 is present in rat aortic endothelial cells.

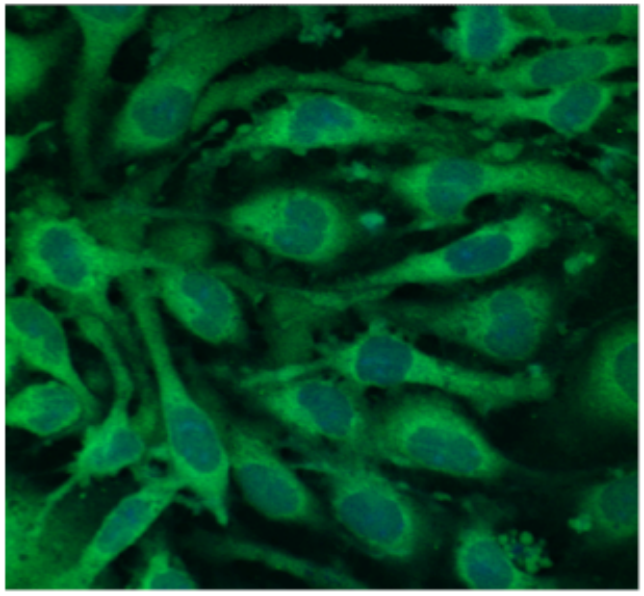

Figure 2.4: Confocal slice through RAEC monolayer showing AQP1 immunohistochemistry staining of RAECs monolayers *en face*. RAECs are stained with rabbit-anti-rat AQP1 primary antibody and goat-anti-rabbit Alexa-488 conjugated secondary antibody. The nuclei are counterstained with DAPI nuclear stain. AQP1 are expressed both in the cytoplasm and on the membrane. The staining is more concentrated around the nuclei (magnification: 400X).

2. In vitro water flux (Jv) measurement on RAECs monolayers transfected with siRNA directly against AQP1 vs. control

Figure 2.5 presents measurements of the water flux (*Jv*) through RAECs monolayer treated with three different *siRNAs* (Target1, Target2 and Target3, each at 20pmol) targeting different regions in the AQP1 mRNA sequence. Aquaporins is crucial to maintaining the cell's osmotic balance and subsequent cell death would damage the integrity of the formed monolayers. Figure 2.5 shows no significant difference between control (no treatment) ($5.03\pm0.57\times10^{-6}$ cm/s) and lipofectamine controls ($4.63 \pm 0.7\times10^{-6}$ cm/s) and scrambled siRNA control ($5.13\pm0.80\times10^{-6}$ cm/s) in terms of *Jv* measurements. However, Target 3 ($3.23\pm1.04\times10^{-6}$ cm/s) shows a significant reduction of 30.3% in *Jv*

compared with control (p=0.003), while Target 1 ($13.61\pm4.69\times10^{-6}$ cm/s) and 2 ($6.95\pm0.95\times10^{-6}$ cm/s) show either shows an increase or no change in *Jv* (n=3, average±standard deviation). After each experiment, the filters were viewed to assess monolayer integrity.

We started our transfection experiments using manufacturer's suggested concentrations for *siRNA* reagent. Since aquaporins are pivotal to cell viability, extensive knockdown might impair the cell's ability to regulate its osmotic balance. This could potentially lead to cell death and, consequently, to compromise monolayer integrity and sharply elevated *Jv* values. Clearly, one would like to accomplish knockdown by using as little *siRNA* reagent as possible while maintaining a tight monolayer configuration and a maximal reduction in *Jv*. Thus we performed a series of optimization experiments using *siRNA* concentrations ranging from 10, 20, 40 to 80pmol/1.5×10^{5} RAECs. See Figure 2.6. Monolayers incubated with >20pmol *siRNA* reagent yielded compromised monolayers, as seen under light microscopy. This was consistent with increased *Jv* values for these monolayers. When using Target3, *siRNA* at a concentration of 10pmol, *Jv* was reduced most significantly from $5.03\pm 0.57\times10^{-6}$ cm/s to $2.19 \pm 0.53\times10^{-6}$ cm/s, a drop of 56.4±8.2% (p=1.9E-7, n=7).

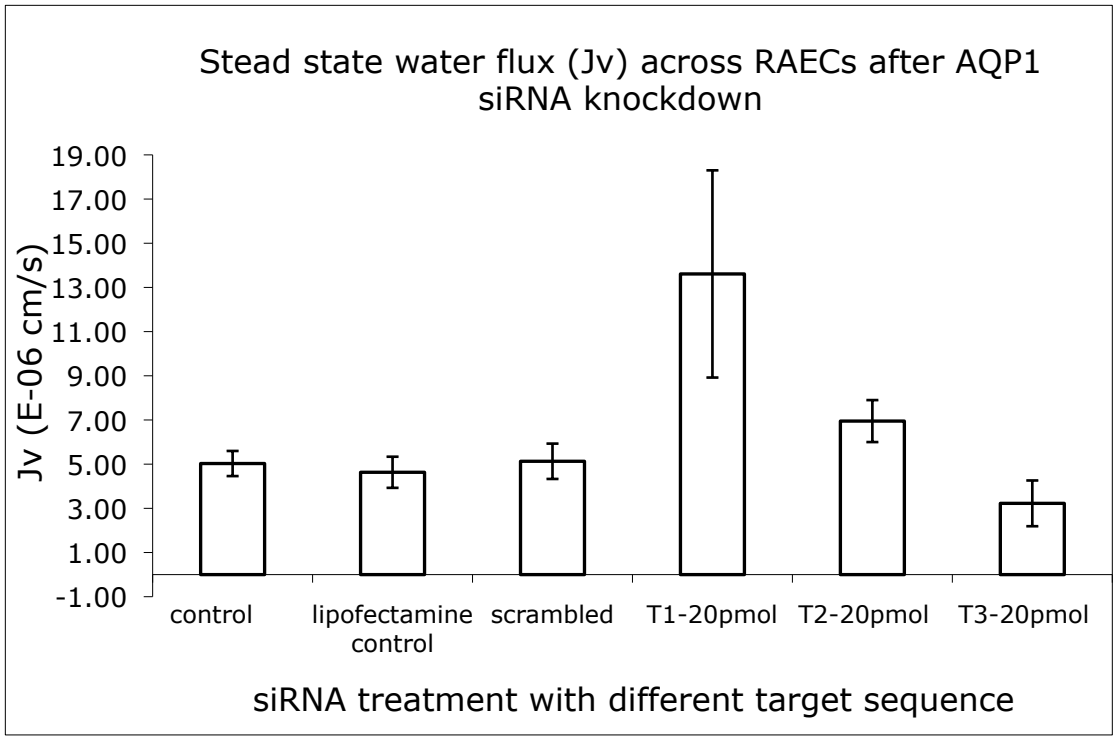

Figure 2.5: The water flux (*Jv*) measurement of RAECs transfected with three custom-designed siRNA target against AQP1. RAECs transfected with Target 3 shows a significant reduction in *Jv* by 30.3% comparing with control, while Target 1 and 2 shows either shows no change or an increase in *Jv*. (n=3, average±standard deviation)

Table 2.2: *Jv* of RAECs transfected at 4 different concentrations of siRNA against AQP1

	0	10pmol	20pmol	40pmol	80pmol
Jv (cm/s)	5.03± 0.57 ×10^{-6}	2.19 ± 0.53 ×10^{-6}	3.23±1.04 ×10^{-6}	6.98±0.17 ×10^{-6}	7.77±1.26 ×10^{-6}

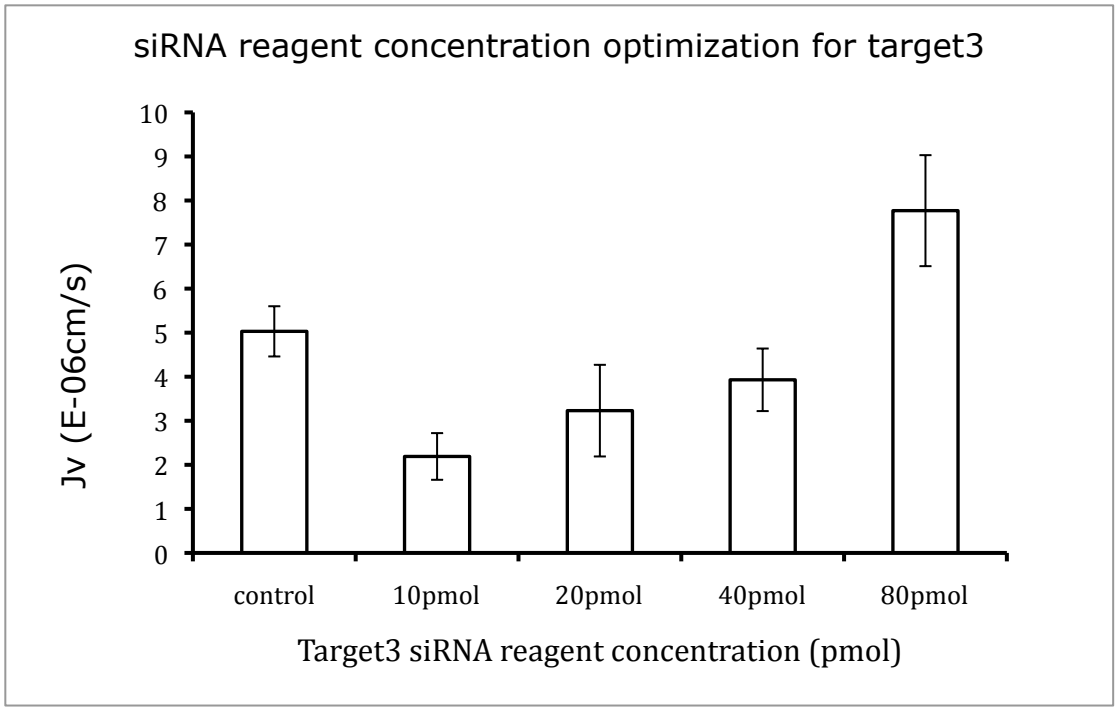

Figure 2.6: The siRNA concentration optimization of Target 3, 10pmol of Target 3 induces a significant drop in *Jv* by 56.4% (n=3, average± standard deviation)

3. Measurement of solute permeability across RAECs

Figure 2.6 shows that aquaporin suppression with 10pmol of target 3 siRNA reduces *Jv* by nearly 56%. RAEC monolayer permeability to the small solutes: tetramethylrhodamine (TAMRA, 1nm in diameter) and tetramethyl-rhodamine-iso-thiocyanate (TRITC)-labeled-albumin (6nm in diameter) under diffusive and pressurized conditions would provide an interesting insight into the true fraction of the direct and indirect contributions of AQP1 knockdown to the reduction of trans-monolayer water flow, since these solutes traverse only the junctions and not the AQP1s. We begin the experiments by applying these tracers in the luminal chamber for 1 hour under diffusive condition; apply a hydrostatic pressure of 10cm water for 2 hours (advective and

diffusive transport); remove the pressure difference and continue to collect data collected (on diffusive transport) for one additional hour. Advective permeability (*Pe*) was calculated based on the second hour of pressure-driven data upon, after cell monolayer's sealing effect had reached steady state. The diffusive permeability (*Po*) was calculated from the final hour of diffusive transport data.

TAMRA, 1nm in diameter, is small enough to pass through the tight junctions. Figure 2.7 shows that the siRNA-transfected group shown a 21.8±7.04% ($p=0.0036$, $n=2$ sets of control and transfected filters measured on the same day, mean±SEM) reduction in TAMRA permeability under convective condition, with no significant difference between the two conditions. This indicates that TAMRA diffusion (through normal junctions, breaks in the tight junctions and through leaky junctions) is far faster than its advection, i.e., its Peclet number is small, due to TAMRA's small size. While albumin, 6nm in diameter, cannot cross the monolayer's tight junctions, it can traverse the breaks in the tight junction as well as the leaky junctions. Figure 2.8 shows that siRNA-transfected RAECs have 29.79±1.72% and 25.69±8.19% ($p=0.008$/$p=0.04$, $n=3$ sets of control and transfected filters measured on the same day, mean±SEM) reductions of albumin permeability by convection and diffusion, respectively, as compared with control group. This indicates order one Peclet numbers, i.e., advection and diffusion of the same order, for albumin. After each experiment, filters were viewed for integrity as above.

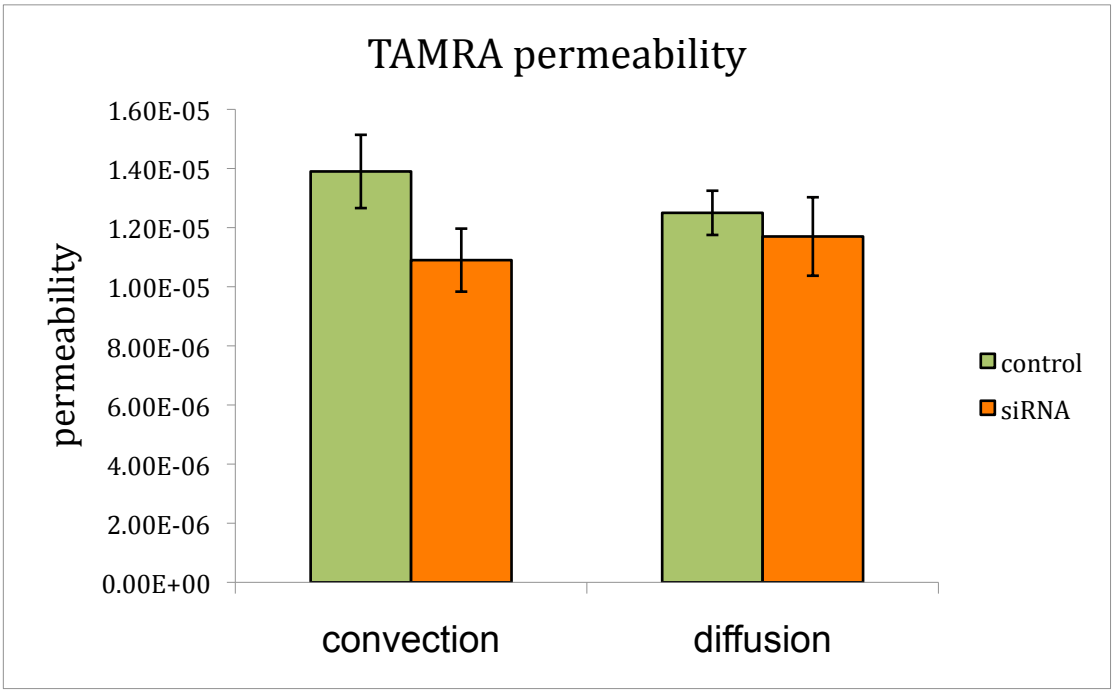

Figure 2.7: TAMRA's convective and diffusive permeability of control and siRNA transfected RAEC monolayers (n=8).

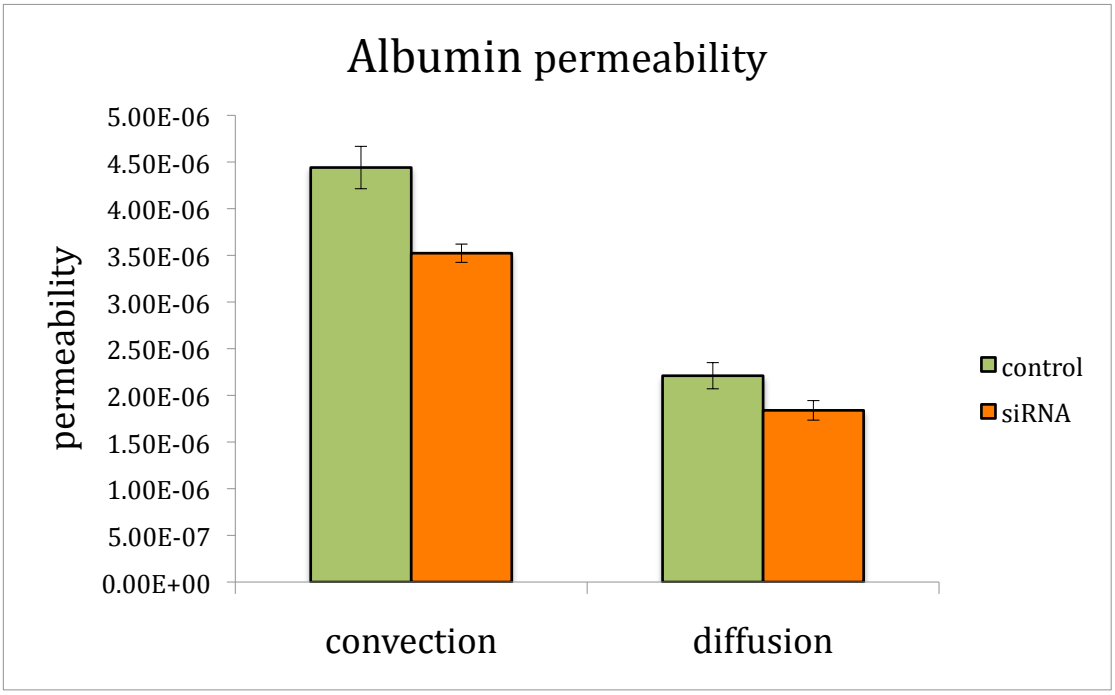

Figure 2.8: Albumin's convective and diffusive permeability of control (n=13) and siRNA transfected RAEC monolayers (n=9).

Table 2.3: Summary of the result for solute permeability experiment

	Po (Diffusion)	*Pe* (Convection)
Control TAMRA	1.25 ± 0.21E-05 (n=8)	1.39 ± 0.35E-05 (n=8)
siRNA TAMRA	1.17 ± 0.38E-05 (n=8)	1.09 ± 0.30E-05 (n=8)
Control Albumin	2.04 ± 0.40E-06 (n=13)	3.74 ± 0.78E-06 (n=13)
siRNA Albumin	1.70 ± 0.39E-06 (n=9)	2.76 ± 0.73E-06 (n=9)

4. Western Blot analysis of protein expression

Using a bovine-specific custom-designed AQP1 siRNA, S. Russell reported an average of 64% drop in *Jv* in BAECs monolayers (S. Russell, 2008). Western blot analysis (Figure 2.9) confirms that siRNA can induce an AQP1 protein knockdown by 70.3% on BAECs (n = 4).

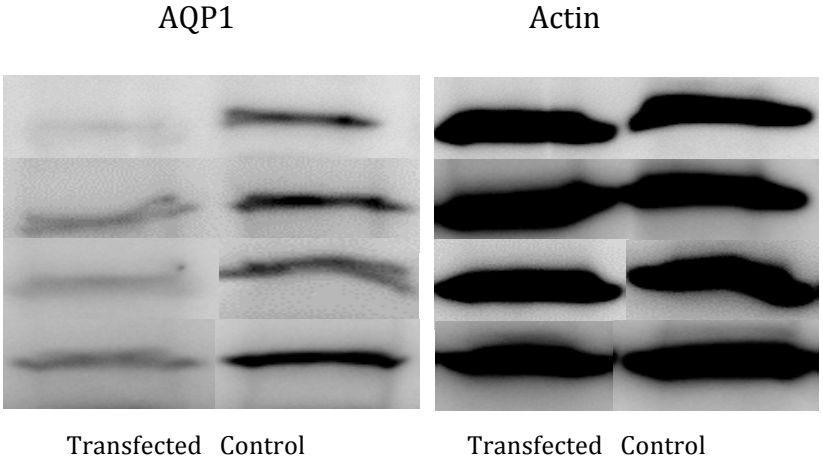

Figure 2.9: Western blots demonstrates an AQP1 knockdown of 70.3% (n=4; $p<0.001$ in BAECs; using NIH ImageJ) relative to vector control.

RAECs cell lysates with and without siRNA reagents were immunoblotted with AQP1 polyclonal antibody. Densitometry analysis using Quantity One software (Biorad, Hercules, CA) shows a 67.9% reduction in protein expression when cells were treated with 10pmol of siRNA reagent compared to the control groups, while there was no difference between control and lipofectamine control (for each concentration n=4, for control n=3, for lipofectamine control n=3), see Figure 2.10.

In our experiments, we found it is very difficult to detect the classic 28kDa band of AQP1 without deglycosylating the protein sample. However, deglycosylation renders AQP1 monomers more prone to aggregation into multimers in the presence of SDS. We incubated with sample buffer for 10 minutes at 60°C (personal communication with Dr. Alfred Van Hoek) to reduce multimer formation before analyzing protein sample by SDS electrophoresis and Western blotting. The anti-AQP1 antibody recognizes multiple bands on the blot, including the 28kDa band, as well as dimer (56kDa), trimer and tetramer bands, both in the transfected and the control RAECs. The 28kDa band represents the unglycosylated monomer protein and the uppers bands are considered as multimers. Incubation with AQP1 blocking peptides, which is a 19 amino acid peptide from rat AQP1 used to neutralize the antibody (AQP11-P, Alpha Diagnostics, San Antonio, Texas), completely abolishes the observed banding pattern on the blot.

Normalized by actin, the single 28kDa band was analyzed by densitometry. This band did not vary significantly between siRNA transfected and control cells either at 10pmol ($p=0.15$) or 20pmol ($p=0.4$) siRNA concentrations. However, the dimer 56kDa

band showed a significant decrease of 67.9% with 10pmol (p=0.001) and 41.0% with 20pmol (p=0.02) siRNA reagents. When combining 28kDa and 56kDa band together for densitometry analysis, there is a 59.2% decrease (p=0.00084) with 10pmol and 43.7% decrease with 20pmol (p=0.001) siRNA reagents. The decrease in AQP1 expression was especially significant in the 56kDa band. The higher multimers don't show any significant difference between transfected and control groups.

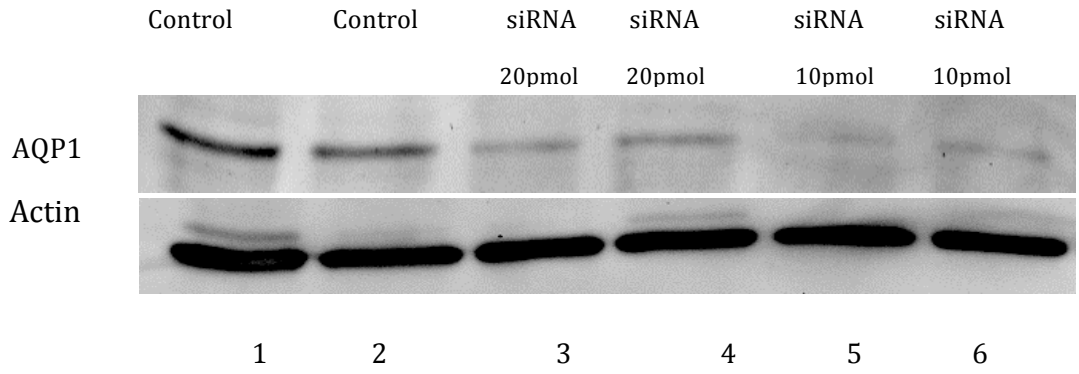

Figure 2.10: Western blot analysis shows the downregulatory effect of rat-specific AQP1 siRNA on RAEC AQP1 protein expression. Lane 1: control without siRNA treatment; Lane 2: control with lipofectamine but no siRNA treatment; Lane 3 and 4: duplicates of 20pmol siRNA treatment; Lane 5 and 6: duplicates of cells treated with 10pmol of siRNA.

5. Reverse Transcription and Quantitative Real Time-Polymerase Chain Reaction (PCR)

Figure 2.11 shows the quantification of *mRNA* suppression of AQP1 in RAECs was quantified by RT-qPCR, The amount of target mRNA (treated with siRNA reagent) normalized to an endogenous control (GAPDH), relative to untreated control was given by $2^{-\Delta\Delta CT}$, which represents a 0.47 fold change of target relative to control (n=3). This is equivalent to about a 53% decrease in mRNA level after AQP1 is knocked down by

siRNA. There was no change in the amount of *von Willebrand factor* (vWF, endothelial cell specific marker) between treated and untreated control groups ($2^{-\Delta\Delta CT}$ equals 0.98).

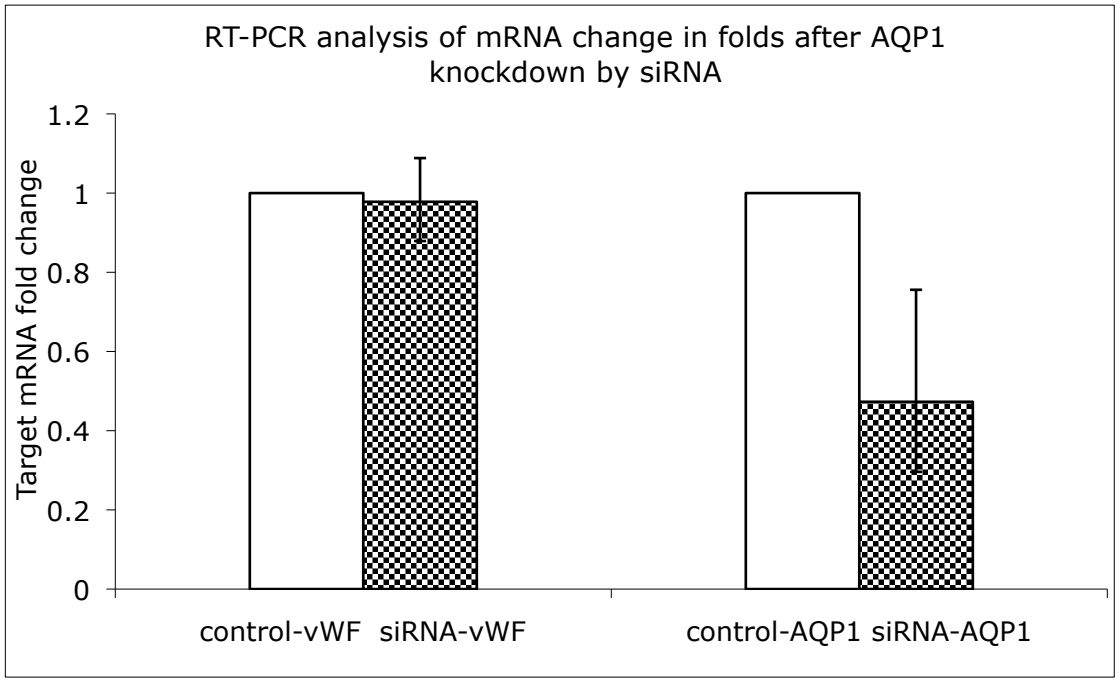

Figure 2.11: AQP1 silencing was examined by RT-qPCR and yield a by fold change of 0.47. There is no significant difference in the mRNA expression level of *von Willebrand factor* (vWF) upon AQP1 silencing.

Discussion

Plasma, mostly water, driven by transmural pressure, advects solutes across the endothelial monolayer, providing nutrients to the arterial wall. When a large pore is present, the flow can also advent LDL into subendothelial intima, which can trigger early lesion formation leading to early arthrosclerosis. It is widely believed that this pressure-driven water flow occurs exclusively paracellularly via the intercellular junctions. We argue here that the aquaporins-mediated transcellular pathway can also contribute to the

total transendothelial water flux. We have carried out a permeability study on RAEC monolayers in culture in order to avoid vessel stretching at elevated pressure and interaction with wall constituents (i.e. smooth muscle cells). We have examined how the siRNA-induced downregulation of AQP1 water channel protein influences the total hydrostatic pressure-driven water flux across the rat aortic endothelial cell (RAEC) monolayer. We also examined RAEC monolayer permeability to two small solutes under both convective and diffusive condition. Our results suggest that AQP1 transcellular pathway contributes significantly to transendothelial water flow, and when inhibited, accounts for a substantial decrease in the total water flux across the RAECs monolayer. This study will provide useful insights for our *ex vivo* study of the hydraulic conductivity (*Lp*) as a function of transmural pressure difference of the whole rat thoracic aorta in chapter 4. The combination of these chapters will allow a fuller assessment of the contribution of AQP1 to the total transmural-pressure-driven water flux through arterial wall in the physiologically relevant setting.

The immunolocalization of aquaporin1 on BAECs

Our data shows abundant AQP1 expression on RAECs *in vitro*. AQP1 is localized to not only the cellular membranes but also substantially to the cytoplasm. There is intense AQP1 staining around the cell nuclei in confocal slices through the monolayers. J. Toussaint of our group has verified the existence of AQP1 by immunohistochemical staining of cross-sections of whole rat thoracic aorta, and found that AQP1 is expressed throughout the aortic endothelial cell, including the apical and basolateral membranes and

the cytoplasm. This result on RAEC monolayer is consistent with studies of AQP1 in other cells and tissues: AQP1 expression was detected on both apical and basolateral surfaces of cultured renal medullary cells *in vitro* by immunoblot (Umenishi, Narikiyo *et al.*, 2004) as well as proximal tubule epithelial *in vivo* (Nielsen, Smith, Christensen e Agre, 1993). The intense reactivity of RAECs to anti-AQP1 antibody is consistent with the role that our knockdown experiments indicate it has in fluid transport across aortic endothelial cells. To determine the finite subcellular localization of AQP1 protein on RAECs, further work with confocal microscopy analysis of immunolabeled serial sections of this monolayer as well as immuno-gold labeling using transmission electron microscopy might be required.

The effect of aquaporins suppression on water permeability

Since aquaporins are important regulators for a cell's response to extracellular osmotic changes, a severe depletion of AQP1 might be very likely to disrupt a cell's ability to regulate such osmotic balance, leading to cell death. This would likely lead to incomplete monolayers having much higher *Jv* values due to holes or leaks in the monolayer. We chose Target 3 in our early experiments because light microscopic evaluation showed that it yielded tight monolayers without apparent sign of cell loss after transfection, indicating minimal cytotoxicity. The observed tightness of the monolayers also correlated with low *Jv* readings. Even for target 3, concentrations higher than 20pmol led to discernable cell loss resulting in 'leaky' monolayers with associated high *Jv* reading. After optimization, we chose a transfection concentration of 10pmol for

siRNA reagent target 3, not only because it induces the most amount of reduction in *Jv*, but also the most knockdown effect in protein expression in our immnuoblotting study. An obvious question is, why does the, siRNA reagent fail to give rise to a higher level of protein knockdown at higher siRNA concentrations? We speculate that the reason is again related to the essential role of aquaporins-driven osmotic water transport to cell viability. A higher amount of siRNA reagent might nearly completely deprive a cell of its endogenous expression of water channel proteins. If a cell can't withstand the consequent loss of function in regulating its osmotic balance, it would die. Since the cells that survive the transfection procedure are likely not to have been uniformly transfected, and since those that received very high transfection efficiencies are likely to have died, the remaining cells are likely a mixture of those that were hardly of poorly transfected. This batch would then exhibit a lower protein knockdown in western blotting than the batches that received the lower (10pmol) dose of siRNA.

When AQP1 expression was suppressed by siRNA, there was a dramatic decrease in the water flux (*Jv*) across the cultured RAECs monolayer. This large reduction in water flow, however, is very unlikely due exclusively to the direct effects of the suppression of the transcellular AQP1 pathway, but rather partially to the indirect elevation of the paracellular flow resistance caused by the suppression of this pathway. Such an increased flow resistance upon aquaporin suppression might be created by the overlapping of the junctional complexes, resulting in a longer, more complex pathway for paracellular water transport. This may be the result of the following mechanisms. In the AQP1 downregulated state, the cell's volume in other systems has been observed to

increase, and the fatter cells might overlap more. A few recent studies have raised this possibility in AQP5-/- mice and in cultured corneal epithelial cells (Verkman, 2005). Moreover, early studies noted that mercuric chloride treatment interfered with a cell's regulatory volume decrease upon a hypotonic challenge. However, as noted, mercuric chloride is not specific for aquaporin-1; they also likely block, for example, membrane ion and osmolytes transporter proteins, which are critical to cell volume restoration.

A second mechanism to explain the induced extension of the paracellular transport path might be the result of cell deformation due to increased pressure-driven axial compression and consequent radial cell expansion. When AQP1 is suppressed and the transcellular pathway for water transport is shut down, there is a larger difference in the pressure on the top surface of the cell and in its intercellular junction. By a Bernoulli argument, one can estimate the increase in the strain between the top and lateral cell surfaces, which should lead to more cell flattening, and more junctions overlapping, and, given a cell's material parameters, one can estimate a resulting cell expansion. Naturally, a careful transmission electron microscopy study on the morphology of pressure-fixed, aquaporins suppressed endothelial cells would be required to reveal the true nature of any morphological change in the cell body as well in the junctional complexes. No matter the reason for increased junction complexity, if present, with decreased aquaporin-1 expression, a more complex intercellular junction would obstruct the conductance of not just water, but also of any small solutes, e.g., TAMRA, that can pass through tight junctions, and slightly larger solutes, e.g., albumin, that can pass through the normal breaks in the tight junctions. We examine the results of just such a test below.

When using siRNA to knockdown AQP1, it might also be possible that the chosen siRNA reagent interferes non-specifically with the gene expression of some of the junction proteins that are responsible for rendering barrier for water transport. To test this speculation, we performed a Basic Local Alignment Search Tool (BLAST) test to compare the nucleotide sequence between Target3 and the NCBI reference mRNA sequence database. We found no sequence similarity between Target 3 and the known junction protein such as Zonula Occludens (ZO-1 and ZO-2) and VE-cadherins. Thus, the observed water permeability across the monolayer is unlikely due to the siRNA reagent's cross reaction with other junction proteins.

The effect of aquaporin-1 knockdown on small solute permeability of RAEC monolayers

Since RAEC monolayers present an array of transport barriers of different sizes, one generally probes them with a battery of tracers of different sizes. One then inserts these tracer data into a four-pore model, an extension of Cancel *et al.*'s (Cancel, Fitting *et al.*, 2007) three pore model, with the fourth, exclusively water pore, being the transcellular aquaporin-1 route, and extracts, among other things, the fraction of *Jv* that passes through each of the pores. By comparing the aquaporin-1 knockdown results to control, one can precisely partition the decrease in trans-aquaporin-1 and in paracellular water flows. Here we only discuss the tracer results qualitatively. My colleagues S. Joshi and C. Raval are currently doing the four-pore model calculations and we plan on including those results in the paper on this work that we intend to submit shortly for publication.

Again, the small solutes that we used are TAMRA and TRITC-albumin. TAMRA is small enough to pass through the tight junctions. We find no significant difference in its transport between advection and diffusion regimes, indicating that its diffusive is far faster than its advective transport, i.e., it has Peclet number much less than one. In contrast, there is a significant difference in TAMRA's permeability between these two conditions, meaning its advective and diffusive transport are similar in size, i.e., its Peclet number is order one. For both tracers the aquaporin-1 knockdown monolayer exhibited significantly decreased transport of both tracers under both advective and diffusive conditions. For TAMRA, which traverses even the normal junctions, this indicates that the normal junctions have become more complex. Albumin transport happens mainly through the breaks in the tight junctions (36%) and the leaky junctions (44%). However, the albumin transport story is more complex, because 20% its transport is accounted by the vesicular pathway (Cancel, Fitting *et al.*, 2007). These results are consistent with increased cell-cell overlap at their peripheries. Again, the four-pour model will make these statements more quantitative.

Our results indicate that AQP1 transcellular pathway play a critical role in transendothelial water flow in RAEC monolayers. Future studies with human aortic endothelial cells would be very useful for the study of water and mass transport in a physiological relevant manner. In whole vessels, as we shall discuss in chapter 4, the level of AQP1 expression may affect the state of SI compaction, which can strongly

impact LDL clearance from the wall, a critical precursor event to prelesion SI LDL accumulation.

Chapter 3 An *ex vivo* aorta organ culture system

Abstract

Aquaporin-1 (AQP1) is the ubiquitous water channel protein that facilitates transcellular water flow. The ultimate goal of our study is to determine the contribution of the AQP1 transcellular pathway to water filtration. Our measurement tool is the hydraulic conductivity (*Lp*, the ratio of water flux (*Jv*) to transmural pressure difference (ΔP)), through the aortic endothelium, as inferred from the *Lp* through the intact and denuded aortic wall, of the excised whole rat thoracic aorta in an *ex vivo* preparation. In chapter 4, we shall compare this endothelial *Lp* of control aortas with those that have undergone siRNA knockdown of endothelial AQP1. Since protein knockdown takes on the order of 50 hours to be effective, the introduction of this siRNA knockdown reagent to endothelial cells through the aortic lumen and its ability to take effect there can only be achieved through a vessel culture system that is designed to maintain vessel architecture and vascular cell integrity intact over a period of days. The system that we describe in this chapter provides a constant perfusion of warm media through the vessel lumen, yielding a physiological shear stress and transmural pressure. By design, one controls the transmural pressure independently of the flow and shear by adjusting the height of a media reservoir. We find that maintenance of both pressure and flow preserves isolated aortic endothelial cell integrity, as monitored by morphological study, as well as maintaining vessel *Lp* at various ΔPs unchanged over a period of days. In particular, the *Lp* vs ΔP curve of cultured rat aortas *ex vivo* does not change after 48 hours of incubation.

Silver nitrate staining demonstrated regular cell shapes and intact cell-cell borders with no distinguishable cell loss even at the entrance of the flow into the vessel. Hematoxylin and Eosin staining reveal an unaltered structure of the aortic wall. In this study/chapter, we describe this novel aorta organ culture system and confirm that rat aorta can be maintained *ex vivo* for 48 hours under controlled pressure and flow. This provides feasibility that the organ culture technique can be used as a potent tool for molecular manipulation of aortic endothelial cells.

Introduction

We aim to study the effect of siRNA suppression of endothelial aquaporins on whole vessel wall hydraulic conductivity (*Lp*) as a function as transmural pressure differences (ΔPs) (Chapter 4). Since aquaporins are ubiquitously expressed throughout the body, especially in the kidney and in erythrocytes, we want to avoid any systemic effect of this molecular manipulation in live animals. In this chapter, we construct and validate an *ex vivo* aorta organ culture system that will permit delivery of the siRNA reagent specifically to aortic endothelial cells while preserving their and the entire wall's morphological as well as functional integrity for 48 hours. This 48-hour period is critical because it allows for the maximal silencing effect of the siRNA reagent to take place, as confirmed by our *in vitro* study.

The aorta is an active organ that has its own distinctly complex structure. It is made of different layers of cells: from the inner most, a monolayer of endothelial cells,

followed by a very thin layer of subendothelial intima (SI) (0.1-0.5μm in rat), which consists of a loose fiber matrix of proteoglycan and collagen fibers and a fenestrated internal elastic lamina (IEL). The media layer immediately following the IEL mainly consists of smooth muscle cells that synthesize extracellular connective matrix such as collagen, elastin and fibronectin. The media accounts for most of the thickness of the aortic wall, about 150μm in rat. The media is covered on the outside by a layer of loose adventitial tissue (Huang, Jan et al., 1998; Lusis, 2000). Involved in numerous physiological functions from regulating vascular tone, lipid metabolism, to mediate inflammatory responses, endothelial viability is crucial to vascular vitality and it's the target of our study. Work by Tedgui and Lever (Tedgui e Lever, 1984), and confirmed in our lab on the *Lp* of intact and denuded aortas have indicated that, even though the endothelial monolayer comprises less than 1% of the thickness of aortic wall, it accounts for nearly 50% of hydraulic resistance (Shou, Jan *et al.*, 2006; Nguyen, 2008).

The arterial wall is continuously exposed to mechanical forces in the form of shear stress and pressure. Shear stress is described as the friction force exerted on the vessel wall by the viscous blood flow. For a purely Poiseuille flow, which would apply to the laminar flow of a Newtonian fluid in a straight, rigid cylinder model of a blood flow in a vessel, for a defined volumetric flow rate, Q, the wall shear stress is directly proportional to the product of $Q \times \mu$ (μ is the fluid viscosity), and inversely proportional to cube radius R_0, while the axial pressure gradient scales as $Q \times \mu / R_0^4$. The measured shear flow is usually high and athero-protective arterial regions. In regions of high curvature (i.e. aortic arch), branches and bifurcations, flow disturbances that result in a relatively

lower wall shear stress occur and these disturbances render these sites susceptible to endothelial disruption and arthrosclerosis (Gimbrone, 1999). The transmural pressure, ΔP, is the pressure difference between the inside and the outside of a vessel. The inside of large arteries is usually at ~100mmHg higher than the outside. ΔP is the driving force that convects plasma (mostly water) and solutes through the vessel wall. Some of the solutes are nutritious: i.e. albumin, while others are not necessarily as beneficial, i.e. LDL, since accumulation of LDL in the subendothelial intima can lead to early lesion formation of arthrosclerosis (Tedgui e Lever, 1985). Overall, these mechanical forces are vital for maintaining vascular health; vascular remodeling associated with changes in these forces reflects an adaptive response to changes in the local environment, usually a long-term process (Epstein, 1994)

1. The effect of pressure and flow on vascular health

As noted above, in order to maintain an excised whole vessel patent over a period of days, our vessel perfusion system endeavors to maintain physiological transmural pressure, ΔP, and wall shear stress. Cultures of endothelial cells at zero or low ΔP result in cell-cell junctions that are far looser than those exposed to physiological ΔP, as measured by a far higher *Lp* upon imposition of a non-zero ΔP than those long exposed to the transmural pressure. This high *Lp* value decays over a period of 10-60 minutes as the junctions seal (Demaio, Tarbell *et al.*, 2004).

Too high ΔP is associated with the physiological condition of hypertension. Hypertension is associated with a much greater risk of the development of cardiovascular diseases such as arthrosclerosis and sudden death. Hypertension affects both the morphology and function of the endothelial monolayer. Functional abnormalities are manifested as increased permeability to colloidal carbon, HRP, albumin and lipoproteins (Wiener, Lattes *et al.*, 1969; Huttner, Boutet *et al.*, 1973; Chobanian, Brecher *et al.*, 1986) and reduced endothelial-mediated vaso-relaxation (Chobanian, 1990). Hypertension disrupts the endothelial monolayer, with accompanying cell swelling and widening of interendothelial junctions (Ooneda, Ooyama *et al.*, 1965). While adult rat aortic endothelial cells rarely replicate, both replication rate and cell density were increased in the early phase of the hypertension (De Chastonay, Gabbiani *et al.*, 1983). Wu *et al.* found that the aortas of male spontaneously hypertensive Wystar Kyoto rats (SHR) displayed triple each the number of mitotic and apoptotic endothelial cells as well as triple the number that were leaky to macromolecular tracers as their normotensive controls of the same strain (Wu, Chi *et al.*, 1990). In addition, endothelial cells of hypertensive rats undergo surface changes, presenting abundant surface projections, which are believed to be related to the spreading of these cells after mitosis as a result of reaction to injury (De Chastonay, Gabbiani *et al.*, 1983). In relation to the media layer, smooth muscle cell (SMC) hypertrophy associated with elevated protein synthesis and DNA content is prominent in SHRs (Owens, 1987). Furthermore, the total amount of elastin and collagen were also increased (Wolinsky, 1970). Enhanced protein synthesis and collagen production are also observed on cultured smooth muscle cells with the application of cyclic stretching (Grande, Glagov *et al.*, 1989). SMCs migration and

proliferation can be induced by endothelial denudation (De Mey, Uitendaal *et al.*, 1989). In an *ex vivo* rabbit aorta organ culture system, a 150mmHg transmural pressure brought about an increase in the total amount of protein synthesis in serum-supplemented media, as compared to the relaxed state ($\Delta p=0$) or to $\Delta p=80$mmHg, while having no effect on DNA synthesis. High transmural pressure also gives rise to increased C-fibronectin production in the media (Bardy, Karillon *et al.*, 1995). SMC phenotype can also be modulated by mechanical forces. *Ex vivo* study has shown that a circumferential stress by a transmural pressure of 80mmHg can prevent the decrease of a differentiated contractile SMC marker, caldesmon, expression. Caldesmon decay is seen on vessels cultured at a relaxed state or $\Delta p=10$mmHg under 1ml/min flow rate within 3 days of rabbit (2-2.5kg) descending thoracic aorta (internal diameter is approximately 3.25 mm) organ culture. Neither flow nor denudation affects caldesmon expression (Bardy, Merval *et al.*, 1996). *In vitro* study has also confirmed that cyclic stretch can induce caldesmon (Birukov, Bardy *et al.*, 1998) and myosin heavy chain production (Smith, Tokui *et al.*, 1995).

Both *in vitro* and *in vivo* study have elucidated the relationship between hemodynamic shear stress and alteration of the integrity of endothelial monolayers. Under unidirectional shear stress, endothelial cells exhibited orderly pattern orienting their long axis parallel to the direction of the flow. Altered endothelial cell morphology was perceived in regions of disturbed flow with cells of irregular spindle-like shape (Reidy e Bowyer, 1977; Gimbrone, 1999). Enhanced influx of plasma proteins and lipids into the arterial wall are also observed there (Friedman e Fry, 1993). Developmentally, blood flow plays a significant role in vascular growth. A long-term decrease in blood

flow results in a time-dependent decrease in lumen diameter and an alteration in vascular structure in young rabbit. Growth inhibition related to young rabbits includes a reduction in DNA and elastin content and in wall mass, but not collagen. However, there is no distinct loss in medial tissue mass or wall constituents in adults. It seems that the initiation of the degradation of wall content doesn't happen after one month in adults (Langille, Bendeck *et al.*, 1989). A chronic increase in blood flow adversely results in blood vessel dilation, intima hyperplasia and increase permeability to proteins such as Evan blue albumin (Fry, Mahley *et al.*, 1977). Excessive shear flow causes the endothelial cells to come off and formation of early atherosclerotic lesion (Kamiya e Togawa, 1980). In an *ex vivo* rabbit aorta culture system, DNA synthesis was induced by flow in serum-free media. This flow-induced mitogenic response is believed to be related to the secretion of growth factors by endothelial cells. Total protein synthesis was increased by flow regardless of the presence or absence of serum (Bardy, Karillon *et al.*, 1995).

2. Ex vivo aorta organ culture system

Endothelial hyperpermeability leads to a reduced restriction on water flow as well as LDL cholesterol transport. Therefore, a great deal of interest is invested in researching the cellular mechanisms related to endothelial cell dysfunction, hyperpermeability to water and macromolecules and atherogenesis. Several experimental approaches are applied to the study of vascular cell structural and functional characteristics. These include *in vitro* cell culture system (see chapter 2), *in vivo* live animal model and *ex vivo* vessel organ culture model (this chapter). Live animals clearly are excellent *in vivo*

models for the study of vascular biology, because the interaction between vascular cells and microenvironment is intact. However, the *in vivo* system is very complex, with numerous factors beyond the control of the experimentalists, and the obtained data are therefore more difficult to interpret. Furthermore, it is technically challenging to deliver chemical reagents to the desired vascular cells without causing any unwanted systemic effects and immune responses (Mangiarua, Moss *et al.*, 1992).

To solve all these problems, researchers have extended their expertise to culturing intact vessels *ex vivo*. This approach preserves the vascular architecture while allowing for independent regulation of mechanical forces as well as molecular interventions. Many early attempts have been employed to culture vessel segments in culture media in suspension without hemodynamic stimuli. However, undesirable structural and functional changes often occur under this culture condition. Scanning electron microscopy (SEM) study of porcine aorta culture showed that, after one day of culture in stasis, the endothelial cells flattened out, changing their shape from enlongated to polygonal and they presented numerous surface microvilli and small gaps in between cells. The author reasoned that the change in shape in the endothelial cells is due to the lack of flow. There is also noticeable subendothelial smooth muscle cell proliferation (Gotlieb e Boden, 1984). This noticeably thicker intima was also observed in a long-term culture of human aorta which was due to the proliferation of smooth muscle cells and extracellular matrix (Barrett, Mergner *et al.*, 1979).

In addition to choosing the appropriate incubation media, to imitate the *in vivo* environment the vessel is experiencing; researchers have introduced fluid mechanical stimuli to the vessel culture system. Rat aortas were cannulated and connected to a peristaltic pump on one end, and left free hanging into a media bottle where the aorta is immersed on the other end. The peristaltic pump provides a perfusion pressure of about 120/36mmHg systolic/diastolic respectively. After 3 days of perfusion, despite the fact that the media and adventitia layer look normal, the intima layer is mostly devoid of endothelial cells. It was suspected by the author that either the shear stress or the culture media was not suitable for the growth of endothelial cells (Mangiarua, Moss et al., 1992). To examine the effect of pressure and flow on the wall structure and DNA and protein syntheses, Bardy and coworkers improved Mangiarua's technique and successfully preserved both endothelial as well as the whole aortic structure of rabbit thoracic aortas in culture for up to 8 days. The aorta was double cannulated and connected to a circulation circuit (flow rate 40ml/min). A separate pressure setup provides the transmural pressure. Similar approaches have also been used to study vascular biology and biomechanical biochemical responses (Birukov, Bardy *et al.*, 1998; Chesler, Ku *et al.*, 1999). Moreover, little attention is paid to the endothelial-dependent whole vessel permeability in the whole aorta in organ culture. We developed a system for the rat aorta and, among other things, monitor vessel *Lp* as a gauge of how well the vessel has been preserved over the incubation period.

3. Examination of endothelial integrity using silver nitrate staining

Introduced by Flinzer in 1854, one of the most useful ways to study aortic endothelium *in situ* is to stain the endothelial border with silver nitrate and to view it transmitted light *en face* (O'nejll J, 1947). This *en face* staining method provides more information than conventional histological cross-sections because it allows for a continuous field of vision of endothelia while providing information with regard to cell size, shape and orientation. It also shows endothelial nuclei much more clearly, an excellent way to assess cell loss, since they generally do not appear in most histological cross-sections. Deposited at the inter-endothelial cell junction as sliver proteinate, this stain is considered a true reflection of the cell border (Poole e Florey, 1958). Since it outlines endothelial borders to a dark brown to black color, 'the silver line' or 'cement line' is used for the characterization of normal, abnormal and for the loss of endothelial cells. Normal endothelial cells present an orderly pattern and alignment while irregularity based on variation in sizes and shapes indicate an abnormal pattern of human aorta endothlelial cells, as Figure 3.1 shows (Cotton e Wartman, 1961)

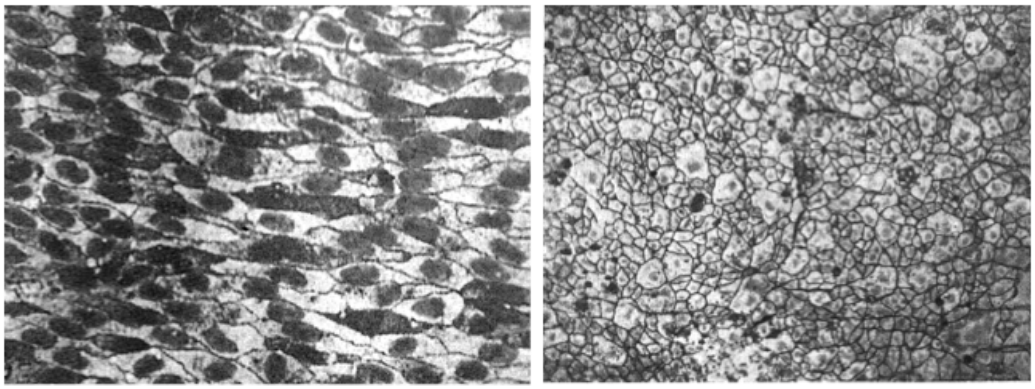

Figure 3.1: Normal regular pattern of human aortic endothelium, the endothelial cells appear regular, with even staining of the silver line (250X) and abnormal aortic endothelium from a showing distinguishable irregularity and variation in sizes and shapes, seemingly related to aging (100X) (Cotton e Wartman, 1961)

Endothelial reaction to injury has been studied intensively using this staining technique. O'Niell reported that when depriving the vein of its blood supply for 6 hours, there occurs focal endothelial losses, which were replaced by black parallel lines perpendicular to the long axis of the vessel. See Figure 3.2. This black line is believed to be staining of the space in between the smooth muscle cells upon loss of the endothelium (O'nejll J, 1947). Rabbit aorta endothelial regeneration was observed upon mechanical scraping. Within 24 hours of deendothelialization, the denuded area was covered by endothelial cells stretched out from the edge of the wounded area. Within 3 days, cell division became apparent and continued to cover up the bare area with new cells. Some irregularity of endothelial cells, so called 'Cement substances', is seen on the surface of these regrown cells. These substances are argyrophilic granular materials, similar to what McGovern has observed on human vein (Poole, Sanders *et al.*, 1958). They are considered to be related to endothelial regenerating and repair (Mc, 1955).

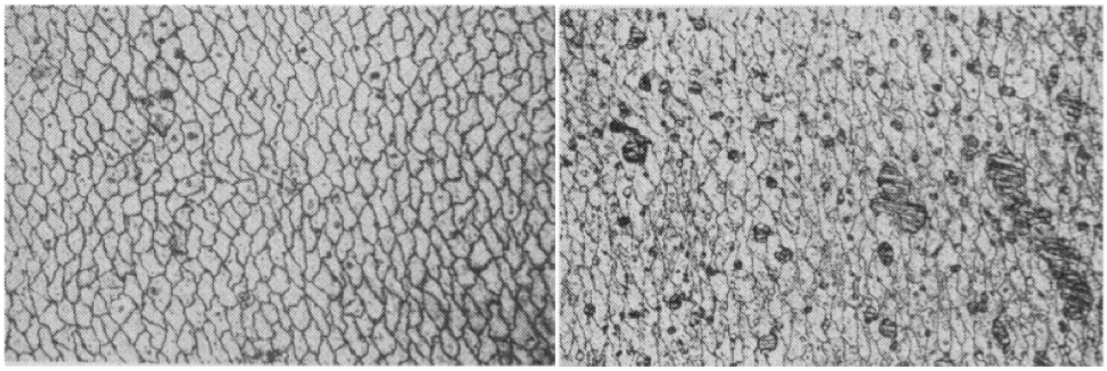

Figure 3.2: Silver nitrate staining of jugular vein of dog. Normal pattern endothelial cells (left), focal loss of endothelial after blood supply was cut off for 6 hours (right). (O'nejll J, 1947)

4. Structure of the aortic wall by Hematoxylin and Eosin staining

Freshly removed rabbit aortic cross-sections stained with Hematoxylin-Eosin (Figure 3.3) displays the basic structure of the aortic wall. It shows a relatively thin sheet

of intima that is comprised of a continuous layer of single nucleated endothelial cells and its underlying basement connective tissue. The media layer, mainly consisting of spindle-shaped smooth muscle cells and its interspersed elastic fibers, occupies the majority of the thickness of the wall. Histological examination of the cultured aorta revealed that the structure of cultured aorta is unchanged in comparison with freshly isolated one (Bardy, Karillon *et al.*, 1995).

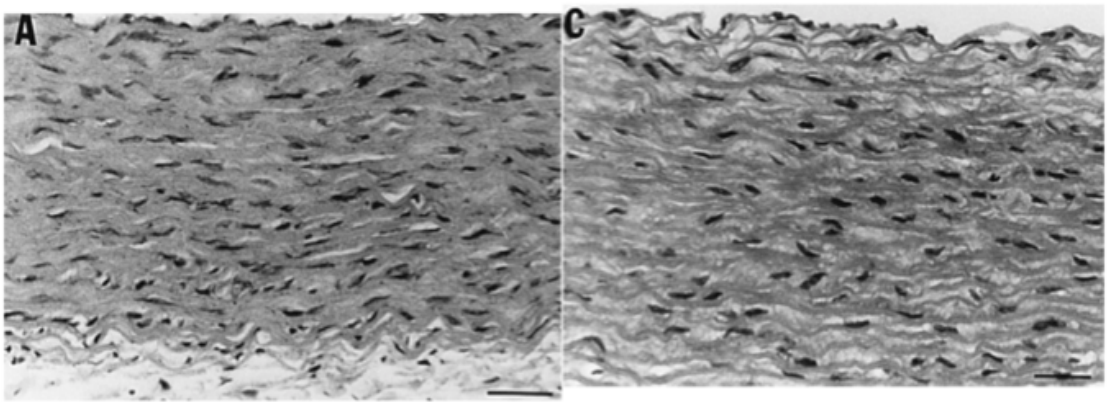

Figure 3.3: Histological cross-sections of aorta. A and C, rabbit aorta freshly removed (A) and cultured for 8 days with perfusion and intramural pressure maintenance (C), both with Hematoxylin and Eosin staining (Bardy, Karillon *et al.*, 1995).

Materials and methods

1. Surgical procedures

For experiments that do not involve long-term vessel culture, and that can be completed in 14 hours or less, we use the following procedure: Male Sprague Dawley rat weighing 400-450 grams were anaesthetized by intraperitoneal (i.p.) injection with 1% sodium pentobarbital (15mg/kg weight). Tracheotomy was performed to mechanically ventilate the lung. The lungs and heart were laterally displaced upon the exposure of

chest cavity. The aorta is cleaned of fat and loose adhering peri-adventitial tissue. Branches of intercostals artery were ligated. The aorta was kept constantly wet with the suffusate solution (4% bovine serum albumin (BSA), 10^{-3}M sodium nitrate ($NaNO_3$) in 1× phosphate buffer saline (PBS)) to prevent it from drying off. The proximal end of the aorta was cannulated with 0.5mm Tygon tubing and flushed with perfusate solution containing (4% BSA, 10^{-3}M $NaNO_3$, 0.03% trypan blue in 1×PBS) at 60mmHg for 10 minutes, which prevents collapse of the aortic wall and subsequent endothelial damage. The vessel was then excised and soaked in suffusate solution bath in a 37°C incubator. The trypan blue clearly marks any leaks in the vessels before cannulation of the distal end as well as acting as a vital stain for cell death at the end of the experiment. $NaNO_3$ relaxes smooth muscle cells (Baldwin e Wilson, 1993). The aorta was pre-conditioned by lowering and raising the vessel ΔP to its minimal (60mmHg) and maximal normal (140mmHg) value 3 times, each for less than 1 minute to reduce hysteresis effects, defined as a vessel's tendency to not return to its original but greater diameter after being pressurized (Baldwin, Wilson *et al.*, 1992).

2. Ex vivo hydraulic conductivity experiment

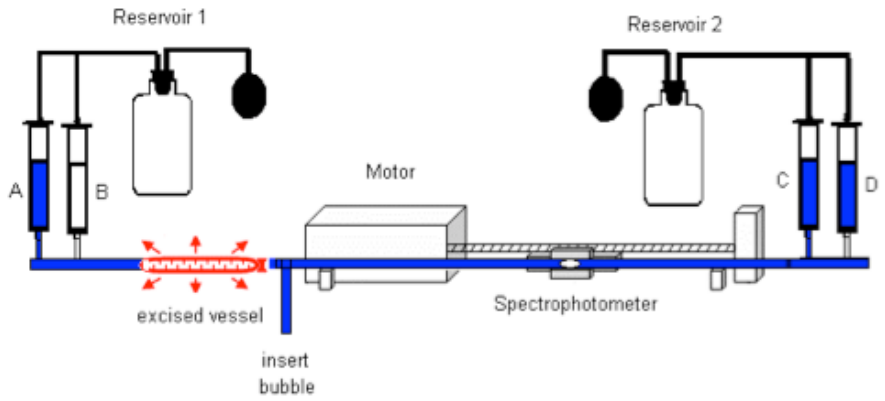

Figure 3.4: Cartoon illustration of *Lp ex vivo* measurement set-up, adapted from (Nguyen, 2008)

The proximal end of the aorta was connected through a spectrophotometer bubble tracking system to Reservoir 2. The distal end of the aorta was connected to Reservoir 1. A mercury sphygmomanometer was used to maintain the proper pressures (ΔPs) with the pressure-bottle setup. Reservoir 2 was pressurized to the desirable ΔP while the distal cannulation was clamped off. An air bubble was positioned under the spectrophotometer in the precision borosilicate capillary tube (1.9913±0.01mm ID x 5.5±0.5mm OD x 550mm; Wilmad Labglass, NJ). The movement of the bubble (cm/second) was tracked by the spectrophotometer and continuously read into a computer. This was used to measure the water infiltration through the vessel wall. After preconditioning, measurement of the transmural water flow was taken at ΔPs of 60 and 100mmHg. A mechanical caliper accurate to 0.1 mm was used to measure the vessel length and outer diameter at the end of each *Lp* measurement. The distal end was untied and a small Epon ball was inserted by rotation motion into the vessel to remove the endothelial cells. After flushing for 10 minutes at 100 mmHg, the distal end was retied and *Lp* measurements were repeated on the denuded vessel.

Jv is calculated based on the following equation:

$$J_V = \frac{\Delta d}{\Delta t} \times \frac{F}{S_A}$$

$\frac{\Delta d}{\Delta t}$ (cm/s) is bubble position per unit of time, S_A (cm^2) is the surface area: $S_A = \pi \times OD \times L$, where OD is the outer diameter and L is the length of the vessel (assuming the vessel is of cylindrical geometry); F is the surface area of the tubing underneath the spectrophotometer, for borosilicate capillary tube, F= 0.00196cm^2. When measuring *Lp*, we assumed that water/perfusate solution crosses the entire surface area of the vessel. The areas of the portions of the intercostals arteries before the ties are regarded small enough to be neglected from the total vessel area calculation. The presence of trypan blue in the perfusate, but not in the suffusate does not generate any significant osmotic pressure difference since the estimated reflection coefficient of the dye is about 0.064, which is 13 times less than that of albumin (0.8-1.0) and since its concentration is low (Knox, Levick *et al.*, 1988; Shou, Jan *et al.*, 2006).

Vessel *Lp* is calculated as

$Lp = Jv/\Delta P$.

From Lp_t of the intact vessel and Lp_{m+I} of the denuded vessel (i.e., for the media plus IEL), we calculate Lp_{e+i} (i.e., for the endothelium plus the subendothelial intima) by a difference of resistances in series as (Tedgui e Lever, 1984)

$1/Lp_{e+i} = 1/Lp_t - 1/Lp_{m+I}$.

3. Ex vivo aorta organ culture system

Aorta harvest procedure was carried out using sterile surgery techniques in a horizontal laminar flow hood. The cannulation of the aorta was modified to accommodate the need for both perfusion and *Lp* measurement. See Figure 3.5, a Petri-dish host for the vessel was rested in an incubator maintaining a temperature of 37°C and 5% CO_2. The aorta was primarily connected to a peristaltic perfusion circuit (orange), composed of a peristaltic pump, a media reservoir and tubing. The pump's flow rate controls the wall shear stress felt by the vessel wall. The height of the media reservoir, which is exposed to the atmospheric pressure of the incubator, can be adjusted to regulate appropriate physiological transmural pressure the aorta experiences, preventing the vessel from collapsing or bursting. The culture media consists of minimal essential media (MEM), supplemented with 2% Pen/Strep, Amphotericin B 10mg/L and 10% fetal bovine serum. Media is continuously perfused to the vessel via a peristalsis pump at a rate16.7ml/min. All of the apparatus except for the peristaltic pump is hosted in the incubator. Via a three-way connector, the proximal end of the aorta is also connected to the *Lp* bubble tracking system (blue), and when distal end is closed off, it permits *Lp* measurement. The experimental perfusate (blue) and suffusate were replaced by culture media at the end of initial *Lp* measurement.

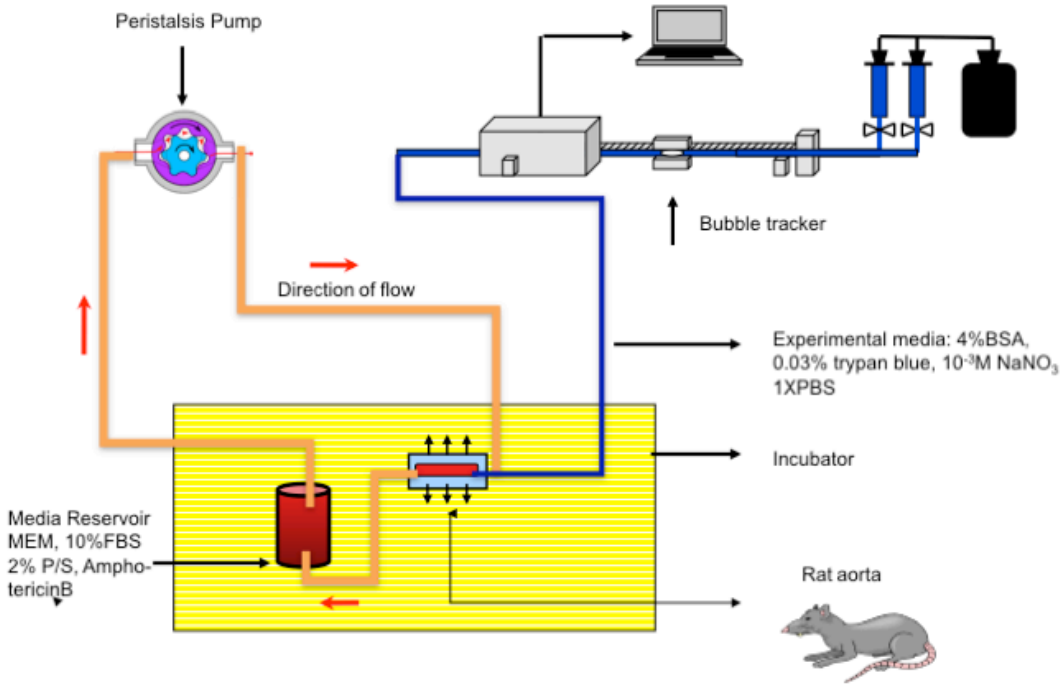

Figure 3.5: The *ex vivo* hydraulic conductivity measurement setup allows switching between connection of the vessel to either the bubble tracking system or the aorta culture system. The aorta is maintained at all times in a media bath in a CO_2 control 37°C incubator. A peristalsis pump constantly provides circulating media through the lumen to maintain a shear stress within a physiological range. The height of a media reservoir is adjusted to maintain a physiological transmural pressure.

4. Silver nitrate staining of whole mount of the arterial wall en face

Ex vivo en face preparation of vessel wall: The vessel was perfusion fixed with 1% paraformaldehyde for 10 minutes and then washed with 1× PBS and 5% glucose for 1 minute. This was followed by the application of 0.05% silver nitrate for 1 minute, washes with glucose for 1 minute, bromides mixture (NH_4Br and CoBr) for 1 minute, and again with glucose for 1 minute. The unopened vessel was post-fixed in 1% paraformaldehyde for 24 hours. The vessel was then washed with water for 3 minutes and slit open longitudinally after careful removal of the adventitial tissue. The aorta was then laid flat on a glass slide with the endothelium facing up, treated with clear-mount and sealed with nail polish.

5. Hematoxylin and Eosin staining

The aorta was fixed in 10% formalin solution and embedded in paraffin. Transverse sections (6μm) were stained with hematoxylin and eosin based on the manufacture's protocol (Hema3 stain set, Fisher diagnostics, Middletown, VA) and examined by light microscopy.

Results

1. Ex vivo hydraulic conductivity measurement

Hydraulic conductivity (*Lp*) is measured on the same aortas upon fresh removal from the rat and after culturing for 48 hours *ex vivo* at transmural pressure differences (ΔPs) of 60 and 100mmHg. This control experiment was performed to evaluate sustainability of the culture system through the functional assessment the whole vessel *Lp*. Based on our group's experience, *Lp* measurement is very sensitive to endothelial as well as whole vessel's integrity. Figure 3.6 shows the *Lp* results: as in previous studies (Tedgui e Lever, 1984; Baldwin, Wilson *et al.*, 1992; Shou, Jan *et al.*, 2006; Nguyen, 2008), there is a significant 22.8% drop in *Lp* from 60mmHg to100mmHg ($p=0.04$, $n=3$, from $3.51\pm0.62\times10^{-8}$ cm/s/mmHg to $2.71\pm0.36\times10^{-8}$cm/s/mmHg) of fresh aortas. There is no significant difference in *Lp* before and after culturing at each transmural pressures (*Lp*=$3.30\pm0.31\times10^{-8}$cm/s/mmHg at 60mmHg and $3.12\pm0.55\times10^{-8}$ cm/s/mmHg at

100mmHg). There is no change in the outer diameter measurement as a function of ΔPs before and after aorta culture *ex vivo* (See Figure 3.7).

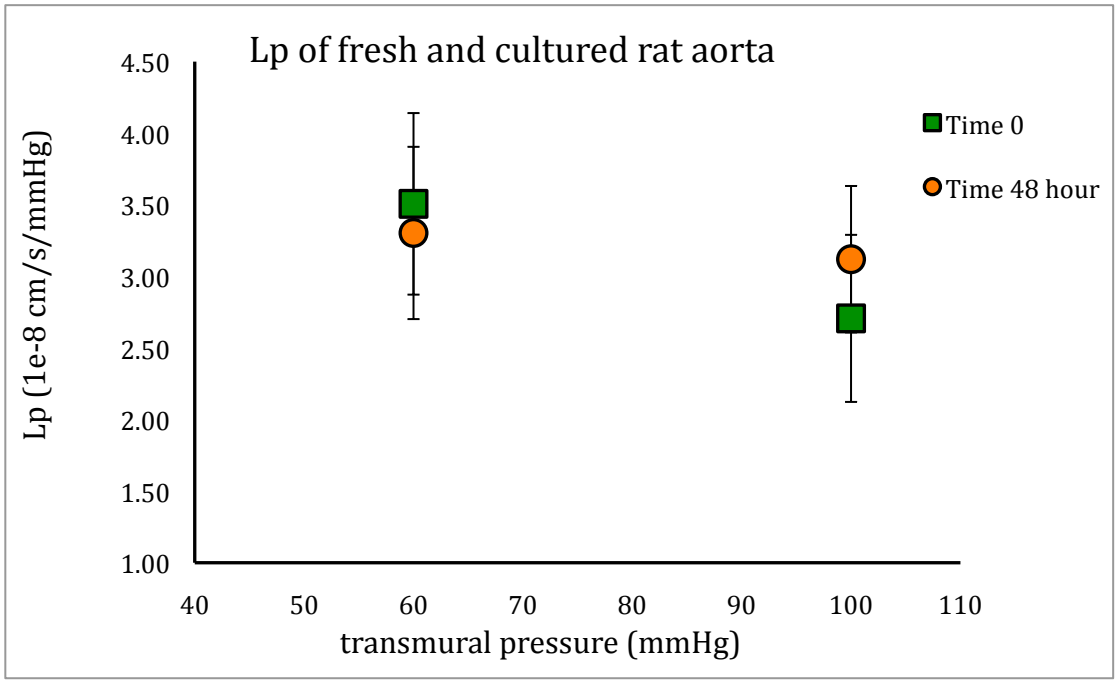

Figure 3.6: Rat aorta hydraulic conductivity as a function of transmural pressure of baseline and after 48 hours of culturing (Values of hydraulic conductivity= mean±Standard Deviation, n=3)

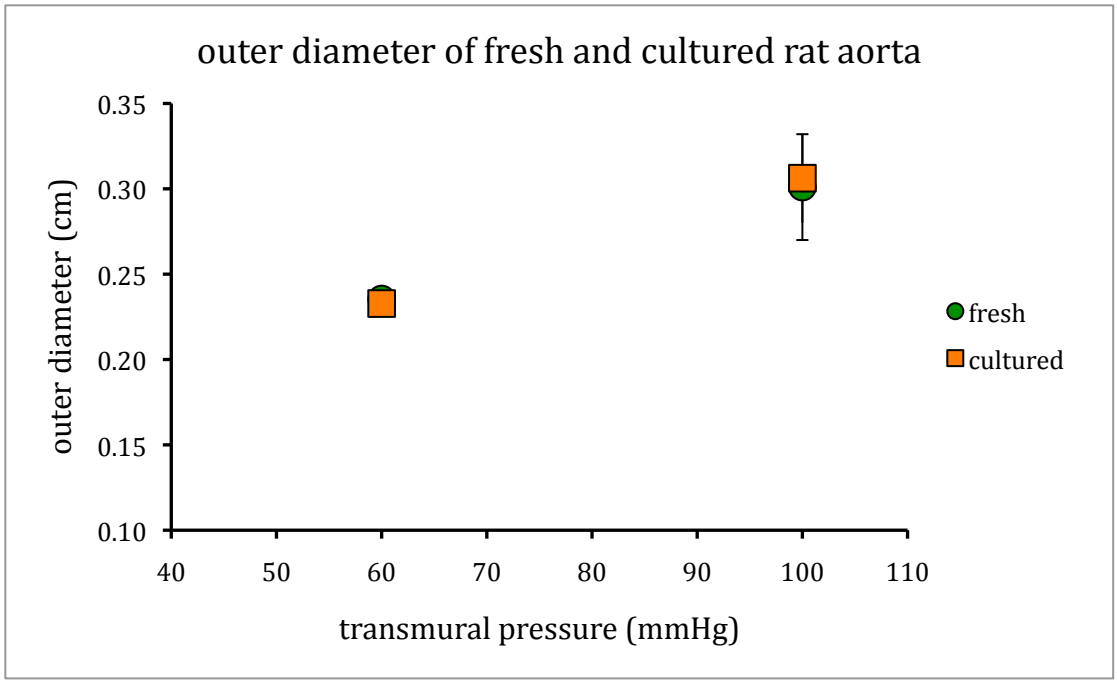

Figure 3.7: Outer diameter measurement of rat aorta before and after 48 hours of culturing (Values of OD (cm)= mean±standard deviation, n=3)

2. Endothelial integrity assessment by silver nitrate staining of the aorta en face

Light microscopic examination (Figure 3.8) of freshly isolated rat aorta in an *en face* preparation shows cell-cell border outlined by silver lines. The silver line is consistently regular, outlining the elongated shapes of the endothelial cells that orderly align in the direction of the flow. The endothelial cells are relatively even in size and staining. This staining pattern agrees with what was observed for both human aorta (Cotton e Wartman, 1961) and rabbit aorta (Poole, Sanders *et al.*, 1958). We notice some variations of silver line from one area to another on the same specimen as well as in between specimens. The cultured aorta showed unchanged patterns and endothelial shapes from the freshly isolated aorta. The endothelial cells still aligned in the orderly fashion with the

longitudinal axis of the aorta. An increase in silver deposit localized to the cell-cell junctions can be observed, which might indicate slight cell injury. Endothelial loss might be seen on some specimen but it is limited to small areas.

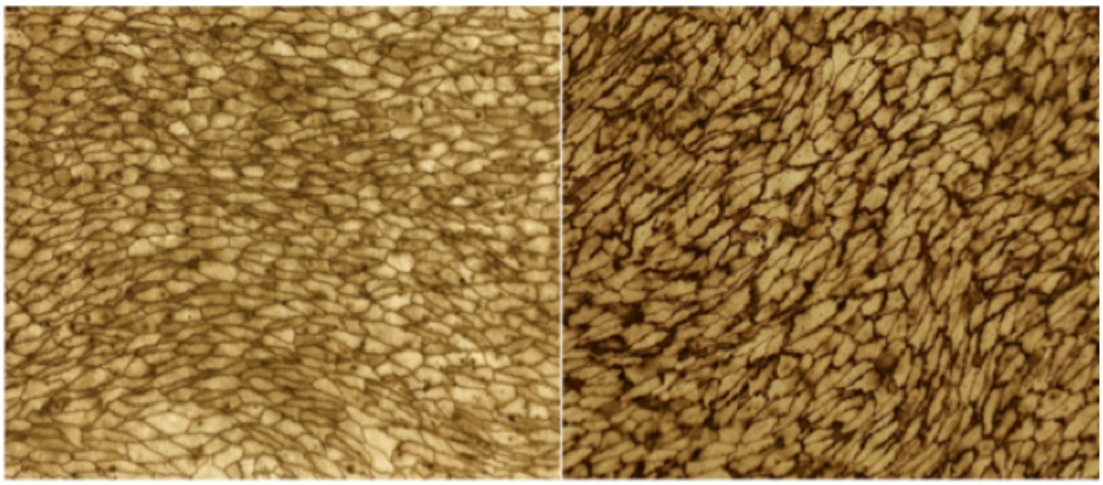

Figure 3.8: Endothelial cell shown in *en face* silver nitrate staining of rat thoracic aortas. Freshly isolated aorta (left) and aorta cultured for 48 hours (right). The endothelial monolayers show the normal pattern (left) and appear unaltered, displaying no visible discontinuity after *ex vivo* perfusion and culturing (right) (magnification 200X)

Figure 3.9 compared the middle portion of the cultured aorta to its end portion where the cannula carries the perfusate to the lumen using silver nitrate staining and low magnification. Concerned with the patchy loss of endothelial cells at the entrance of the flow into the vessel due to possible entrance eddy formation that we had observed in our first experiments, we scale down the flow rate from 60ml/min (calculated shear stress 10 dynes/cm^2) to 16.7ml/min. The result was no more discernable endothelial loss at the entrance of the flow.

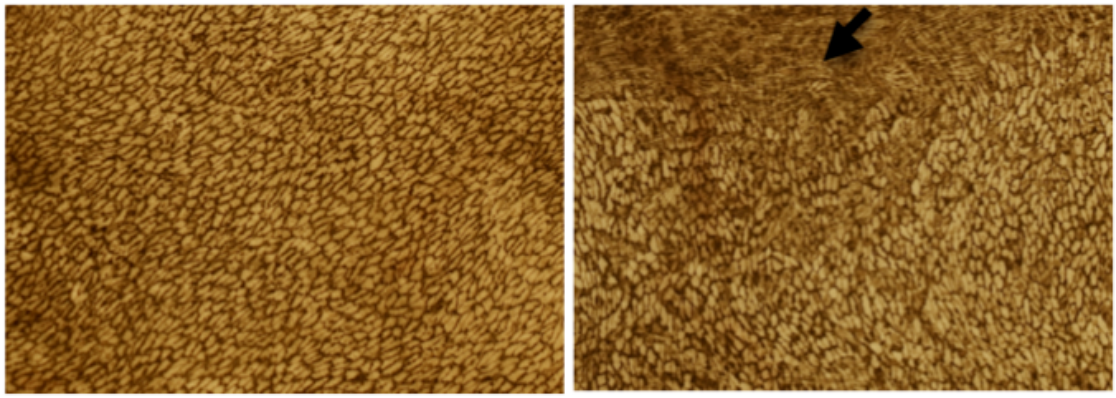

Figure 3.9: Comparison by silver nitrate staining at low magnification of the middle portion of the cultured aorta after perfusion (left) to the entrance portion of the same aorta near the cannulation site after 48-hour perfusion (right). There is no apparent loss of endothelia beyond the cannulation area with threaded marks (black arrow)

3. Aortic wall integrity assessment by Hematoxylin and Eosin staining of aorta cross-section

Figure 3.10 examined the integrity of the endothelium and of the aortic wall by light microscopy, using both freshly isolated and cultured aorta. As can be seen from the freshly isolated rat aorta cross-section stained with Hematoxylin and Eosin, the media layer with its spindle-shaped smooth muscle cells and interspersed elastic fibers comprises the majority of the thickness of the wall. The media layer is followed on the outside by an adventitia of some loose connective tissue. There is a relatively thin layer of intima that is comprised of a continuous layer of mono-nucleated endothelial cells and its underlying basement connective tissue. Histological examination of the cultured aorta reveals that the structure of the cultured aorta remains unchanged in comparison with that of the freshly isolated one. The media is well preserved; smooth muscle cells are well oriented, without any distinct cell injury or loss. Silver nitrate staining outlines the

continuous layer of endothelial cells facing the lumen without distinguishable evidence of cell death. Thus, the cultured aorta doesn't show any alternation associated with *ex vivo* culturing.

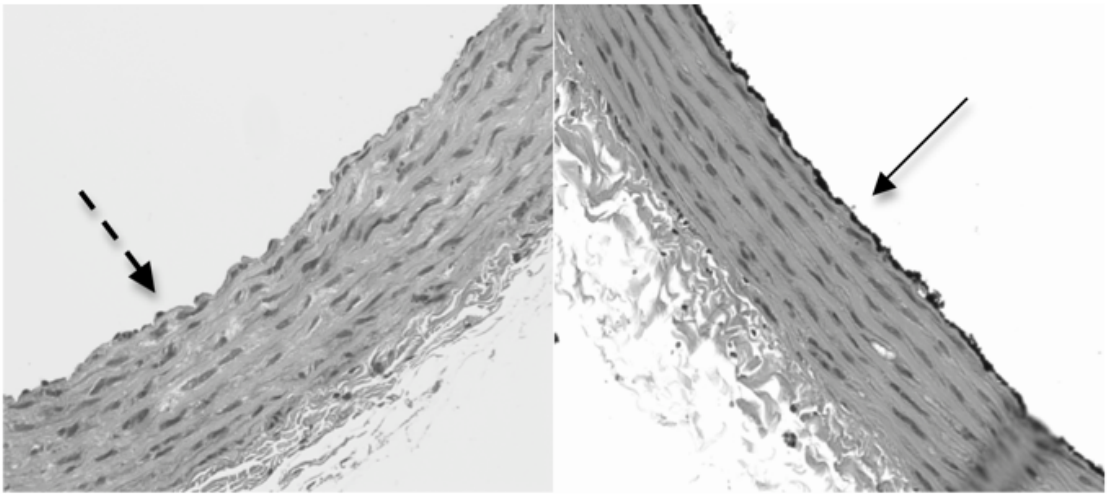

Figure 3.10: Histological cross-sections of the aorta. In freshly isolated rat aorta (left) endothelial cell nuclei are visible (dashed arrow) on the inner side of the aorta. In aorta cultured for 2 days with flow and pressure (right), a continuous endothelium, outlined by silver nitrate co-staining (black arrow) is still evident. In both frames, smooth muscle cells have normal appearance. (200X)

Discussion

Vessel culture technique is a powerful tool for the study of vascular biology. It provides a foundation, which enables gene manipulation of vascular cell in a controlled environment for better understanding of vascular cell function in normal and diseased state. An *ex vivo* vessel culture system has definite advantages over both the *in vivo* animal model and the *in vitro* cell culture model. *In vivo* systems are complex with its many uncontrollable variables and unwanted systemic effects that make interpret the interpretation of the effect of individual substances difficult (Mangiarua, Moss *et al.*, 1992). Simple cell culture models suffer from the fact that they often can not imitate the

function of intact vessel with which changes vascular cell phenotypes and gene expressions sufficiently well (Nagel, Resnick *et al.*, 1999). The *ex vivo* model, however, preserves the *in vivo* cellular phenotypes and matrix architecture while allowing experimental manipulation of a single target cell type. In our case (Chapter 4), this targeting amounts to the specific gene silencing of the aortic endothelial cells. This culture apparatus serves as a critical connection between *in vitro* cell culture and the *in vivo* animal model.

The ex vivo aorta culture setup

Maintaining a piece of vessel intact in an *ex vivo* environment has been accomplished for various species: i.e. porcine, rabbit and hamster (Bardy, Karillon *et al.*, 1995; Chesler, Ku *et al.*, 1999; Bolz, Pieperhoff *et al.*, 2000). These apparatus have been used to investigate the biomechanical and biochemical responses of vascular cells, i.e. endothelial-dependent vasomotor function, protein and DNA synthesis, extracellular matrix contents (Bardy, Merval *et al.*, 1996; Birukov, Bardy *et al.*, 1998; Chesler, Ku *et al.*, 1999; Bolz, Pieperhoff *et al.*, 2000). To our knowledge, rat aorta, however, has not been successfully cultured *ex vivo* for an extended period of time. Furthermore, little attention has been paid to the study of the endothelial-dependent whole vessel hydraulic conductivity property of whole rat thoracic aorta in organ culture.

We have constructed and performed an initial validation of an *ex vivo* rat aorta organ culture system. Our *ex vivo* culturing system is designed to preserve an isolated rat

aorta in a controlled incubating environment that provides the vessels with nutrients as well as mechanical forces similar to what an vessel would experience *in vivo*. Using a similar setup, Bardy and coworkers successfully cultured rabbit aorta for 8 days with independent flow and pressure applications (Bardy, Karillon et al., 1995). Our system consists of a peristalsis pump, which constantly drives warm media supplemented with serum through the aortic lumen at a desired flow rate and shear stress. The cardiac output of a rabbit is 97ml/kg body weight/min (Cumming e Nutt, 1962), so the calculated flow rate was 194-242.5ml/min for Bardy's experimental rabbits. Those authors set the perfusion rate for their rabbit aorta culture at 40ml/min, which is 20% of its physiological flow rate and the aorta was well preserved and the endothelial monolayer intact (Bardy, Karillon et al., 1995). Under a claimed perfusion pressure of 120/36mmHg systolic/diastolic respectively, however, the intima of cultured rat aorta is devoid of endothelial cells, as observed by Mangiarua and coworkers (Mangiarua, Moss et al., 1992). We set the flow rate, measured at the entrance of the aortic segment where it is cannulated, to be about 16.7ml/min. For male Wistar Kyoto rats, the cardiac output at their normal resting state is 25.8ml/min/100g body weight as determined by Beznak (Beznak, 1959). So for a rat of 400-450g, this means its cardiac output is about 100-116ml/min. We are scaling down the flow rate to 16.7% of physiological flow rate, based on our observation from early experiments that higher flow rates, i.e. 60ml/min (calculate shear stress 10 dynes/cm^2), cause massive endothelial damage in the entrance region, likely due to eddy formation at in the entrance region, and subsequent drastic increase in the measured vessel *Lp* value. Our design allows simple adjustment of the transmural pressure felt by the aortic segment by adjusting the height of the fluid media reservoir

within the incubator. Unit operations calculation predicted, and our directly measured lumen pressure at the proximal cannula showed a value of about 60mmHg. This pressure is within the physiological range and is appropriate to prevent the aortic lumen from collapsing, which would lead to endothelial damage.

Guyton considers diameter growth as a long-term process, generally accompanied by structural changes in wall mass (Guyton e Hartley, 1985). Langille also notice that carotid artery diameter reduction doesn't happen until a month after the onset of experimental restriction of blood flow, and it is not accompanied by any wall mass reduction for adult rabbits (Langille, Bendeck *et al.*, 1989). We did not observe any significant difference in the measured outer diameter of our aortas at either 60mmHg or 100 mmHg before and after 48-hour culture, probably because 48-hour is too short a time for the vessel to initiate an adaptation response or a degradation reaction.

Histological study

Considered as the true reflection of cell border by silver outlining (Poole, Sanders *et al.*, 1958), the silver nitrate staining technique was utilized to examine aorta *en face*. Comparing the silver nitrate endothelial cell staining pattern between freshly isolated and cultured aortas, we noticed no change in orientation or shape of the aortic endothelial cells. Artifacts such as breaks in the silver line, loss of endothelial cells, uneven staining or variation in cell sizes may be produced due to stretching or distortion of the aorta preparation. In addition, since as variations in the silver line may occur from one area to

the other on the same specimen as well as between samples, one must use caution when interpreting silver deposits on cell borders (Cotton e Wartman, 1961). These results do, however, give us an overall estimate of the endothelial cell size, shape and number. 'Cement substances', seen on the surfaces of endothelial cells, have been described as an indicator of cell injury or inflammatory responses (Mc, 1955). We did not observe such signs on the cells after 48-hour culture.

Light microscopic examination shows an unaltered media layer and most importantly, a continuous undisrupted endothelial layer in the aortic wall before and after culturing *ex vivo*. Even though smooth muscle cell proliferation can occur under static culture condition (Barrett, Mergner *et al.*, 1979; Gotlieb e Boden, 1984), we did not observed such proliferation using our *ex vivo* culture system.

The well-preserved endothelial monolayer examined by both staining methods is indicative that our application of shear stress and pressure has been successful in sustaining vessel and endothelial viability. Also, we suspect that any possible loss of endothelial cells during the early trauma of surgical removal of the aorta from the live animal and mirrored in the initial pre-culturing *Lp* measurement might be recovered by proliferation from adjacent endothelial cells, since endothelial cells are known to respond rapidly to injury by turning up their mitosis rate. As observed by Poole, endothelial cells stretch out from the edge of a denuded area in rabbit aorta within 24 hours of denudation; within 3 days, cell division becomes apparent and continues to cover up the bare area with new cells (Poole, Sanders *et al.*, 1958). The presence of functional endothelial cells

in our cultured vessel is also demonstrated by *Lp* measurement, the focus of the next paragraph. In some early experiments, after perfusing the aorta for 48 hours *ex vivo* at high flow rates, patchy losses of endothelial cells, due to flow entrance effects, on the intima surface appeared, which resulted in an *Lp* measurement that were significantly higher than from vessels having intact monolayers.

Lp measurements

Our *Lp* results show a 22.8% drop in *Lp* from 60mmHg to100mmHg (from $3.51\pm0.62\times10^{-8}$ cm/s/mmHg to $2.71\pm0.36\times10^{-8}$cm/s/mmHg) on fresh aortas. There is no significant difference in *Lp* before and after culturing at either transmural pressure (Lp=$3.30\pm0.31\times10^{-8}$cm/s/mmHg at 60mmHg and $3.12\pm0.55\times10^{-8}$cm/s/mmHg at 100mmHg). These unchanged *Lp* values further indicate that our culture technique was able to preserve the aorta intact, compared with its pre-culture state.

Tedgui and Lever's rabbit aorta results and Shou and Nguyen's *Lp* results for freshly isolated whole rat thoracic aorta as a function of transmural pressure (ΔP) showed similar trends to our measurements. Shou's found that *Lp* dropped by 40% as ΔP increased from 60mmHg to 100mmHg (4.69 to $2.79\pm0.62\times10^{-8}$cm/s/mmHg). Shou's data agree with Tedgui and Lever's of rabbit aorta *Lp* data. Tedgui and Lever found that when transmural pressure increase from 70 to 180mmHg, *Lp* decreased from 4.0 to 2.44×10^{-8} cm/s/mmHg for individual rabbit aortas by nearly 40%. Nguyen found a drop of 27.5%

from 60 to 100mmHg (2.55±0.15 to 1.84±0.15×10^{-8}cm/s/mmHg), with numbers that were consistently ~ 20% lower at each ΔP than that of Shou's data. Our measured *Lp* drop over this pressure range is smaller than those of both Shou and Nguyen's, but is quite close to Nguyen's result. Factors that may explain the difference in this *Lp* drop with pressure include a slight difference in the technique of vessel handling. We used a technique more similar to Nguyen: pre-conditioning the aorta to avoid hysteresis effect and measuring *Lp* using a precision glass tube and optical bubble tracking system, rather than a flexible tube mounted on a ruler together with a stop watch and measurement of bubble position at 5 minute intervals. Clearly the continuous readout and the precision glass tubing should lead to more accurate results, including a more accurate assessment of when the transmural flow and vessel area have become steady. Another difference between our measurements and those of Shou and Nguyen is that our more complex setup required us to use a much longer (about 3 meters long) section of tygon tubing, which needs to enter the back of the incubator to cannulate the proximal end of the aorta. In our system, we incubate the aorta in the enclosed environment of an incubator, rather than using either a heating pad or a large liquid reservoir hooked to a circulating heating-cooling bath to continuously warm the bottom of the petri-dish that hosts the vessel in the open air, as these two previous investigators had done. It is also worth noting that Shou and Nguyen's both used 350-400g rats, whereas the animals used for this study are larger, ranging from 400 to 450g to ensure maximal RNA harvest and subsequent RT-qPCR analysis for gene knockdown. Nonetheless, it is not clear why these differences in technique, other than possible problems with assessing steady state or in rat size, should account for the measured differences in *Lp*. Although we cannot with certainty pin down

the nature of this difference in the magnitude of the *Lp* drop, the absolute *Lp* values and the their trend has been consistent amongst all of these experimenters.

Chapter 4 The role of AQP1 in the transmural water flux across whole rat aortic endothelium *ex vivo* by siRNA knockdown

Abstract

By downregulating the expression of AQP1 in rat aortic endothelial cells and measuring its effect on the hydraulic conductivity (*Lp*) as a function of transmural pressure (ΔP) of the wall of excised whole rat aorta, we supply the missing piece of evidence needed to establish the transcellular water pathway across the aortic endothelium. The *ex vivo* preparation of aorta, as demonstrated by the functional and morphological integrity examinations detailed in Chapter 3, permits us to knockdown endothelial AQP1. We begin by measuring *Lp* at two ΔPs of 60 and 100mmHg, followed by introduction of AQP1 siRNA reagent in transfection medium through the lumen, flushing and re-measurement of *Lp* on the same vessel at the same pressures 48 hours post-transfection *ex vivo*. Finally, the endothelial layer was mechanical removed and *Lp* measured again on the same vessel at the same pressures a third time. The average percentages drop in total *Lp* (Lp_t) is more pronounced (37.35±12.97%) at 60mmHg and less drastic (8.71±3.76%) at 100mmHg, for n=5. The corresponding calculated drop in *Lp* attributed to the endothelia plus the subendothelial intima (SI) (Lp_{e+i}) is 59.8±11.6% and 15.5±9.1% at 60 and 100 mmHg respectively. These apparently pressure-dependent drops in Lp_t likely reflect, in part, a change in intrinsic endothelial permeability (Lp_e). We argue that AQP1 blocking decreases the number of pores available for water transport through the endothelial cells, thus shifting a larger fraction of the overall transmural pressure from the media to the endothelium. The resulting increase in force/unit surface

area on the endothelial layer causes early subendothelial intima compression and consequent endothelial cell blockage of the IEL fenestral holes to happen, leading to a portion of the sharp reduction in Lp_t. Our results show that aquaporin-1 contributes significantly to transmural water permeability. We argue the potential significance of a transcellular water flux pathway via AQP1 water channel proteins in the endothelial cell membranes in parallel with the clear paracellular route. Water flux through the leaky junctions surrounding very rare endothelial cells whose junctions are temporarily not tight carries LDL into subendothelial intima (SI), water passing through normal endothelial junctions (both through normal inter-endothelial cell junctions and transcellularly through endothelial aquaporins), might play an essential role in diluting the local LDL concentration in the SI region as LDL spread from the focal leaks, thereby slowing its rate of binding to SI extracellular matrix. This uniform flow is also likely active in flushing unbound lipid out of the SI and, subsequently, from the aortic wall. This could play beneficial role in terms of disease prevention and regression.

Introduction

The pressure-driven LDL transport into the aortic wall is considered as one of the most important factors that determine the likelihood that LDL will deposit in the SI and participate in early lesion formation. In this study we aim to clarify the nature of transendothelial water flow in the vessel by identifying the contribution of water flux through the transcellular route via aquaporin channels.

1. Transmural pressure driven water transport

Water filtration through the vessel wall is believed to occur predominantly paracellularly through inter-endothelial junctions (Huang, Rumschitzki *et al.*, 1994). Driven by transmural pressure, water and hydrophilic solutes smaller than the size of albumin are carried through the functional clefts between endothelial cells (ECs) into the aortic wall. Rarely, there exist transient "leaky junctions" associated with cell turnovers (mitosis/cell death). Even though at any given time only a small proportion of ECs undergo mitosis (~0.01%) or death (~0.1%) (Chen, Jan *et al.*, 1997), numerous groups have shown that the 'leaky junctions' associated with ECs turnover are frequently highly associated with endothelial hyperpermeability to macromolecules i.e. LDL, HRP, EBA (Weinbaum, Tzeghai *et al.*, 1985; Stemerman, Morrel *et al.*, 1986; Lin, Jan *et al.*, 1988; Truskey, Roberts *et al.*, 1992). Transmural water flux can also direct the deposit of LDL to pre-existing lesions. After incubating the arteries with LDL and albumin at 70mmHg for 2 hours and at 160 mmHg for 5 minutes, 30 minutes and 1 hour and 2 hours, *Curmi et al.* (Curmi, Juan *et al.*, 1990) examined the transmural distribution of these solutes on serial frozen sections. They observed an overall increase in the wall's uptake of albumin and LDL at the higher transmural pressure, which is probably due to endothelial hyperpermeability and pressure-driven convection. After 1-hour incubation at 160mmHg the distribution of labeled albumin was uniform throughout the artery while the majority of labeled LDL accumulated in the inner layers (closer to the lumen) with decreasing concentration in the outer two thirds of the media layers. They explained this distribution

pattern in conjunction with the result from a washout experiment: the vessels were subject for 30-minutes to a tracer-free solution after a 30-minute incubation with each tracer at the same pressures. The washout removed albumin from the artery wall, but did not affect the concentration of LDL. Thus as one increases the transmural pressure, there is an enhanced endothelial hyperpermeability and pressure-driven convection of LDL. They interpreted these data as meaning that the higher transmural pressure causes the arterial wall to compact, thereby trapping the LDL that is convected into inner media. Actually, in order to draw such a conclusion, they should have dropped the pressure to 70 mmHg and carried out the washout experiment. Had the LDL then washed out, they could have concluded that it was indeed wall compaction that had trapped the LDL. The reported results could also have resulted from the LDL in the SI having mostly (a small portion of it was indeed washed out) bound to SI extracellular matrix and LDL in the media might have been internalized via the smooth muscle cell scavenger receptor. If this was the case, then a washout at 70 mmHg would have had no effect. In either case, it is clear that, transmural water flux plays an essential role in controlling the delivery and retention of LDL leading to early lesion formation of arthrosclerosis.

The Starling's hypothesis depicts that the fluid movement in the microvessel wall is determined by the hydrostatic and oncotic transmural pressure differences. Water filtration can be characterized by the medium's hydraulic conductivity (*Lp*), which is the ratio of the steady-state transmural water influx (*Jv*) to the pressure differences (ΔP). It is described in the following equation:

$$Lp = \frac{Jv}{(\Delta P - \sigma\Delta\pi)}$$

Lp is the hydraulic conductivity (cm/s/mmHg), *Jv* is the transmural water flux, expressed as volume flow rate per unit surface area through which water flows (cm^3/s), ΔP is the hydrostatic pressure difference, Δπ is the osmotic pressure difference and σ is the osmotic reflection coefficient. Because in the context of our study the effect of osmotic pressure is trivial in comparison to hydrostatic pressure (Tedgui e Lever, 1984), the hydraulic conductivity (*Lp*) of the aorta can be simplified to be equal to:

$$Lp = \frac{Jv}{\Delta P}$$

Tedgui and Lever were one of pioneers characterizing water filtration through intact aortic whole walls. They discovered that when one raises a rabbit aorta's transmural pressure augmented from 70 to 180mmHg, its hydraulic conductivity (*Lp*) decreased from 4.0 to 2.44×10^{-8}cm/s/mmHg by nearly 40%. Upon endothelial denudation, they found that *Lp* increased to 5.36 and 5.27×10^{-8}cm/s/mmHg at 60 and 100mmHg, respectively. They argued that this reduction the resistance to water flow was likely due to both the removal of a layer of resistance and the relief of a portion of the strain of the interstitial matrix via denudation. The hydraulic conductivity of the vessel wall apparently turned out to be dependent on the transmural pressures as well as on the integrity of the endothelial monolayer. Further changes in these factors can alter the

resulting water permeability through the vessel wall (Tedgui e Lever, 1984). The facts that Tedgui and Lever used different vessels for different *Lp* measurements, and that the variations between individual vessels can be high add additional complexities to the interpretation of their data. Baldwin and Wilson improved the *Lp* measurement technique by using the same rabbit aorta for *Lp* measurements at multiple hydrostatic pressure points. Their study showed a similar *Lp* trend: a nearly 40% drop in *Lp* from 50 to 75mmHg and pressure-insensitive with further increase in transmural pressure. However, their data obtained at lower pressures (50 and 75mmHg) showed very large standard deviations, and these large deviations robbed any apparent trends in *Lp*(ΔP) at these pressures of statistical significance. In addition, their *Lp* values were nearly double those of Tedgui and Lever (Baldwin, Wilson *et al.*, 1992).

Shou *et al.* (Shou, Jan *et al.*, 2006) adapted Baldwin and Wilson's technique to the much smaller rat vessels and, with far more reasonable error bars, measured *Lp*(ΔP) at six transmural pressures, both with intact and denuded endothelia, on the same vessel. They found (see Figure 4.1) the trends observed by Tedgui and Lever indeed persists when measurements are made on a single vessel with finer ΔP resolution and, moreover, that Tedgui and Lever's rabbit data superimpose upon their rat data. It appears that variations between these species in the aorta are negligible. Beginning with Shou, our group has developed extensive experience in measuring *Lp* as a function of transmural pressure using very small rat aortas, both with intact and denuded endothelium. Y. Shou, T. Nguyen and Y. Sun all have carried measured *Lp* vs.ΔP with intact and denuded endothelium on the same vessel. Shou showed that *Lp* dropped by 40% as ΔP increased

from 60mmHg to 100mmHg and remained flat till 140mmHg. T. Nguyen showed a similar *Lp* trend, a drop of 27.5% from 60 to 100mmHg, but her values were consistently 20% lower at each ΔP than those of Shou. Our lab's *Lp* values for the deendothelialized vessels are again higher than for the intact vessels, nearly doubles that of intact vessels, and are pressure-insensitive, as in Tedgui and Lever. The aortic endothelium accounted for about 47% (Shou) and 37% (Nguyen) of the total aortic resistance (1/*Lp*) by calculation. The difference between the *Lp* data of these two investigators might be attributed to differences in technique in measuring *Lp*. For example, Shou used a traditional method of measuring the movement of the bubble in flexible tubing taped against a ruler by eye at 5-minute time intervals clocked by a stopwatch. Nguyen modified the *Lp* measurement system by introducing a sphectrophotomic mounted on a motor-driven ball screw with feedback that automatically and continuously tracked the front bubble meniscus (Nguyen, 2008). This bubble tracking system is similar to that used by the Tarbell group used for its *in vitro* work (Cancel, Fitting *et al.*, 2007). Slight differences in the vessel preconditioning protocol might have also been a factor in these differences.

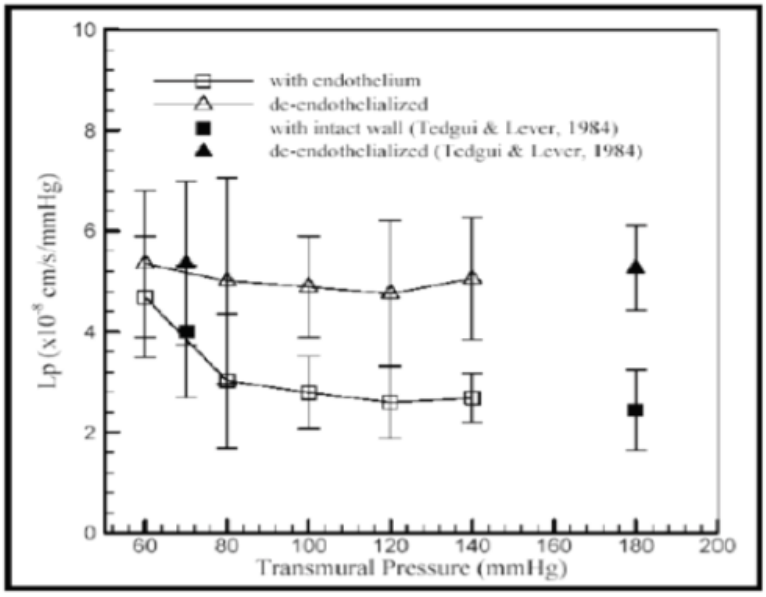

Figure 4.1: A graph of the hydraulic conductivity (*Lp*) measured as a function of transmural pressure of rat aorta at multiple pressures, with and without endothelium, on the same vessel. The data were plotted with experimental rabbit *Lp* data from Tedgui and Lever, 1984. Our rat aorta *Lp* data quantitatively agreed with those of the rabbit aorta both with and without endothelia (Shou, Jan *et al.*, 2006).

2. The convection-diffusion model and intima compaction theory

Is macromolecule transport dominated by diffusion or convection? In studies of macromolecular transport, horseradish peroxidase (HRP) is often used as a macromolecular tracer and injected into rat for various circulation times. It was found that, for circulation times less than ~4 minutes, HRP tracer displays in rare localized spots rather than spreading into the aortic wall in a uniform fashion. HRP spot sizes increase rapidly with increasing circulation times, reaching ~200μm diameter within 2 minutes, and seem to slow down markedly, possibly to a steady value, around 4 minutes circulation. Beyond 4 minutes, a diffuse HRP staining pattern was observed that makes it

difficult to distinguish spot from background (Chuang, Cheng *et al.*, 1990). If the growth of an HRP spot were diffusion dominated, a much slower early growth and continuous growth at longer times would be observed. In fact, the tracer spot growth as a function of circulation time was far too fast for any realistic diffusivity. The only other possibility was that this type of transport might be advection-mediated (Huang, Rumschitzki *et al.*, 1994).

An initial advection-diffusion model was developed that took into account that the SI and the media were separated by an IEL, but this theory showed very little improvement over the earlier pure diffusion theories (Yuan, Chien *et al.*, 1991). Huang *et al*. extended these earlier models to take into accounts of the difference in the transport property of the SI and the media layers of the aortic wall. Using Frank and Fogelman's ultra-rapid freezing, rotary shadow imaging scanning electron micrographs of the aortic SI, Huang et al noticed the detailed, sparse SI ultrastructure and extracted its characteristic fiber sizes and spacings. Using these numbers they constructed an *ab initio* fiber matrix theory for the SI transport parameters. They found that the permeability of the more porous SI, which is made of a loose extracellular matrix of proteoglycan and collagen, is two orders of magnitude greater (130-250 times) than that of media. As a result, the theory showed that transmural pressure drives water flow that advects solutes across the localized leaky junction into the subendothelial intima (SI) space. Once inside the SI space, water flows (and advects tracer) predominantly parallel to the endothelium and radially away from the leaky junction in the SI and, eventually, through the fenestrated pores of internal elastic lamina (IEL) and into the media. This SI water flow is

the key to the rapid macromolecular spread in the SI (See Figure 4.2) (Huang, Rumschitzki *et al.*, 1994)

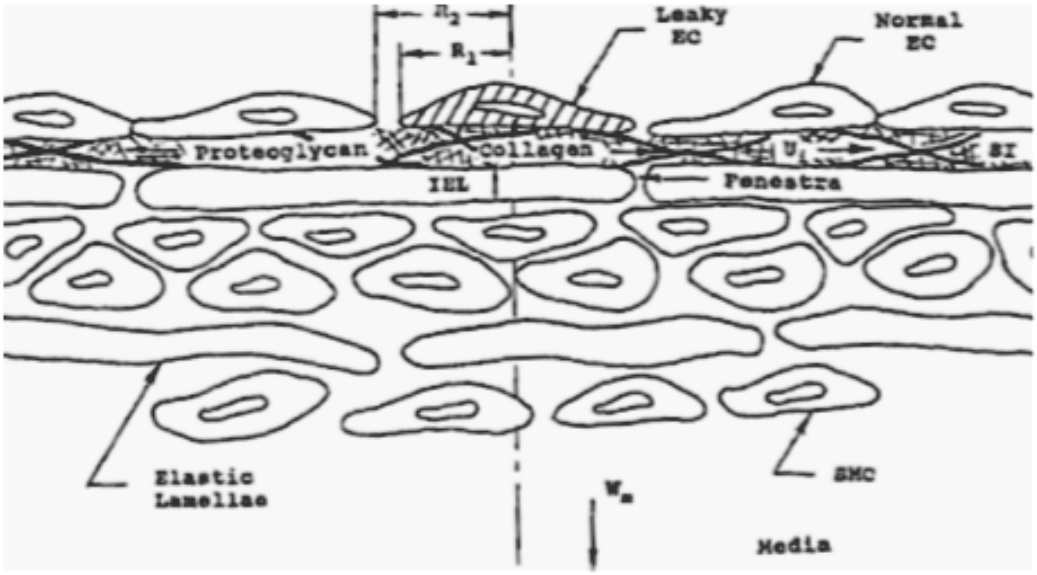

Figure 4.2: Schematic illustration of macromolecular transport via water convection. Macromolecules are carried in the SI away from the leaky site in a direction parallel to the endothelial monolayer and eventually the flow proceeds through the fenestral holes in the IEL and into the media (Huang, Rumschitzki *et al.*, 1994).

As the transmural pressure increases, the driving force for convective flow also increases; however, over the range 60-~100mmHg, *Lp* decreases. Huang *et al.* proposed a mathematical model to explain the difference in hydraulic conductivity upon increasing the transmural pressures based on Tedgui & Lever and Baldwin & Wilson's studies. As noted above, the calculated (from Frank and Fogelman's freeze etchings) permeability of the much more porous SI is much higher than that of the more dense media (Huang, Rumschitzki *et al.*, 1994). As a result, the SI is far more compressible under increasing pressure than the media, whose potential degree of compaction with increasing pressure in the physiological range is negligible. When the aortic SI is compressed under pressure loading, the resulting increase in fiber density raises resistance to flow and reduces water

permeability. More significantly, though, under maximal loading, the endothelial cells can partially block the fenestrated pores in internal elastic lamina (IEL), which drastically increase resistance to water flow into the media and therefore the wall's overall decrease in water permeability. Beyond the maximum compaction, the far stiffer collagen fibers prevent the SI from being further compressed and vessel filtration properties suffer no further alteration with increasing transmural pressure within the physiological range. The data suggest that the SI is maximally compressed somewhere between 80-100mmHg. Deendothelialization removes the endothelial resistance and also the potential for blockage of the IEL fenestrate, resulting in an elevated *Lp* that is ΔP-independent, in accordance with observation. According to this theory, at even lower pressures than measured in the two early studies, the SI would be even less compacted and vessel *Lp* might even be higher although the difference is likely small since, even at 60mmHg, the IEL fenestrae are likely fully unblocked. This intimal compaction theory successfully models the *Lp*-trends observed by both group (Huang, Rumschitzki *et al.*, 1997). Shou *et al.*'s *Lp* data on other rat vessels suggest that SI compression under ΔP loading may also play a role in *Lp* (ΔP) in these other vessels (Shou, Jan *et al.*, 2006).

3. The effect of aquaporins blocking on whole aortic hydraulic conductivity

$HgCl_2$ is the most well-known aquaporin water channel blocker. It binds to cysteine189 located near the entrance to aquaporin-1's narrow aqueous pore, which blocks the passage of water molecule (Preston, Jung *et al.*, 1993). Mercuric compounds have been used extensively for its effect on reducing the water permeability of

erythrocytes and renal tubules epithelial cells in response to a step change in extracellular osmolarity (Macey e Farmer, 1970; Whittembury, Carpi-Medina *et al.*, 1984). Unfortunately, this mercury treatment, at high enough concentration and exposure times, can be cytotoxic; it can lead to cell swelling and impaired normal cell volume regulation and possibly cell death in situation of osmotic challenges. Since the binding of mercuric compounds is non-specific, it might also disrupt major membrane transporter proteins that are responsible for ion or solute transport, contributing to the cell's inability regulate its volume, as observed in hepatocytes and lymphocytes (Sarkadi, Cheung *et al.*, 1985; Ballatori e Boyer, 1996).

Blocking aquaporins with $HgCl_2$ enables one to elucidate the contribution of the aquaporin-mediated transcellular pathway to transmural water permeability. To achieve this goal, one should measure *Lp*(ΔP) on a whole aorta *ex vivo*, introduce $HgCl_2$ into the lumen of the aorta, flush and re-measure *Lp*(ΔP) on the same vessel. To the best of our knowledge, such experiments in our group are the first experiments that used $HgCl_2$ to alter aortic wall *Lp*. Shou reported a pilot *Lp* experiment using 10μM $HgCl_2$. Shou found an *Lp* decrease occurs throughout the entire range of ΔPs, mostly notably by 27.5% at 60 mmHg and less at 100mmHg (Shou, 2005). Nguyen, in more careful follow-up experiments, found essentially the same result: that AQP1 blocking induces a significant decrease in *Lp*, and this decrease is most pronounced at 60mmHg, i.e. the decrease is pressure-dependent. It decreases by 32±4% at 60mmHg, 11±2% at 100mmHg and by 5±3% at 140mmHg. Note all of these changes are statistically significant because all measurements were made on the each vessel, and each vessel showed a drop in *Lp* at

each ΔP. This inhibitory effect could be reversed by reduction of the cis-Hg+ bond by β-mercaptoethanol (ME). *Lp* of the denudated aorta showed no significant change with and without AQP1 inhibitory treatment, indicating that water transport in the media occurred mainly around SMCs, which do not have tight junctions, and not across them (Nguyen, 2008).

Our group attempted to explain this observed pressure-dependent decrease in *Lp* after AQP1 blocking with a theory that posited that endothelial AQP1 inhibition promotes the shift of a portion of the overall ΔP from the media to the endothelium, leading to the critical force/area on the endothelium for SI compression being reached at a lower overall ΔP. Since this SI compression can block the fenestrated holes in the IEL, it can reduce *Lp* at lower ΔP. HRP has been commonly used as a tracer to study the transport properties of large vessel such as the aorta. If this explanation of the change in *Lp* with increasing ΔP is correct, then this SI compression at a lower ΔP upon $HgCl_2$ treatment should lead to different rates of HRP spot growth. Using Zeng *et al*'s (Zeng, 2006) corrected version of Huang *et al.*'s theory of water and macromolecular transport in the artery wall, Sun predicted and measured these differences. A reduced *Lp* should lead to a decrease in transmural clearance of the tracer, resulting in larger, not smaller spots. The theory predicted and the experiment quantitatively confirmed this prediction that $HgCl_2$ treatment indeed leads to faster-growing observable HRP spots (Sun, 2008).

Despite extensive controls to find dosages and exposure times that were not cytotoxic, the generic cytotoxicity and non-specific action of $HgCl_2$ inhibition means that

some will never be fully convinced by a mercury-based study. As such, an alternative improved intervention method to alter AQP1 expression is required. In this study, we use siRNA to suppress endogenous AQP1 expression and test to see if this knockdown of AQP1 lowers whole rat aortic hydraulic conductivity (*Lp*) as a function of transmural pressure (ΔP) *ex vivo*. The *ex vivo* preparation of the aorta, as demonstrated by the functional and morphological integrity examinations in Chapter 3, permits us to knockdown endothelial AQP1 in the whole vessel preparation *ex vivo*. AQP1 siRNA can be introduced into the vessel lumen and endothelial cells can be harvested for quantitative assessment of gene knockdown. *Lp*(ΔP) is first measured with intact endothelia immediately after vessel excision and then again, after endothelial AQP1 knockdown and, finally, a third time after endothelial denudation, all on the same vessel at the same transmural pressures. If our original mercury experiments were indeed valid, one would expect that such a suppression of AQP1 would have a significant impact on water filtration through aortic wall, but not differ substantially from our previous experiment with $HgCl_2$ inhibition.

Materials and methods

1. siRNA transfection

Using sterile technique, we isolate rat thoracic aorta with intact endothelia under physiological pressure, as described in Chapter 3, and hooked to the apparatus described therein. Baseline *Lp* measurement was immediately performed. After initial *Lp*

measurement, experimental media was flushed out and aortic endothelial cells were transfected either with Lipofectamine 2000 (Invitrogen) lipid carrier either alone or with siRNA reagent plus lipid carrier complexes in OPTI-MEM based on the concentration that was tested for *in vitro* transfection. The *in vitro* data has shown that using 10pmol of siRNA per 1.5×10^5 cells gave the maximum protein knockdown while minimizing toxicity by maintaining endothelial monolayer integrity (Chapter 2). The endothelial cells were incubated with transfection reagent for 6 hours. OPTI-MEM was then removed and the lumen was flushed briefly to remove any excess lipofectamine. The vessel was cultured for 48 hours following our *ex vivo* vessel culture protocol (Chapter 3). A second *Lp* measurement was performed after 48 hours. This is followed by a third *Lp* measurement upon denudation as described in Chapter 3. In some cases, instead of performing endothelial denudation, we extracted the endothelial cells for PCR study 48 hours post transfection.

In order to ensure that introducing tranfection reagent alone without siRNA wouldn't cause any endothelial damage or experimental artifacts, we conducted control experiment where we introduced into the vessel lumen lipofectamine lipid carrier alone (with no siRNA) and incubated it there for 6 hours based on the manufactures' protocol. The lumen was then flushed with OPTI-MEM briefly to remove any remaining lipofectamine. The vessel was then perfused and superfused based on our *ex vivo* vessel culture protocol with culture media (Chapter 3). *Lp* was then measured 48 hours later on the same vessel at the same pressures and compared with earlier technique controls that involved *Lp* measurement after 48-hour incubation, but with no lipofectamine incubation.

2. Lumenal extraction of endothelial RNA

We increase the RNA yield for qPCR by combining two aortas' RNA harvest. Due to the restriction of our *ex vivo* aorta organ culture setup, we are only able to transfect and maintain the vitality of one aorta at a time. The first aorta after transfection for 48 hours is submersed in a chemical RNA preservative called RNAlater (Ambion) while we carried out the second aorta transfection. The two aortas' lumens were quickly flushed with PBS and with 800μl of TRIzol reagent using a 1ml syringe. The run-through was collected into a microcentrifuge tube and incubated for 5 minutes at room temperature. The mixture was centrifuged at 4°C for 15 minutes upon addition of chloroform (0.2ml chloroform per 1ml Trizol reagent used). The resulting colorless aqueous phase was transferred into a new tube and mixed with an equal amount of 70% cold ethanol. RNA purification was performed using an RNeasy mini kit (QIAGEN) according to the manufacturer's instructions.

3. RT-qPCR (see chapter 2)

4. Calculation of Lp_{e+i}

For the intact vessel, the measured *Lp* stands for the total *Lp* (Lp_t). For the denuded vessels, *Lp* represents *Lp* of the media + IEL (Lp_{m+I}). 1/ Lp_t is the total

resistance of the intact aorta. 1/ Lp_{m+I} is the resistance of the vessel of the media and IEL. 1/ Lp_{e+i} is the resistance of the endothelium plus SI. The resistance of endothelium plus intima ($1/Lp_{e+i}$) can be extracted from to the overall wall resistance (1/ Lp_t) and the resistance of media + IEL (1/ Lp_{m+I}) from the following equation:

$$\frac{1}{Lp_t} = \frac{1}{Lp_{e+i}} + \frac{1}{Lp_{m+I}}$$

Results

1. Verification of RNA knockdown by RT-qPCR

Dancu *et al.* and Nam *et al.* have harvested endothelial cells in rabbit aorta and mouse common carotid artery using the Trizol method *in situ*, which protects vulnerable RNA against attack from natural endonuclease upon cell lysis (Dancu e Tarbell, 2007; Nam, Ni *et al.*, 2009). Using similar methods, we are able to increase the RNA yield by combining two aortas' harvests using a chemical RNA preservative, as described above. Figure 4.3 shows the fold change ($2^{-\Delta\Delta CT}$) of the transfected AQP1 mRNA relative to non-transfected controls, which is considered as 1. The amount of AQP1 RNA (treated or untreated with siRNA) is normalized to an endogenous control (GAPDH) (two aortas combined sample). Overall, there is an 84.5% knockdown in AQP1 RNA when comparing transfected vessels to controls.

To test the purity of the harvested RNA, we carried out RT-qPCR analysis using smoothelin (smooth muscle cell-specific marker) and vWF (*Von Willebrand factor*, endothelial cell-specific marker). RT-qPCR results confirmed (Figure 4.4) the excellent purity of the endothelial cells harvested. The fold change of endothelial cell smoothelin to vWF, which is considered as 1, is 0.015 and 0.018 for control vessels and transfected vessels respectively. Our results showed that luminal RNA can be obtained using Trizol method from both freshly excised control aorta and cultured aorta. This method provides sufficient quantity and purity without significant smooth muscle RNA contamination.

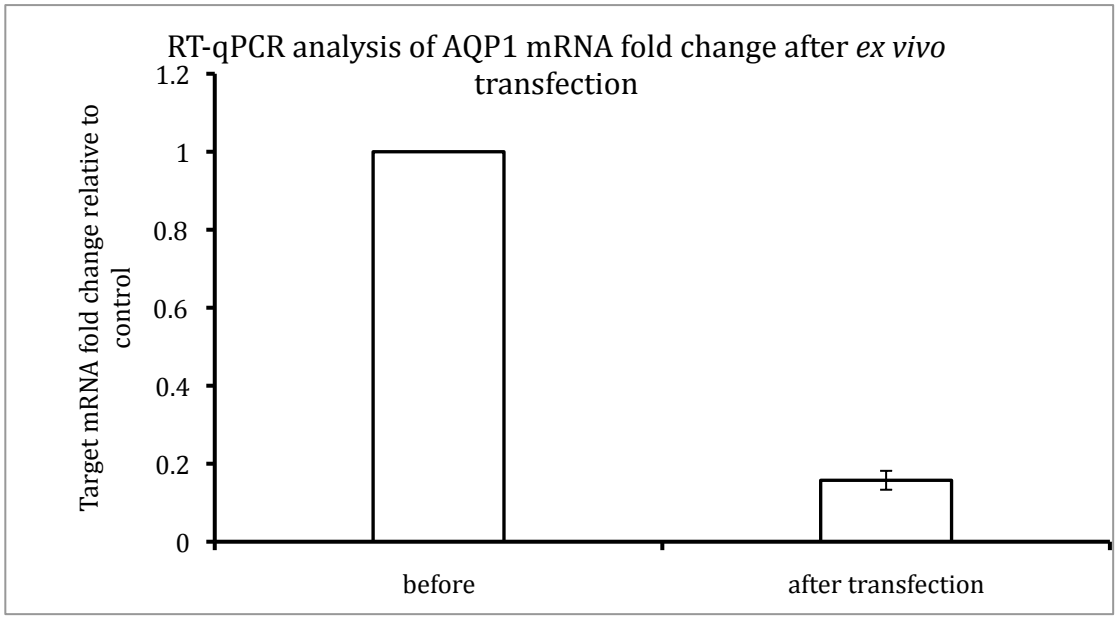

Figure 4.3: Shows the fold change ($2^{-\Delta\Delta CT}$) of transfected AQP1 mRNA relative to non-transfected controls, which is considered as 1. The amount of AQP1 mRNA (treated with siRNA) is normalized to an endogenous control (GAPDH) (2 aortas combined sample). Overall, there is an 84.5% knockdown in AQP1 RNA when comparing transfected vessels to controls.

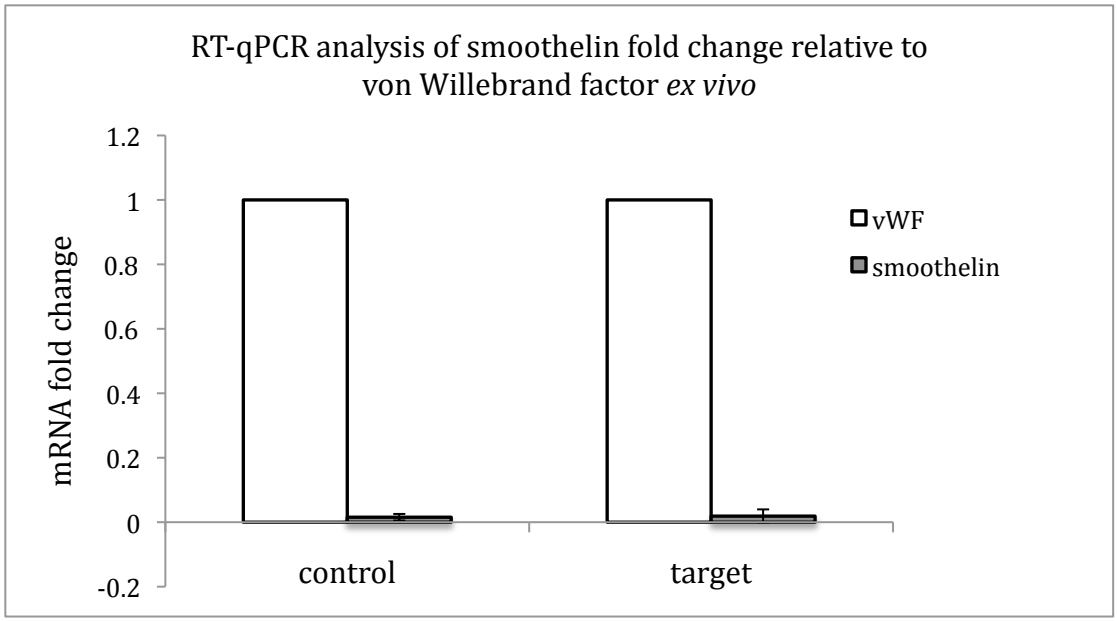

Figure 4.4: Shows high purity of endothelial cells harvested. For control vessels, smoothelin (smooth muscle cell-specific marker) is only 0.015 fold change to vWF (endothelial cell-specific marker), while transfected vessels, smoothelin is 0.018 fold relative to vWF (2 aortas combined sample).

2. Control study: intact vessel transfected with lipofectamine alone and with lipofectamine with containing scrambled siRNA

Lipofectamine 2000 lipid carrier and non-target control (scrambled siRNA) were tested as a control, before transfecting cells with siRNA against AQP1, to ensure that the lipid carrier alone or scrambled RNA would not compromise the integrity of the aortic endothelial cells. *Lp* values were measured on newly isolated aortas at 60 and 100mmHg transmural pressures and re-measured 48 hours after lipofectamine and scrambled siRNA treatment. Table 4.1 shows the result of *Lp* measurements before and after lipofectamine incubation. There is no significant difference between *Lp* values before and after lipofectamine and scrambled siRNA treatment at each transmural pressure.

Table 4.1: Control experiments: *Lp* of aorta before and after lipofectamine (n=3) and lipofectamine with scrambled siRNA treatment (n=1) (Values are means ± standard deviation)

	Lp (E-8cm/s/mmHg)	Time 0	Time 48 hour
Lipofectamine control (n=3)	60mmHg	3.15 ± 0.21	3.03 ±0.21
	100mmHg	2.67 ±0.14	2.85 ± 0.22
Scrambled siRNA (n=1)	60mmHg	3.59	3.48
	100mmHg	2.69	2.68

3. Control experiments: endothelial denudation

The endothelial layer can be mechanically removed using a small Epon ball with a slow rotary motion during withdrawal for the vessel. This denudation process removes the flow resistance attributed to the endothelial layer. The *Lp* measured after denudation is the *Lp* of the media plus IEL (Lp_{m+I}), which reflects the hydraulic filtration property of the media+IEL layer. Lp_{m+I} is $6.29\pm0.49\times10^{-8}$ cm/s/mmHg at 60mmHg and $6.09\pm0.85\times10^{-8}$cm/s/mmHg at 100mmHg for control vessels without transfection. These values nearly double those of intact vessel (see Chapter 3, for fresh aorta *Lp* is $3.51\pm0.62\times10^{-8}$ cm/s/mmHg and $2.71\pm0.36\times10^{-8}$cm/s/mmHg and for cultured aortas *Lp*=$3.30\pm0.31\times10^{-8}$ cm/s/mmHg and $3.12\pm0.55\times10^{-8}$cm/s/mmHg at 60 and100mmHg, respectively). These data agrees with Tedgui and Lever, Baldwin and Wilson, Shou and Nguyen's results.

Table 4.2 shows that there is no significant difference between Lp_{m+I} values of control vessels and that of post-transfected ones, indicating that siRNA inhibition of

endothelial AQP1 via lumen incubation doesn't affect Lp_{m+l} (n=3, p=0.12 at 60mmHg and p=0.84 at 100mmHg between control and transfected vessels).

Table 4.2: Lp_{m+l} values of vessels that were either denuded or transfected with siRNA and then denuded. Values are means ± standard deviation (n=3)

Lp value of denuded aortas ($\times 10^{-8}$cm/s/mmHg)	60mmHg	100mmHg
Control	6.29±0.49	6.09±0.85
Transfected	5.74±0.33	5.90±0.83

4. The effect of AQP1 suppression on aortic Lp measured as a function of transmural pressure

We measured hydraulic conductivity (*Lp*) at two different transmural pressures, 60 and 100mmHg. We then introduce AQP1 siRNA knockdown reagent through the lumen and re-measure *Lp* on the same vessel at the same pressures 48-hours post-transfection *ex vivo*. Finally, the endothelial layer is mechanical removed and *Lp* measured again on the same vessel at the same pressures. Figure 4.5 shows that when using siRNA at 20pmol, cell loss is very discernible.

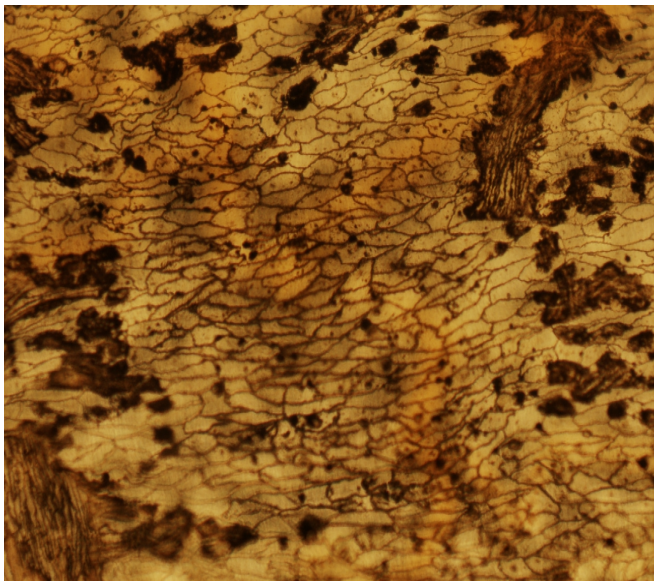

Figure 4.5: Shows endothelial cell silver nitrate staining of rat thoracic aorta *en face* with discernable cell loss (dark areas) after a 20pmol of siRNA treatment (Magnification: 200X)

Figure 4.6 shows *Lp* baseline values, which demonstrates similar trend as measured by Tedgui and Lever, Baldwin and Wilson and Shou and Nguyen. Denuded vessel nearly doubles the values of the intact vessel Lp_t giving denuded values of 5.74±0.33 and 5.90±0.83 $\times 10^{-8}$cm/s/mmHg at 60mmHg and 100mmHg, respectively.

Figure 4.6 also shows AQP1 at 10pmol inhibition causes a significant drop of Lp_t of roughly 37.35±12.97% at 60mmHg from 3.32±0.16 to 2.07±0.42$\times 10^{-8}$cm/s/mmHg (n=5, mean±standard deviation). At this pressure, the endothelium + intima ($1/Lp_{e+i}$) contributes about 30.5±4.0% of the total wall resistance ($1/ Lp_t$). AQP1 suppression decreases Lp_{e+i} by 59.8±11.6 % from 7.98±0.64 to 3.17±0.85$\times 10^{-8}$cm/s/mmHg. At 100mmHg, the decrease in Lp_t is attenuated to about 8.71±3.76% at from 2.95±0.29 to 2.69±0.20$\times 10^{-8}$cm/s/mmHg. And this drop in Lp_{e+i} was less pronounced as well

(15.5±9.1%). To conclude, the average percentage drop in Lp_t (Lp_{e+i}) is 37±12.97% (59.8±11.6 %), 8.71±3.76 % (15.5±9.1%), at 60 and 100 mmHg respectively.

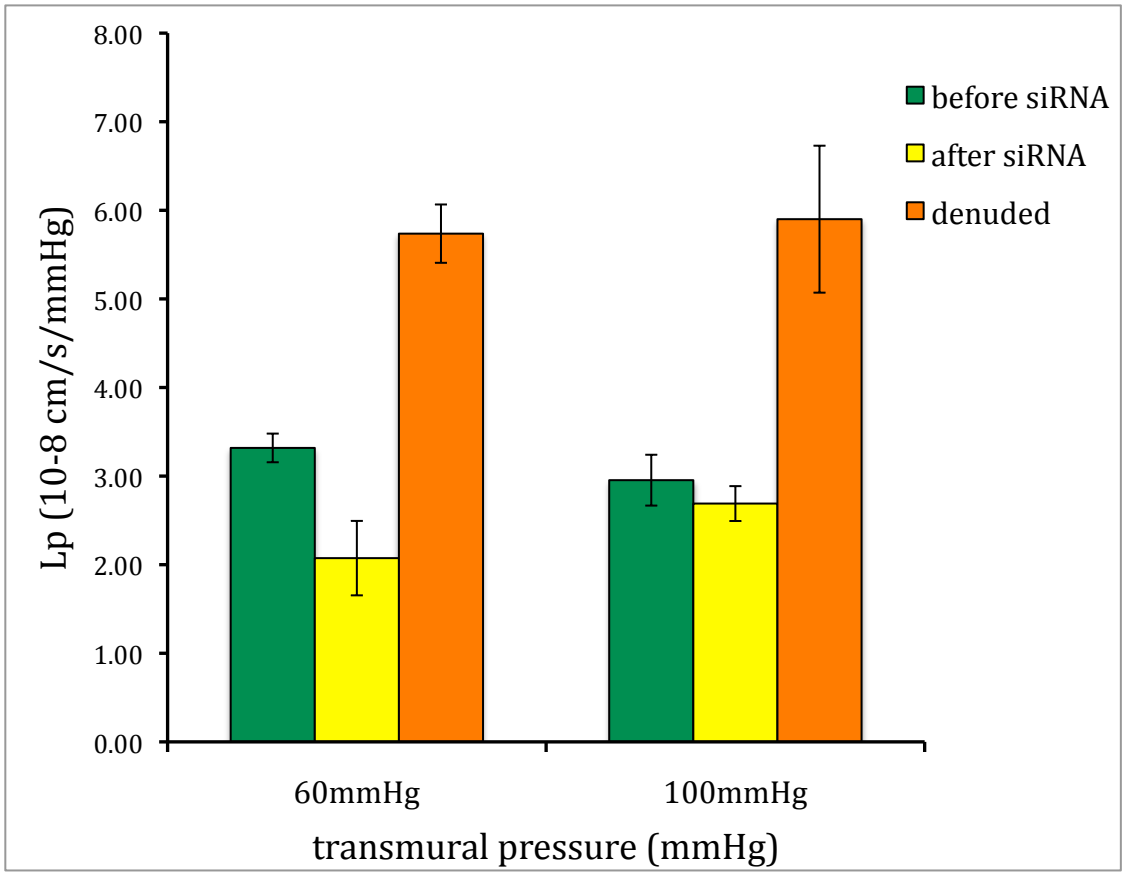

Figure 4.6: The effect of AQP1 suppression on whole aorta hydraulic conductivity *Lp* (ΔP) before and after treatment with AQP1 siRNA reagent. (Values are means ±standard deviation)

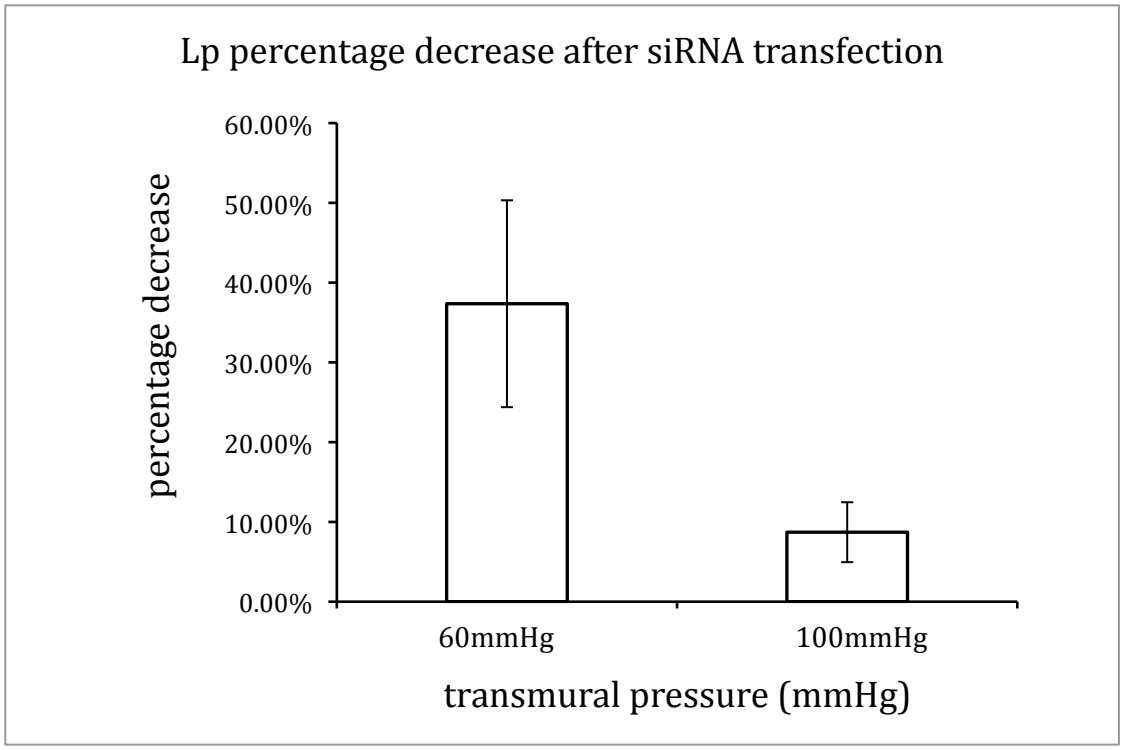

Figure 4.7: Percent drop in *Lp* upon endothelial AQP1 knockdown by siRNA reagent in the intact rat aorta. Values area means ± standard deviation (n=3).

Discussion

AQP1-mediated transcellular water transport plays an important physiological function in fluid transport in the kidney and in erythrocytes. Transmural-pressure-driven water transport is assumed to occur only paracellularly through the endothelial cell-cell junctions (including both normal and leaky junction clefts). Our experiments challenged this conventional belief and argue that the transcellular pathway via aquaporins likely also contributes to the water filtration property of the aorta. In this study, we have investigated the nature of such water filtration by extracting, i.e., shutting off, the contribution of the transcellular route via aquaporin water channels from total water filtrated and measured the resulting change in water filtration. That is, we have measured

the water flux through the walls of intact, whole rat aortas *ex vivo* and calculated the corresponding hydraulic conductivity (*Lp*) at two different transmural pressures (60 and 100mmHg) immediately after the aorta is freshly isolated from the rat. We then lumenally expose the endothelia to AQP1 siRNA knockdown reagent and re-measured *Lp* on the same vessel at the same pressures a second time after a 48-hour incubation, so as to allow for maximal siRNA aquaporin-1 knockdown. Finally, the endothelial layer was removed by mechanical denudation and *Lp* was measured a third time on the same vessel at the same pressures. Our studies show that AQP blocking decreases *Lp* for cultured aorta, indicating AQP1 contributes significantly to aortic endothelial hydraulic conductivity in whole rat thoracic aorta.

A simple method of luminal endothelial cell RNA extraction

We described here a simple method of harvesting endothelial cell RNA from rat aorta with very little smooth muscle cell contamination. Due to the relatively small size of the rat aorta compared with aortas of larger animals (i.e. rabbits, pigs, etc.), it is very difficult to isolate aortic endothelial cell in large quantity. Vascular endothelial cells can be isolated by an outgrowth method from aortic rings (Mcguire e Orkin, 1987), enzymatic dissociation (Folkman, Haudenschild *et al.*, 1979) and mechanical scraping (Lewis, Hoak *et al.*, 1973; Ryan, 1984). However, these techniques require a large population of endothelial cell to work with and unavoidably produce of a mixed population of cells, which then requires additional sorting steps such as magnetic bead sorting and fluorescence-activated cytometry using endothelial cell-specific markers

(Chen, Sega *et al.*, 2004). Recently, a technique has been developed to directly harvest endothelial RNA using the Trizol reagent. Subsequently RT-qPCR using both EC and smooth muscle cell marker can help verify the purity of extraction simultaneously with the test of target gene expression (Dancu e Tarbell, 2007; Nam, Ni *et al.*, 2009). Developed by Chomczynski and Sacchi, Trizol reagent is a mixture of guanidine isothiocyanate and phenol-chloroform utilized in the single-step RNA isolation method for biological samples The acidic mixture of guanidine isothiocyanate, sodium acetate phenol and chloroform act as strong protein denaturants of ribonucleases in order to protect the integrity of RNA, while disrupting cell and dissolving cellular components. Subsequently, the RNA harvested can be separated from DNA and protein and later recovered by precipitating with isopropanol alcohol (Chomczynski e Sacchi, 1987). We are able to increase RNA yield by running the Trizol solution through the lumen for just a few seconds. In addition, we combine two aortas Trizol run-through using a chemical RNA preservative called RNAlater. In summary, our results show that luminal RNA can be obtained using the Trizol method from freshly excised control aorta, cultured aorta and RNAlater preserved aorta. This method provides sufficient quantity of RNA to run RT-qPCR and purity without significant smooth muscle cell contamination.

AQP1 suppression accounts for a significant drop in Lp_{e+i}

$HgCl_2$ impedes with water transport in AQP1 by binding to cystein189 at its pore entrance. Previously, our group has shown that water transport inhibition by $HgCl_2$ leads to a drastic pressure-dependent reductions in whole vessel *Lp* and Lp_{e+i} (Shou, 2005;

Nguyen, 2008). This result allows one to extract the apparent contribution of the transcellular pathway from the total transmural water flux. However, given the potential for $HgCl_2$ to block other molecules besides the water pore in AQP1, this apparent transcellular contribution may not truly reflect the contribution of the AQP1 transcellular pathway. Moreover, since $HgCl_2$ is cytotoxic at high concentration and longer exposure times and thus may in fact cause some increase in *Lp* due to this toxicity. When measuring water permeability (*Jv*) using bovine aortic endothelial cells (BAECs) *in vitro*, we noted in Chapter 2 that custom-designed AQP1 siRNA induced nearly a decrease in *Jv* that was three times higher than that induced in $HgCl_2$ treated monolayers (64% vs. 22.1%) (Nguyen, 2008; Russell, 2008). As discussed there, it is likely that the low concentrations of $HgCl_2$ used by Nguyen in order to avoid cytotoxicity was low enough to only block ~1/3 of the aquaporins (Yang, Kim *et al.*, 2006). In contrast, it seems that the dosage of the siRNA reagent used was able to maintain the monolayer's integrity, and, at the same time, knock down the majority of AQP1 protein expression (nearly 70%) in BAECs, while avoiding the cytotoxic side effects. To minimize cytotoxicity and maximize the inhibitory effect, we use siRNA as an $HgCl_2$ alternative to silence AQP1 expression in target rat aortic endothelial cells in excised whole rat aortas *ex vivo*. Both Shou and Nguyen's $HgCl_2$ results found a large drop at 60mmHg and smaller, yet statistically significant drops in *Lp* that at the higher transmural pressures.

Our experiments were performed only at two lower transmural pressures of 60 and 100mmHg. We showed that blocking AQP1 via siRNA reagent knocks down 85% of AQP1 gene expression, resulting in a decrease in Lp_t (Lp_{e+i}) by 37.35±12.97%

(59.8±11.6%) and 8.71±3.76% (15.5±9.1%) at 60 and 100 mmHg respectively. At 60mmHg, the endothelium + intima ($1/Lp_{e+i}$) contributes 30.5±4.0% of the total wall resistance ($1/ Lp_t$), while AQP1 suppression decreases Lp_{e+i} by 59.8±11.6%. These drops represent the change of Lp_{e+i} that is attributed by AQP1. Denuded aortas showed no significant change in *Lp* with and without siRNA treatment, suggesting that water transport through the media happens mainly around SMCs, since they have no tight junctions, and not across them. As a result, the endothelium, subendothelium intima (SI) and internal elastic lamina (IEL) are indicative as the primary cause of the pressure-dependence of the effect of AQP1 suppression on Lp_t (Lp_{e+i}).

Recall that Nguyen's $HgCl_2$-induced reduction in *Lp* was also ΔP-dependent in the same way that our results were. Thus the likely explanation is the same, i.e., that reducing the AQP1 transcellular water pathway likely shifts a larger portion of the overall ΔP from the media to the endothelium, thereby achieving the critical pressure for SI compaction at lower overall ΔP. That is, this blocking shifts a larger fraction of the overall transmural pressure to the endothelial layer, leading to an early compaction of otherwise uncompressed SI, increasing the partial blockage of fenestrated holes and thus the resistance to water flow at lower pressures (Huang, Jan *et al.*, 1998). As noted earlier, one of my colleagues, S. Joshi, has worked out a fluid mechanical theory for this effect and confirmed that it indeed can explain those earlier data. We presume that it can explain these data quantitatively as well. An indirect proof of this theory comes from Sun *et al*.'s observation that AQP1 blocking leads to larger, not smaller HRP tracer spots at a fixed ΔP low enough that, without disabling AQP1, the SI is uncompressed, because

reduced *Lp* lessens the extent of transmural clearance of the tracer while the tracer's transport and spreading in SI is driven by a fixed pressure but through a SI of narrowed cross-section (Sun, 2008). Clearly, at maximal compaction aquaporins blocking cannot impact on SI compression, therefore, the observed changes in Lp_t (Lp_{e+i}) are smaller and reflect changes in the intrinsic endothelial *Lp*.

When the AQP1 pathway is more completely blocked by siRNA reagent than by using a low concentration of $HgCl_2$, one might at first blush expect a much higher drop in *Lp* than Nguyen found. This was, in fact, the case for our *in vitro* permeability study, although Nguyen's n value was quite small (n=4) and her standard deviation was large. However, as we noted, the results of Nguyen's $HgCl_2$-induced and our siRNA-induced reductions in *Lp* are, in fact, quite consistent. We argue that the similarity between these two sets of experiments lies in the fact that most of the observed drop is due to SI compaction, which is only indirectly due to AQP blockage or knockdown, and not directly to the intrinsic drop in Lp_e. That is, when enough endothelial AQPs are blocked or knocked down, a sufficient fraction of the overall transmural pressure is shifted from the media to the endothelium so as to exceed the critical force/area on the endothelium to cause maximal SI compaction at 60mmHg. It is this compaction that accounts for the bulk of the drop in the observed Lp_t. Any further AQP blocking or knockdown, while increasing the force across the endothelium, cannot further compact the already maximally compressed SI, and thus only effects a change in the intrinsic Lp_e, which has a minor effect on Lp_t. That is why, if even at such a low concentration, $HgCl_2$ treatment can cause a maximal SI compaction, the observed Lp_t will not differ much from that

found with the far more extensive AQP deactivation of siRNA knockdown. Recall that, in the presence of $HgCl_2$, Nguyen estimated and experimentally verified that reducing ΔP for $HgCl_2$ treatment to ΔP =27 mmHg is enough to sufficiently reduce the force/area on the endothelium so as to decompress the SI in the presence of $HgCl_2$ to the extent that it is decompressed without $HgCl_2$ at 60 mmHg. According to this reasoning, one ought to have to go to an even lower transmural pressure (ΔP) at which the Lp_t measured in the presence of siRNA reagent above its value at 60 mmHg and approaches the siRNA-free value at that pressure.

Potential roles for AQP1 transcellular water flux

Our results show that aquaporins contribute significantly to transmural water permeability. We argue the potential significance of a transcellular water flux pathway via AQP1 water channel proteins in the endothelial cell membranes. Plasma (mostly water) convects LDL into subendothelial intima (SI) through transient leaky junctions. Water flux, however, can also determine whether LDL can spend enough time at high enough concentration in the SI to deposit, that is, to bind to with SI extracellular matrix, and thus to set of the chain of events that potentially lead to atherogenesis. Lever *et al*. showed that the steady state LDL concentration in the media of the carotid artery was 50 times higher with collars around the vessel than without collars. They explained this result as the collars restricting transmural water flux. This retarded flux then cannot flush LDL out of the vessel wall, resulting in LDL accumulation in the media (Lever, Jay *et al.*, 1996). Thus, water flow is not only crucial to macromolecule transport into, but also to its

drainage/clearing out of arterial wall. We consider that water passing through the normal, non-leaky endothelium, including endothelial aquaporins, is responsible for diluting the local LDL concentration as they spread from the leak and can flush them from the SI and through the artery's wall. AQP1 knockdown and HRP tracer spot study can be combined in the future to study the local dilution function of transcellular water flux.

AQP1 is expressed on both the luminal and abluminal sides of the rat endothelial membrane and in the cell's interior, as determined by rat aorta transverse sections using immunohistochemical staining (Toussaint, 2009). In addition, two types of hypertensive rats (SHR and 2K1C) expressed much more AQP1 in their aortic endothelial cells and Lp_{e+i} was significantly higher than their normotensive littermates (Nguyen, 2008). These result supports our theory that AQP1 is critical in regulating endothelial hydraulic conductivity and aortic wall's *Lp* in response to chronic transmural pressures (hypertension) by actively switching its gene expression on and off (Toussaint, 2009). Thus, it is intriguing to suspect that the endothelium can actively regulate water transport into the vessel wall, in contrast to the passive transmural flow though normal and leaky clefts in response to transmural pressure changes. The ability of AQP1 to actively and rapidly regulates its expression and function to facilitate transendothelial flow may be used in a beneficial way to influence LDL transport across the vessel wall and its subsequent deposition into the extracellular matrix of SI, as to lead to potential strategies for disease prevention and regression. Compounds that potentially induce the overexpression of AQP1 might be identified and used to enhance such transcellular water

fluxes. My colleague Raval is currently using pharmacological approach to upregulate AQP1 expression to see its potential effects on atherogenesis.

The physiological impact of the transcellular pathway via aquaporins

Aquaporins are widely expressed in epithelial and endothelial cells in various tissues, such as the kidney, lung and brain. They are involved with fluid transport, which is important for tissue fluid homeostasis both in normal physiology, and when abnormal, pathophysiology. In this work we have shown explicitly that cell-expressed aquaporin can not only foster water entry into and exit from a cell, but also transport across a cell monolayer. Moreover, we demonstrated that in addition to the well-known ability of an osmotic pressure difference, a hydrostatic pressure difference can also drive a trans-aquaporin flow. Below we review some well-known physiological localization of aquaporins and what these new insights might mean for them.

Aquaporins deficiency is linked to the kidney's inability to concentrate urine and thus to conserve fluid, resulting in a pathological state of polyuria and dehydration. AQP1 is expressed in epithelial cells of the proximal tubules and thin descending limb of Henle and endothelial cells of the descending vasa recta, indicating a fluid transport pathway from the tubular lumen to the interstitial space and finally to the vascular compartment. AQP1-deficient mice display a drastic decrease in transepithelial water permeability and a reduced net fluid reabsorption, resulting in a severely reduced ability to produce concentrated urine (Schnermann, Chou *et al.*, 1998). These facts about the kidneys are consistent with aquaporins as the pathway for osmotically driven

transcellular water transport; our studies directly show that such transport is possible. It is not difficult to understand that aquaporins inhibitors should have therapeutic effects in diuretic-refractory edematous state, causing the body to lose more water than salt (diuresis) (Verkman, 2009). While lacking AQP1, renal collecting ducts express AQP2 on their apical surface, which is regulated by the anti-diuretic hormone: vasopressin. Vasopressin could cause the trafficking of intracellular AQP2 vesicles to the plasma membrane. AQP2 is believed to help move water from the duct lumen to the interstitial space. It is suggested that AQP2 underexpression is involved with diabetes insipidus. AQP2 inhibitor might impose effects similar to vasopressin receptor-2 (V_2) antagonist in the treatment of hyponaturemia (Verkman, 2009).

The lung expresses AQP1 in microvascular endothelial cells and AQP5 in alveolar epithelial cells, which facilitate water movement between the airspace, and the interstitial and capillary spaces, resulting in the hydration of the airway and the absorption of alveolar fluid. Again, rather than simply supposing that the presence of aquaporins facilitates such transport, we have explicitly demonstrated that this transport is possible. In addition, the expression of AQP1 in pulmonary capillary endothelial cells appears to be upregulated by corticosteroids. Aquaporins' expression is very high in the lung at birth. It is predicted that premature infants would have trouble clearing fluid in the lungs and therefore difficulties in breathing. Aquaporins' deficiency would also impair the lung's ability to return fluid back to the vascular space to resolve pulmonary edema (Agre, King *et al.*, 2002).

AQP4 is expressed in astroglial cells, which are located in close proximity to the subarachnoid space and the capillaries. It is suggested that AQP4 is involved in the brain's water balance across the blood-brain barrier. AQP4 inhibitor might have a neuro-protective function in reducing cerebral edema (Verkman, 2009) .

As mentioned above, aquaporins are implicated in various physiological and diseased states. So far, the connection between aquaporins and cardiovascular disease such as atherosclerosis has been unclear. AQP7 is expressed in adipose tissue, particularly in periadventitial fat. Dysfunction of AQP7 is implicated in obesity. Overexpression of aquaporins may have beneficial effect of reducing adipose tissue mass in obesity and therefore decreasing the risk of cardiovascular disease (He, Liang *et al.*, 2008). In this work, we have shown that AQP1 is expressed in rat aortic endothelial cells and that it can facilitate the transendothelial transport of water. Since such water transport may be important in diluting LDL that has entered the arterial subendothelial intima and flushing it from that region, thereby affecting the kinetics of its binding to intimal extracellular matrix, these results suggest additional potential influences of aquaporins on atherogenesis.

Polymorphism is observed in AQP1 in sickle cell anemia and diabetic nephropathy (Ewens, George *et al.*, 2005); AQP4 in stroke patients (Kleffner, Bungeroth *et al.*, 2008) and AQP7 in obesity and diabetes (Prudente, Flex *et al.*, 2007). Though promising, the importance of such polymorphism as potential disease marker is yet to be determined.

Chapter 5 Summary and future works

Atherosclerosis, a disease affecting the aorta and other large arteries, is the leading causes of death in America and in all Western countries. It is initiated by the transport and deposition of low density lipoprotein (LDL) cholesterol from the arterial lumen to its subendothelial intima (SI), triggering early lesions/ fatty streaks formation (Baldwin, Wilson *et al.*, 1992). Driven by transmural pressure differences, plasma, mostly water and solutes, advects LDL, into the SI space, where it can be retained (Rader e Daugherty, 2008). There are two major transendothelial transport pathways by which macromolecules can traverse the arterial endothelia. Normally, large-molecular-weight molecules (such as LDL) cannot pass through the tight inter-endothelial cell junction clefts, but rather are taken up by receptor-mediated endocytosis and brought into the cells (Rudenko, Henry *et al.*, 2002). Studies with large circulating tracers show endothelial hyperpermeability to macromolecules is associated with 'leaky junctions': transient widening of endothelial junctions (Weinbaum, Tzeghai *et al.*, 1985). Water flow is not only crucial to macromolecule transport into, but also to its drainage/clearing out of arterial wall (Lever, Jay *et al.*, 1996). This determines whether LDL molecules can spend enough time at high enough local concentration in the SI to bind to SI extracellular matrix.

The purpose of our study is to investigate the mechanisms of transmural water flux that are relevant to atherogenesis, which might lead to potential strategies for disease prevention and regression. It is natural to presume that water transport occurs

predominantly through the paracellular pathway. In this thesis we have presented experimental evidence that a parallel transcellular water flux pathway via AQP1 water channel proteins in the endothelial cell membranes plays an important role in transendothelial water flow. Discovered in erythrocytes and renal epithelial cells, aquaporins are the transmembrane proteins that facilitates high throughput water transport in response to osmotic gradients (Denker, Smith *et al.*, 1988). Our group had previously identified the presence of AQP1 protein in rat aortic endothelial cells in whole rat aorta *ex vivo* and in bovine aorta endothelial cells *in vitro* by immunohistochemistry staining. Our group had also shown that aortas can actively regulate their endothelial cells' aquaporin-1 expression (elevation) in response to chronic hypertension, resulting in an increase in the hydraulic conductivity (Lp_{e+i}) of the endothelium plus SI measured as a function of transmural pressure (ΔP) in rat aorta. Our group has also shown the inhibitory effect of mercuric chloride on rat aorta hydraulic conductivity and on cultured BAEC monolayer. AQP1 blocking by mercuric chloride significantly decreases $Lp(\Delta P)$ of excised aorta *ex vivo* and this decrease is pressure-dependent. *In vitro* study shows reduction in *Jv* induced by the siRNA knockdown method nearly triples that induced by concentration of $HgCl_2$ low enough to avoid any trace of toxicity on BAECs under a 10-cm hydrostatic pressure (Nguyen, 2008; Russell, 2008).

The aim of the first part of my study is to determine the contribution of the transcellular pathway via AQP1 to water filtration through rat aortic endothelial cells (RAECs), cultured monolayers *in vitro*. RAECs' AQP1 expression is confirmed by immunohistochemistry staining and by Western blotting. Water flux (*Jv*) studies show a

56.4±8.2% decrease in *Jv* comparing with control monolayers not exposed to siRNA. This significant decrease in *Jv* is assumed to be due not only to the direct effects of the suppression of the purported transcellular AQP1 pathway, but also partially to the indirect flow resistance caused by this pathway suppression. That is, when the aquaporins are knocked down, cell volume may tend to increase and the pressure difference across the monolayer pushes the monolayer against the stiff filter on which they are grown. This flattens the bigger endothelial cells, which increases the overlap of their junctional complexes. RAECs' permeability to small solutes: tetramethylrhodamine (TAMRA, 1nm) and tetramethyl-rhodamine-iso-thiocyanate (TRITC)-labeled-albumin (6nm) under diffusive and pressurized conditions provide an interesting insight into the fractional contribution of AQP1 to the reduction of water flow, since these solutes traverse only the junctions and not the AQP1s. For TAMRA and albumin, the siRNA-transfected groups have, respectively, a 21.8±7.04% and 29.79±1.72%/25.69±8.19% reduction in permeability under convection/diffusion conditions. As hydrostatic pressure is applied, the change in permeability of TAMRA and albumin could reflect the change in paracellular water flux for different pathways excluding aquaporins, i.e. tight junctions, and breaks in tight junction and leaky junctions. From similar experiments with labeled albumin and LDL and an assumed three-pore model, Cancel L. was able to calculate the contribution of different paracellular pathways to the total water and solute transports through the assumed three pores. One can modify the 3-pore model to include a fourth pore, the water-only AQP1 pathway to calculate the contribution of each of above-mentioned pathways, including AQP1, to water filtration through RAECs monolayers. My colleagues, S. Joshi and C. Raval, are doing this now.

The ultimate goal of our study is to determine the contribution of the AQP1 transcellular pathway to transendothelial water filtration, as measured by the hydraulic conductivity (*Lp*, the ratio of water flux to transmural pressure difference (ΔP)), across aortic endothelial cells and through rat thoracic aorta. The technique that we have chosen is siRNA knockdown of endothelial AQP1. The second part of my thesis work involves constructing an *ex vivo* aorta organ culture system to preserve endothelial and overall aorta structural integrity for 48 hours. This 48-hour time period is critical for allowing maximal knockdown effect to take place following siRNA transfection. Our vessel culture system provides a constant perfusion of media through the vessel lumen, yielding a physiological shear stress. Independent of the flow manipulation, our device allows one to set a physiological transmural pressure by adjusting the height of a media reservoir. We find that maintenance of both pressure and flow preserves isolated aortic endothelial cell integrity, as confirmed by both the examination of vessel hydraulic conductivity ($Lp = Jv/\Delta P$) and morphology study. The *Lp* vs ΔP curve of cultured rat aortas *ex vivo* does not change after 48 hours of incubation. Silver nitrate staining demonstrates regular cell shapes and intact cell-cell borders with no distinguishable cell loss even at the entrance region of the flow into the excised vessel. Hematoxylin and Eosin staining reveal unaltered aortic wall structure. Thus, in this study, we describe a somewhat novel aorta organ culture system and confirm that rat aorta can be maintained *ex vivo* for 48 hours under controlled pressure and flow. These facts demonstrate the feasibility that the organ culture technique can be used as a potent tool for molecular manipulation of aortic endothelial cells, as we subsequently have done, and also a useful platform for the study

of mass transport of macromolecules (i.e. HRP, LDL). A more careful study of the characteristics of different layers of the cultured aorta, i.e. DNA, protein extracellular matrix contents, would be useful in the future to gain a better understanding and to improve the system for long-term study uses.

The final part of my work intends to test if siRNA knockdown of AQP1 lowers whole rat aortic hydraulic conductivity (*Lp*) *ex vivo*. This would help us assess AQP1's contribution to the transcelluar water flow in whole rat aorta. Our group is very experienced at measuring *Lp* of whole rat vessel as a function of transmural pressure (ΔP) *ex vivo*, first with intact and then after endothelial denudation, on the same vessel. We measure *Lp* vs ΔP at 60 and 100mmHg on a freshly excised rat aorta, transfect the endothelium of excised whole rat aorta with siRNA in order to knock down its AQP1 expression, culture for 48 hours and then re-measure *Lp* vs ΔP on the same vessel. Finally, the endothelial layer was removed by mechanical denudation and *Lp* was measured a third time on the same vessel at the same pressures. We showed that blocking AQP1 via siRNA reagent knocks down 85% of AQP1 gene expression, resulting in a decrease in Lp_t (Lp_{e+i}) by 37.35±12.97% (59.8±11.6%) and 8.71±3.76 % (15.5±9.1%) at 60 and 100 mmHg respectively. At 60mmHg, the endothelium + intima ($1/Lp_{e+i}$) contributes about 30.5±4.0% of the total wall resistance ($1/ Lp_t$), while AQP1 suppression decreases Lp_{e+i} by 59.8±11.6 %, n=3. These drops represent the fraction of Lp_{e+i} that is attributed to the AQP1 transcellular pathway. Denuded aortas showed no significant change in *Lp* with and without previous siRNA treatment, suggesting that water transport through the media occurs mainly around SMCs and not across them. Why is the drop in

Lp_t (Lp_{e+i}) pressure dependent? We propose the same explanation used fro a similar pressure-dependent drop upon AQP1 blocking with $HgCl_2$ applies here as well. That is, blocking or knocking down aquaporins at a constant ΔP shifts a larger fraction of the overall transmural pressure ΔP (considered as force per unit area) to the endothelium. In conjunction with SI compaction theory, this shift induces a compaction of otherwise uncompressed SI and increases fenestral blocking, leading to a sharp drop in *Lp* at lower overall ΔP. In the future, we can estimate, based on the above reasoning, a lower value of ΔP, at which in the presence of aquaporins blocker, the force on the endothelium and the degree of SI compaction are equivalent to what is found at 60 mmHg without blocker. And measurements of Lp_t at this low ΔP with and without siRNA can be carried out to verify this prediction.

AQP1 is found both on the luminal and abluminal surface of aortic endothelia in transverse sections of rat aorta using quantitative immunohistochemistry technique (Toussaint, 2009). In addition, both genetically bred spontaneous hypertensive rats (SHR) and Goldblatts surgery-induced hypertensive rats (2K1C) expressed much more AQP1 on aortic endothelial cells than controls. The measured Lp_{e+i} of SHR and 2K1C hypertensive rat aorta was significantly higher than their normotensive littermates (Nguyen, 2008). J. Toussaint's result supports our theory that AQP1 is critical to the regulation of transcellular water flow since in response to chronic hypertension, the vessel actively switch its endothelial cells' AQP1 gene expression on (Toussaint, 2009).

AQP1 contribute significantly to the hydraulic conductivity of endothelial cells. AQP1 might affect lipid transport in a beneficial way with regard to disease progression. To better understand the mechanism of disease initiation, progression and regression, we would like test in the future how molecular manipulation of aquaporins transmembrane protein (up and downregulation) and transcellular water pathway might affect macromolecule tracer spot growth (i.e. HRP and LDL) in both live animals and our *ex vivo* organ culture system.

Chapter 6 References

Agre, P., L. S. King*, et al.* Aquaporin water channels--from atomic structure to clinical medicine. J Physiol, v.542, n.Pt 1, Jul 1, p.3-16. 2002.

Anderson, J. M. Molecular structure of tight junctions and their role in epithelial transport. News Physiol Sci, v.16, Jun, p.126-30. 2001.

Baldwin, A. L. e L. M. Wilson. Endothelium increases medial hydraulic conductance of aorta, possibly by release of EDRF. Am J Physiol, v.264, n.1 Pt 2, Jan, p.H26-32. 1993.

Baldwin, A. L., L. M. Wilson*, et al.* Effect of pressure on aortic hydraulic conductance. Arterioscler Thromb, v.12, n.2, Feb, p.163-71. 1992.

Ballatori, N. e J. L. Boyer. Disruption of cell volume regulation by mercuric chloride is mediated by an increase in sodium permeability and inhibition of an osmolyte channel in skate hepatocytes. Toxicol Appl Pharmacol, v.140, n.2, Oct, p.404-10. 1996.

Bardy, N., G. J. Karillon*, et al.* Differential effects of pressure and flow on DNA and protein synthesis and on fibronectin expression by arteries in a novel organ culture system. Circ Res, v.77, n.4, Oct, p.684-94. 1995.

Bardy, N., R. Merval*, et al.* Pressure and angiotensin II synergistically induce aortic fibronectin expression in organ culture model of rabbit aorta. Evidence for a pressure-induced tissue renin-angiotensin system. Circ Res, v.79, n.1, Jul, p.70-8. 1996.

Barrett, L. A., W. J. Mergner*, et al.* Long-term culture of human aortas. Development of atherosclerotic-like plaques in serum-supplemented medium. In Vitro, v.15, n.12, Dec, p.957-66. 1979.

Beznak, M. Hemodynamic changes in hypophysectomized rats. Circ Res, v.7, Nov, p.907-16. 1959.

Birukov, K. G., N. Bardy*, et al.* Intraluminal pressure is essential for the maintenance of smooth muscle caldesmon and filamin content in aortic organ culture. Arterioscler Thromb Vasc Biol, v.18, n.6, Jun, p.922-7. 1998.

Bolz, S. S., S. Pieperhoff*, et al.* Intact endothelial and smooth muscle function in small resistance arteries after 48 h in vessel culture. Am J Physiol Heart Circ Physiol, v.279, n.3, Sep, p.H1434-9. 2000.

Cancel, L. M., A. Fitting*, et al.* In vitro study of LDL transport under pressurized (convective) conditions. Am J Physiol Heart Circ Physiol, v.293, n.1, Jul, p.H126-32. 2007.

Chen, S., M. Sega*, et al.* "Lumen digestion" technique for isolation of aortic endothelial cells from heme oxygenase-1 knockout mice. Biotechniques, v.37, n.1, Jul, p.84-6, 88-9. 2004.

Chen, Y. L., K. M. Jan, *et al.* Relationship between endothelial cell turnover and permeability to horseradish peroxidase. Atherosclerosis, v.133, n.1, Aug, p.7-14. 1997.

Chesler, N. C., D. N. Ku, *et al.* Transmural pressure induces matrix-degrading activity in porcine arteries ex vivo. Am J Physiol, v.277, n.5 Pt 2, Nov, p.H2002-9. 1999.

Cho, A., L. Mitchell, *et al.* Effects of changes in blood flow rate on cell death and cell proliferation in carotid arteries of immature rabbits. Circ Res, v.81, n.3, Sep, p.328-37. 1997.

Chobanian, A. V. 1989 Corcoran lecture: adaptive and maladaptive responses of the arterial wall to hypertension. Hypertension, v.15, n.6 Pt 2, Jun, p.666-74. 1990.

Chobanian, A. V., P. I. Brecher, *et al.* EFFECTS OF HYPERTENSION AND OF ANTIHYPERTENSIVE THERAPY ON ATHEROSCLEROSIS - STATE-OF-THE-ART LECTURE. Hypertension, v.8, n.4, Apr, p.15-21. 1986.

Chomczynski, P. e N. Sacchi. Single-step method of RNA isolation by acid guanidinium thiocyanate-phenol-chloroform extraction. Anal Biochem, v.162, n.1, Apr, p.156-9. 1987.

Chou, C. L., M. A. Knepper, *et al.* Reduced water permeability and altered ultrastructure in thin descending limb of Henle in aquaporin-1 null mice. J Clin Invest, v.103, n.4, Feb, p.491-6. 1999.

Chuang, P. T., H. J. Cheng, *et al.* Macromolecular transport across arterial and venous endothelium in rats. Studies with Evans blue-albumin and horseradish peroxidase. Arteriosclerosis, v.10, n.2, Mar-Apr, p.188-97. 1990.

Cotton, R. e W. B. Wartman. Endothelial patterns in human arteries. Their relationship to age, vessel site and atherosclerosis. Arch Pathol, v.71, Jan, p.3-12. 1961.

Cumming, J. D. e M. E. Nutt. Bone-marrow blood flow and cardiac output in the rabbit. J Physiol, v.162, Jun, p.30-4. 1962.

Curmi, P. A., L. Juan, *et al.* Effect of transmural pressure on low density lipoprotein and albumin transport and distribution across the intact arterial wall. Circ Res, v.66, n.6, Jun, p.1692-702. 1990.

Dancu, M. B. e J. M. Tarbell. Coronary endothelium expresses a pathologic gene pattern compared to aortic endothelium: correlation of asynchronous hemodynamics and pathology in vivo. Atherosclerosis, v.192, n.1, May, p.9-14. 2007.

De Chastonay, C., G. Gabbiani, *et al.* Remodeling of the rat aortic endothelial layer during experimental hypertension. Changes in replication rate, cell density, and surface morphology. Lab Invest, v.48, n.1, Jan, p.45-52. 1983.

De Mey, J. G., M. P. Uitendaal, *et al.* Acute and long-term effects of tissue culture on contractile reactivity in renal arteries of the rat. Circ Res, v.65, n.4, Oct, p.1125-35. 1989.

Demaio, L., J. M. Tarbell, *et al.* A transmural pressure gradient induces mechanical and biological adaptive responses in endothelial cells. Am J Physiol Heart Circ Physiol, v.286, n.2, Feb, p.H731-41. 2004.

Denker, B. M., B. L. Smith*, et al.* Identification, purification, and partial characterization of a novel Mr 28,000 integral membrane protein from erythrocytes and renal tubules. J Biol Chem, v.263, n.30, Oct 25, p.15634-42. 1988.

Desjardins, L. M. e J. P. Macmanus. An adherent cell model to study different stages of apoptosis. Exp Cell Res, v.216, n.2, Feb, p.380-7. 1995.

Dewey, C. F., Jr., S. R. Bussolari*, et al.* The dynamic response of vascular endothelial cells to fluid shear stress. J Biomech Eng, v.103, n.3, Aug, p.177-85. 1981.

Dimmeler, S., J. Haendeler*, et al.* Shear stress inhibits apoptosis of human endothelial cells. FEBS Lett, v.399, n.1-2, Dec 9, p.71-4. 1996.

Dolman, D., S. Drndarski*, et al.* Induction of aquaporin 1 but not aquaporin 4 messenger RNA in rat primary brain microvessel endothelial cells in culture. J Neurochem, v.93, n.4, May, p.825-33. 2005.

Dull, R. O., H. Jo*, et al.* The effect of varying albumin concentration and hydrostatic pressure on hydraulic conductivity and albumin permeability of cultured endothelial monolayers. Microvasc Res, v.41, n.3, May, p.390-407. 1991.

Epstein, M. Hepatorenal syndrome: emerging perspectives of pathophysiology and therapy. J Am Soc Nephrol, v.4, n.10, Apr, p.1735-53. 1994.

Ewens, K. G., R. A. George*, et al.* Assessment of 115 candidate genes for diabetic nephropathy by transmission/disequilibrium test. Diabetes, v.54, n.11, Nov, p.3305-18. 2005.

Fire, A., S. Xu*, et al.* Potent and specific genetic interference by double-stranded RNA in Caenorhabditis elegans. Nature, v.391, n.6669, Feb 19, p.806-11. 1998.

Folkesson, H. G., M. A. Matthay*, et al.* Transcellular water transport in lung alveolar epithelium through mercury-sensitive water channels. Proc Natl Acad Sci U S A, v.91, n.11, May 24, p.4970-4. 1994.

Folkman, J., C. C. Haudenschild*, et al.* Long-term culture of capillary endothelial cells. Proc Natl Acad Sci U S A, v.76, n.10, Oct, p.5217-21. 1979.

Frank, J. S. e A. M. Fogelman. Ultrastructure of the intima in WHHL and cholesterol-fed rabbit aortas prepared by ultra-rapid freezing and freeze-etching. J. Lipid Research, v.30, p.967-978. 1989.

Friedman, M. H. e D. L. Fry. Arterial permeability dynamics and vascular disease. Atherosclerosis, v.104, n.1-2, Dec, p.189-94. 1993.

Frokjaer-Jensen, J. The plasmalemmal vesicular system in striated muscle capillaries and in pericytes. Tissue Cell, v.16, n.1, p.31-42. 1984.

Fry, D. L., R. W. Mahley*, et al.* Simultaneous accumulation of Evans blue dye and albumin in the canine aortic wall. Am J Physiol, v.233, n.1, Jul, p.H66-79. 1977.

Fu, D., A. Libson, *et al.* Structure of a glycerol-conducting channel and the basis for its selectivity. Science, v.290, n.5491, Oct 20, p.481-6. 2000.

Gimbrone, M. A., Jr. Endothelial dysfunction, hemodynamic forces, and atherosclerosis. Thromb Haemost, v.82, n.2, Aug, p.722-6. 1999.

Goldblatt, H., Lynch J, Hanzel Rf, Summerville, Ww. Studies on experimental hypertension. 1. The production of persistent elevation of systolic blood pressure by means of renal ischemia. J Exp Med, v.59, p.347-379. 1934.

Goldstein, J. L. e M. S. Brown. The LDL receptor. Arterioscler Thromb Vasc Biol, v.29, n.4, Apr, p.431-8. 2009.

Gonzalez, E., A. Nagiel, *et al.* Small interfering RNA-mediated down-regulation of caveolin-1 differentially modulates signaling pathways in endothelial cells. J Biol Chem, v.279, n.39, Sep 24, p.40659-69. 2004.

Gotlieb, A. I. e P. Boden. Porcine aortic organ culture: a model to study the cellular response to vascular injury. In Vitro, v.20, n.7, Jul, p.535-42. 1984.

Grande, J. P., S. Glagov, *et al.* Effect of normolipemic and hyperlipemic serum on biosynthetic response to cyclic stretching of aortic smooth muscle cells. Arteriosclerosis, v.9, n.4, Jul-Aug, p.446-52. 1989.

Grundmann, S., S. H. Schirmer, *et al.* Endothelial glycocalyx dimensions are reduced in growing collateral arteries and modulate leucocyte adhesion in arteriogenesis. J Cell Mol Med, v.13, n.9B, Sep, p.3463-74. 2009.

Guyton, J. R. e C. J. Hartley. Flow restriction of one carotid artery in juvenile rats inhibits growth of arterial diameter. Am J Physiol, v.248, n.4 Pt 2, Apr, p.H540-6. 1985.

He, Z. Q., C. Liang, *et al.* Dysfunction of AQP7 in the periadventitial fat: A novel trigger of atherosclerosis. Med Hypotheses, v.70, n.1, p.92-5. 2008.

Hermann, R. A., R.A. Malinauskas and G.A. Truskey. Characterization of sites with elevated LDL permeability at intercostal, celiac, and iliac branches of the normal rabbit aorta. Arteriosclerosis and Thrombosis, v.14, p.313-323. 1994.

Herrera, M. e J. L. Garvin. Novel role of AQP-1 in NO-dependent vasorelaxation. Am J Physiol Renal Physiol, v.292, n.5, May, p.F1443-51. 2007.

Herrera, M., N. J. Hong, *et al.* Aquaporin-1 transports NO across cell membranes. Hypertension, v.48, n.1, Jul, p.157-64. 2006.

Huang, Y., K. M. Jan, *et al.* Structural changes in rat aortic intima due to transmural pressure. J Biomech Eng, v.120, n.4, Aug, p.476-83. 1998.

Huang, Y., D. Rumschitzki, *et al.* A fiber matrix model for the growth of macromolecular leakage spots in the arterial intima. J Biomech Eng, v.116, n.4, Nov, p.430-45. 1994.

Huang, Y., D Rumschitzki, *et al.* A fiber matrix model for the filtration through fenestral pores in a compressible arterial intima. Am J Physiol, v.272, n.4 Pt 2, Apr, p.H2023-39. 1997.

Huttner, I., M. Boutet, *et al.* Studies on protein passage through arterial endothelium. 3. Effect of blood pressure levels on the passage of fine structural protein tracers through rat arterial endothelium. Lab Invest, v.29, n.5, Nov, p.536-46. 1973.

Insull, W., Jr. The pathology of atherosclerosis: plaque development and plaque responses to medical treatment. Am J Med, v.122, n.1 Suppl, Jan, p.S3-S14. 2009.

Jung, J. S., R. V. Bhat, *et al.* Molecular characterization of an aquaporin cDNA from brain: candidate osmoreceptor and regulator of water balance. Proc Natl Acad Sci U S A, v.91, n.26, Dec 20, p.13052-6. 1994.

Jung, J. S., G. M. Preston, *et al.* Molecular structure of the water channel through aquaporin CHIP. The hourglass model. J Biol Chem, v.269, n.20, May 20, p.14648-54. 1994.

Kamiya, A. e T. Togawa. Adaptive regulation of wall shear stress to flow change in the canine carotid artery. Am J Physiol, v.239, n.1, Jul, p.H14-21. 1980.

Kim, M. H., N. R. Harris, *et al.* Regulation of hydraulic conductivity in response to sustained changes in pressure. Am J Physiol Heart Circ Physiol, v.289, n.6, Dec, p.H2551-8. 2005.

King, L. S. e P. Agre. Pathophysiology of the aquaporin water channels. Annu Rev Physiol, v.58, p.619-48. 1996.

King, L. S., S. Nielsen, *et al.* Aquaporin-1 water channel protein in lung: ontogeny, steroid-induced expression, and distribution in rat. J Clin Invest, v.97, n.10, May 15, p.2183-91. 1996.

Kleffner, I., M. Bungeroth, *et al.* The role of aquaporin-4 polymorphisms in the development of brain edema after middle cerebral artery occlusion. Stroke, v.39, n.4, Apr, p.1333-5. 2008.

Knox, P., J. R. Levick, *et al.* Synovial fluid--its mass, macromolecular content and pressure in major limb joints of the rabbit. Q J Exp Physiol, v.73, n.1, Jan, p.33-45. 1988.

Krane, C. M., J. E. Melvin, *et al.* Salivary acinar cells from aquaporin 5-deficient mice have decreased membrane water permeability and altered cell volume regulation. J Biol Chem, v.276, n.26, Jun 29, p.23413-20. 2001.

Kuang, K., M. Yiming, *et al.* Fluid transport across cultured layers of corneal endothelium from aquaporin-1 null mice. Exp Eye Res, v.78, n.4, Apr, p.791-8. 2004.

Langille, B. L. e S. L. Adamson. Relationship between blood flow direction and endothelial cell orientation at arterial branch sites in rabbits and mice. Circ Res, v.48, n.4, Apr, p.481-8. 1981.

Langille, B. L., M. P. Bendeck, *et al.* Adaptations of carotid arteries of young and mature rabbits to reduced carotid blood flow. Am J Physiol, v.256, n.4 Pt 2, Apr, p.H931-9. 1989.

Lever, M. J., M. T. Jay, *et al.* Plasma protein entry and retention in the vascular wall: possible factors in atherogenesis. Can J Physiol Pharmacol, v.74, n.7, Jul, p.818-23. 1996.

Lewis, L. J., J. C. Hoak, *et al.* Replication of human endothelial cells in culture. Science, v.181, n.98, Aug 3, p.453-4. 1973.

Lin, S. J., K. M. Jan, *et al.* Role of dying endothelial cells in transendothelial macromolecular transport. Arteriosclerosis, v.10, n.5, Sep-Oct, p.703-9. 1990.

Lin, S.J., K.M. Jan, *et al.* Enhanced macromolecular permeability of aortic endothelial cells in association with mitosis. Atherosclerosis, v.73, n.2-3, Oct, p.223-32. 1988.

Lin, S. J., K. M. Jan, *et al.* Transendothelial transport of low density lipoprotein in association with cell mitosis in rat aorta. Arteriosclerosis, v.9, n.2, Mar-Apr, p.230-6. 1989.

Lusis, A. J. Atherosclerosis. Nature, v.407, n.6801, Sep 14, p.233-41. 2000.

Macey, R. I. Transport of water and urea in red blood cells. Am J Physiol, v.246, n.3 Pt 1, Mar, p.C195-203. 1984.

Macey, R. I. e R. E. Farmer. Inhibition of water and solute permeability in human red cells. Biochim Biophys Acta, v.211, n.1, Jul 7, p.104-6. 1970.

Mangiarua, E. I., N. Moss, *et al.* Morphological and contractile characteristics of rat aortae perfused for 3 or 6 days in vitro. Artery, v.19, n.1, p.14-38. 1992.

Mc, G. V. Reactions to injury of vascular endothelium with special reference to the problem of thrombosis. J Pathol Bacteriol, v.69, n.1-2, Jan-Apr, p.283-93. 1955.

Mcguire, P. G. e R. W. Orkin. Isolation of rat aortic endothelial cells by primary explant techniques and their phenotypic modulation by defined substrata. Lab Invest, v.57, n.1, Jul, p.94-105. 1987.

Mcmanus, M. L., K. B. Churchwell, *et al.* Regulation of cell volume in health and disease. N Engl J Med, v.333, n.19, Nov 9, p.1260-6. 1995.

Mora, R., F. Lupu, *et al.* Prelesional events in atherogenesis. Colocalization of apolipoprotein B, unesterified cholesterol and extracellular phospholipid liposomes in the aorta of hyperlipidemic rabbit. Atherosclerosis, v.67, n.2-3, Oct, p.143-54. 1987.

Murata, K., K. Mitsuoka, *et al.* Structural determinants of water permeation through aquaporin-1. Nature, v.407, n.6804, Oct 5, p.599-605. 2000.

Nagel, T., N. Resnick, *et al.* Vascular endothelial cells respond to spatial gradients in fluid shear stress by enhanced activation of transcription factors. Arterioscler Thromb Vasc Biol, v.19, n.8, Aug, p.1825-34. 1999.

Nakhoul, N. L., B. A. Davis, *et al.* Effect of expressing the water channel aquaporin-1 on the CO2 permeability of Xenopus oocytes. Am J Physiol, v.274, n.2 Pt 1, Feb, p.C543-8. 1998.

Nakhoul, N. L., K. S. Hering-Smith, *et al.* Transport of NH(3)/NH in oocytes expressing aquaporin-1. Am J Physiol Renal Physiol, v.281, n.2, Aug, p.F255-63. 2001.

Nam, D., C. W. Ni, *et al.* Partial carotid ligation is a model of acutely induced disturbed flow, leading to rapid endothelial dysfunction and atherosclerosis. Am J Physiol Heart Circ Physiol, v.297, n.4, Oct, p.H1535-43. 2009.

Nguyen, T. H. Aquaporin-1 contribution to rat aortic endothelial hydraulic conductivity and how chronic transmural pressure affects it. (Thesis (Ph D)). City University of New York, 2008. [Graduate Faculty in Engineering], 2008. xi, 107 leaves p.

Nielsen, L. B. Transfer of low density lipoprotein into the arterial wall and risk of atherosclerosis. Atherosclerosis, v.123, n.1-2, Jun, p.1-15. 1996.

Nielsen, S., B. L. Smith, *et al.* Distribution of the aquaporin CHIP in secretory and resorptive epithelia and capillary endothelia. Proc Natl Acad Sci U S A, v.90, n.15, Aug 1, p.7275-9. 1993.

Nielsen, S., B. L. Smith, *et al.* CHIP28 water channels are localized in constitutively water-permeable segments of the nephron. J Cell Biol, v.120, n.2, Jan, p.371-83. 1993.

O'nejll J, F. The Effects on Venous Endothelium of Alterations in Blood Flow Through the Vessels in Vein Walls, and the Possible Relation to Thrombosis. Ann Surg, v.126, n.3, Sep, p.270-88. 1947.

Ooneda, G., Y. Ooyama, *et al.* Electron Microscopic Studies on the Morphogenesis of Fibrinoid Degeneration in the Mesenteric Arteries of Hypertensive Rats. Angiology, v.16, Jan, p.8-17. 1965.

Owens, G. K. Influence of blood pressure on development of aortic medial smooth muscle hypertrophy in spontaneously hypertensive rats. Hypertension, v.9, n.2, Feb, p.178-87. 1987.

Pallone, T. L., A. Edwards, *et al.* Requirement of aquaporin-1 for NaCl-driven water transport across descending vasa recta. J Clin Invest, v.105, n.2, Jan, p.215-22. 2000.

Poole, J. C. e H. W. Florey. Changes in the endothelium of the aorta and the behaviour of macrophages in experimental atheroma of rabbits. J Pathol Bacteriol, v.75, n.2, Apr, p.245-51. 1958.

Poole, J. C., A. G. Sanders, *et al.* The regeneration of aortic endothelium. J Pathol Bacteriol, v.75, n.1, Jan, p.133-43. 1958.

Preston, G. M. e P. Agre. Isolation of the cDNA for erythrocyte integral membrane protein of 28 kilodaltons: member of an ancient channel family. Proc Natl Acad Sci U S A, v.88, n.24, Dec 15, p.11110-4. 1991.

Preston, G. M., T. P. Carroll, *et al.* Appearance of water channels in Xenopus oocytes expressing red cell CHIP28 protein. Science, v.256, n.5055, Apr 17, p.385-7. 1992.

Preston, G. M., J. S. Jung, *et al.* The mercury-sensitive residue at cysteine 189 in the CHIP28 water channel. J Biol Chem, v.268, n.1, Jan 5, p.17-20. 1993.

Preston, G. M., B. L. Smith, *et al.* Mutations in aquaporin-1 in phenotypically normal humans without functional CHIP water channels. Science, v.265, n.5178, Sep 9, p.1585-7. 1994.

Prudente, S., E. Flex*, et al.* A functional variant of the adipocyte glycerol channel aquaporin 7 gene is associated with obesity and related metabolic abnormalities. Diabetes, v.56, n.5, May, p.1468-74. 2007.

Rader, D. J. e A. Daugherty. Translating molecular discoveries into new therapies for atherosclerosis. Nature, v.451, n.7181, Feb 21, p.904-13. 2008.

Reidy, M. A. e D. E. Bowyer. Scanning electron microscopy of arteries. The morphology of aortic endothelium in haemodynamically stressed areas associated with branches. Atherosclerosis, v.26, n.2, Feb, p.181-94. 1977.

Rensen, S. S., P. M. Niessen*, et al.* Contribution of serum response factor and myocardin to transcriptional regulation of smoothelins. Cardiovasc Res, v.70, n.1, Apr 1, p.136-45. 2006.

Ross, R. The pathogenesis of atherosclerosis: a perspective for the 1990s. Nature, v.362, n.6423, Apr 29, p.801-9. 1993.

Rudenko, G., L. Henry*, et al.* Structure of the LDL receptor extracellular domain at endosomal pH. Science, v.298, n.5602, Dec 20, p.2353-8. 2002.

Russell, S. Energy depletion causes endothelial hyperpermeability in hyperglycemia. (Thesis (Ph D)). City University of New York, 2008. [Graduate Faculty in Engineering], 2008. ix, 165 leaves p.

Russell, S., L. M. Cancel*, et al.* A protein diffusion model of the sealing effect. Chemical Engineering Science, v.64, n.22, Nov, p.4504-4514. 2009.

Ryan, U. S. Isolation and culture of pulmonary endothelial cells. Environ Health Perspect, v.56, Jun, p.103-14. 1984.

Sarkadi, B., R. Cheung*, et al.* Cation and anion transport pathways in volume regulatory response of human lymphocytes to hyposmotic media. Am J Physiol, v.248, n.5 Pt 1, May, p.C480-7. 1985.

Savage, D. F. e R. M. Stroud. Structural basis of aquaporin inhibition by mercury. J Mol Biol, v.368, n.3, May 4, p.607-17. 2007.

Schnermann, J., C. L. Chou*, et al.* Defective proximal tubular fluid reabsorption in transgenic aquaporin-1 null mice. Proc Natl Acad Sci U S A, v.95, n.16, Aug 4, p.9660-4. 1998.

Shi, Z. D., X. Y. Ji*, et al.* Interstitial flow induces MMP-1 expression and vascular SMC migration in collagen I gels via an ERK1/2-dependent and c-Jun-mediated mechanism. Am J Physiol Heart Circ Physiol, v.298, n.1, Jan, p.H127-35. 2010.

Shou, Y. Water and macromolecular transport into the walls of vessels with differing atherogenic susceptibilities. (Ph.D.). Department of Chemical Engineering, City University of New York, New York, 2005. 146 p.

Shou, Y., K. M. Jan*, et al.* Transport in rat vessel walls. I. Hydraulic conductivities of the aorta, pulmonary artery, and inferior vena cava with intact and denuded endothelia. Am J Physiol Heart Circ Physiol, v.291, n.6, Dec, p.H2758-71. 2006.

Smith, B. L. e P. Agre. Erythrocyte Mr 28,000 transmembrane protein exists as a multisubunit oligomer similar to channel proteins. J Biol Chem, v.266, n.10, Apr 5, p.6407-15. 1991.

Smith, P. G., T. Tokui, *et al.* Mechanical strain increases contractile enzyme activity in cultured airway smooth muscle cells. Am J Physiol, v.268, n.6 Pt 1, Jun, p.L999-1005. 1995.

Snelting-Havinga, I., M. Mommaas, *et al.* Immunoelectron microscopic visualization of the transcytosis of low density lipoproteins in perfused rat arteries. Eur J Cell Biol, v.48, n.1, Feb, p.27-36. 1989.

Stemerman, M. B., E. M. Morrel, *et al.* Local variation in arterial wall permeability to low density lipoprotein in normal rabbit aorta. Arteriosclerosis, v.6, n.1, Jan-Feb, p.64-9. 1986.

Sui, H., B. G. Han, *et al.* Structural basis of water-specific transport through the AQP1 water channel. Nature, v.414, n.6866, Dec 20-27, p.872-8. 2001.

Sun, Y. The focal spread of macromolecular tracers in vessel walls: frequency and effect of intima compaction and blood pressure. Chemical Engineering, The City College of New York, New York, 2008. 154 p.

Tarbell, J. M. Mass transport in arteries and the localization of atherosclerosis. Annu Rev Biomed Eng, v.5, p.79-118. 2003.

Tarbell, J. M. Shear stress and the endothelial transport barrier. Cardiovasc Res, v.87, n.2, Jul 15, p.320-30. 2010.

Tedgui, A. e M. J. Lever. Filtration through damaged and undamaged rabbit thoracic aorta. Am J Physiol, v.247, n.5 Pt 2, Nov, p.H784-91. 1984.

Tedgui, A. e M. J. Lever. The interaction of convection and diffusion in the transport of 131I-albumin within the media of the rabbit thoracic aorta. Circ Res, v.57, n.6, Dec, p.856-63. 1985.

Toussaint, J. D. Aquaporin-1 and pressure-driven water transport across aortic endothelia : aquaporin-1 expression, distribution and regulation. (Thesis (Ph D)). City University of New York, 2009. [Graduate Faculty in Engineering], 2009. xxii, 156 leaves p.

Truskey, G. A., W. L. Roberts, *et al.* Measurement of endothelial permeability to 125I-low density lipoproteins in rabbit arteries by use of en face preparations. Circ Res, v.71, n.4, Oct, p.883-97. 1992.

Turner, M. R. Flows of liquid and electrical current through monolayers of cultured bovine arterial endothelium. J Physiol, v.449, Apr, p.1-20. 1992.

Umenishi, F., T. Narikiyo, *et al.* Hypertonic induction of aquaporin-1 water channel independent of transcellular osmotic gradient. Biochem Biophys Res Commun, v.325, n.2, Dec 10, p.595-9. 2004.

Van Hoek, A. N., M. L. Hom, *et al.* Functional unit of 30 kDa for proximal tubule water channels as revealed by radiation inactivation. J Biol Chem, v.266, n.25, Sep 5, p.16633-5. 1991.

Van Hoek, A. N., L. H. Luthjens*, et al.* A 30 kDa functional size for the erythrocyte water channel determined in situ by radiation inactivation. Biochem Biophys Res Commun, v.184, n.3, May 15, p.1331-8. 1992.

Van Hoek, A. N. e A. S. Verkman. Functional reconstitution of the isolated erythrocyte water channel CHIP28. J Biol Chem, v.267, n.26, Sep 15, p.18267-9. 1992.

Van Itallie, C. M. e J. M. Anderson. The molecular physiology of tight junction pores. Physiology (Bethesda), v.19, Dec, p.331-8. 2004.

Vasile, E., M. Simionescu*, et al.* Visualization of the binding, endocytosis, and transcytosis of low-density lipoprotein in the arterial endothelium in situ. J Cell Biol, v.96, n.6, Jun, p.1677-89. 1983.

Verkman, A. S. More than just water channels: unexpected cellular roles of aquaporins. J Cell Sci, v.118, n.Pt 15, Aug 1, p.3225-32. 2005.

Verkman, A. S. Aquaporins: translating bench research to human disease. J Exp Biol, v.212, n.Pt 11, Jun, p.1707-15. 2009.

Weinbaum, S., G. Tzeghai, P. Ganatos, R. Pfeffer and S. Chien. Effect of cell turnover and leaky junctions on arterial macromolecular transport. Am. J. Physiol., v.248, p.H945-H960. 1985.

Weinbaum, S., G. Tzeghai*, et al.* Effect of cell turnover and leaky junctions on arterial macromolecular transport. Am J Physiol, v.248, n.6 Pt 2, Jun, p.H945-60. 1985.

Whittembury, G., P. Carpi-Medina*, et al.* Effect of para-chloromercuribenzenesulfonic acid and temperature on cell water osmotic permeability of proximal straight tubules. Biochim Biophys Acta, v.775, n.3, Sep 5, p.365-73. 1984.

Wiener, J., R. G. Lattes*, et al.* The cellular pathology of experimental hypertension. IV. Evidence for increased vascular permeability. Am J Pathol, v.54, n.2, Feb, p.187-207. 1969.

Wolinsky, H. Response of the rat aortic media to hypertension. Morphological and chemical studies. Circ Res, v.26, n.4, Apr, p.507-22. 1970.

Wu, C. H., J. C. Chi*, et al.* Transendothelial macromolecular transport in the aorta of spontaneously hypertensive rats. Hypertension, v.16, n.2, Aug, p.154-61. 1990.

Yang, B., J. K. Kim*, et al.* Comparative efficacy of HgCl2 with candidate aquaporin-1 inhibitors DMSO, gold, TEA+ and acetazolamide. FEBS Lett, v.580, n.28-29, Dec 11, p.6679-84. 2006.

Yuan, F., S. Chien*, et al.* A new view of convective-diffusive transport processes in the arterial intima. J Biomech Eng, v.113, n.3, Aug, p.314-29. 1991.

Zeidel, M. L., S. V. Ambudkar*, et al.* Reconstitution of functional water channels in liposomes containing purified red cell CHIP28 protein. Biochemistry, v.31, n.33, Aug 25, p.7436-40. 1992.

Zeidel, M. L., S. Nielsen*, et al.* Ultrastructure, pharmacologic inhibition, and transport selectivity of aquaporin channel-forming integral protein in proteoliposomes. Biochemistry, v.33, n.6, Feb 15, p.1606-15. 1994.

Zeng. Macromolecular transport in heart valves and blood vessel walls. (microform). 2006.